universitätbonn
Rheinische
Friedrich-Wilhelms-
Universität Bonn

The Influence of the Xin Repeat-Containing Proteins on the Development of Pressure Induced Cardiac Hypertrophy in Mice

Dissertation

zur

Erlangung des Doktorgrades (Dr. rer. nat.)

der

Mathematisch-Naturwissenschaftlichen Fakultät
der

Rheinischen Friedrich-Wilhelms-Universität Bonn

vorgelegt von

Tippaporn Bualeong

Aus

Thailand

Bonn, 2015

Angefertigt mit der Genehmigung der Mathematisch-Naturwissenschaftlichen

Fakultät der Rheinischen-Friedrich-Wilhelms-Universität Bonn

am Institut für Physiologie II, Universitätsklinikum Bonn.

Prüfungsausschuss:

Erstgutachter:	Herr Prof. Dr. Rainer Meyer
Zweitgutachter:	Herr Prof. Dr. Dieter O. Fürst
Fachnahes Mitglied:	Frau PD. Dr. Gerhild van Echten-Deckert
Fachangrenzendes Mitglied:	Herr Prof. Dr. Gerhard von der Emde

Tag der Promotion: October 1, 2015

Erscheinungsjahr: 2015

Contents

Abbreviation…… v

1. Introduction…… 1

1.1 The heart an overview …… 1

1.1.1 Physiological function of the heart……. 1

1.1.2 Cellular morphology of the cardiac muscle tissue…….. 4

1.1.3 The cytoskeleton of cardiomyocytes…….. 8

1.1.4 Xin repeat-containing proteins as part of the cardiac cytoskeleton 11

1.1.5 The excitation-contraction coupling of cardiomyocytes…… 15

1.2 Cardiac remodeling and hypertrophy …….. 19

1.2.1 Adaptive or maladaptive remodeling……..…… 19

1.2.2 Development of cardiac hypertrophy……. 20

1.2.3 Contribution of cardiomyocytes to hypertrophy…… 23

1.2.4 Mechanism of fibrosis……..…….. 25

1.3 Aim of the study…….. 27

2. Material and Methods…… 29

2.1 Experimental animals…….. 29

2.2 Experimental protocols…… 29

2.3 In *vivo* Experiments…….. 33

2.3.1 Transverse aortic constriction……. 33

2.3.1.1 The operating field…..…… 33

2.3.1.2 Endotracheal intubation……. 35

2.3.1.3 Ligation of the transverse aorta……. 37

2.3.1.4 Post-operative recovery…….. 39

2.3.2 Hemodynamic measurement…….. 39

2.3.2.1 The catheter preparation…… 39

2.3.2.1.1 The equipments……... 39

2.3.2.1.2 Calibration method…….. 39

2.3.2.2 Running the experiment…….... 41

2.3.2.3 Preparing the mouse…….. 41

2.3.3 Hemodynamic data analysis……... 44

2.3.3.1 Setting the module to analyze the data…….. 44

2.4 Light microscopy……. 46

2.4.1 Histology……. 46
2.4.1.1 PFA fixation…….. 46
2.4.1.1.1 Heart cannulation…… 46
2.4.1.1.2 Perfusion of the heart……... 47
2.4.1.2 Automated tissue processor……... 47
2.4.1.3 Paraffin embedding……... 47
2.4.1.4 Sectioning with a microtome……. 48
2.4.1.5 Masson's trichrome staining…….. 49
2.4.1.6 Image analysis and quantification……. 50
2.4.1.6.1 LV thickness…… 50
2.4.2 Morphometric measurements……. 52
2.4.3 Immunohistochemical staining of isolated cerdiomyocytes…… 52
2.4.3.1 Isolation of ventricular cardiomyocytes……. 52
2.4.3.2 Immunofluorescence staining of ventricular cardiomyocytes 53
2.5 Statistics……... 55
2.6 Equipment and materials……..... 55
2.6.1 Animals and materials for animal husbandry……. 55
2.6.2 Equipment and materials for the operation……. 56
2.6.3 Equipment and materials for the hemodynamic measurement…... 57
2.6.4 Equipment for histology……. 58
2.6.5 Immunohistochemistry staining…….. 59
2.6.6 Others…….. 61

3. Results……... 63

3.1 Animals…… 63
3.1.1 Animal numbers…….. 63
3.1.2 Mortality rate…….. 63
3.1.3 Age of the mice…… 63
3.1.4 Characterization of protein expression of the mouse model…….. 64
3.1.5 Body weight of the mice…….. 66
3.1.6 Tibia length of the mice…….. 67
3.1.7 HW, HW/BW ratio, and HW/TL ratio…… 67
3.1.8 LVW, LVW/BW ratio, and LVW/TL ratio……. 68
3.1.9 LW, LW/BW ratio, and LW/TL ratio……. 69
3.2 The effect of TAC surgery…… 71
3.2.1 The effect of surgery on BW…….. 71

3.2.2 HW, HW/BW ratio, and HW/TL ratio…… 72
3.2.3 LVW, LVW/BW ratio, and LVW/TL ratio……. 73
3.2.4 LW, LW/BW ratio, and LW/TL ratio…….. 74
3.2.5 Left ventricular and septum thickness……. 75
3.2.6 Fibrosis…… 76
3.3 Studies on isolated cardiomyocytes……. 78
3.3.1 Immunolocalization of different proteins…… 78
3.3.2 Cell size of cardiomyocytes……. 82
3.3.3 The distribution of ICDs…….. 83
3.4 Hemodynamic parameters…… 85
3.4.1 Hemodynamic data after 14 days TAC…… 85
3.5 Electrocardiogram……. 87
3.5.1 Surface ECG parameters……. 88
3.5.2 The ECG variations……. 89
3.6 Comparison three month old with one year old mice…….. 93
3.6.1 HW, HW/BW ratio, and HW/TL ratio…… 93
3.6.2 LVW, LVW/BW ratio, and LVW/TL ratio……. 94
3.6.3 LW, LW/BW ratio, and LW/TL ratio……. 96
3.6.4 HW, HW/BW ratio and HW/TL ratio after TAC…… 97
3.6.5 LVW, LVW/BW ratio and LVW/TL ratio after TAC……. 99
3.6.6 LW, LW/BW ratio, and LW/TL ratio after TAC……. 100
3.6.7 Hemodynamic parameters in 3 month and 1 year-old mice after 14 days of TAC…… 102

4. Discussions…… 105

4.1 Mouse model……. 107
4.2 Hypertrophy model (TAC)…… 107
4.3 TAC-induced changes in macroscopic parameters…… 108
4.3.1 Mortality…… 108
4.3.2 Body weight…….. 109
4.3.3 Age of the mice……. 109
4.3.4 HW, LVW, and LW……. 110
4.3.5 Left ventricular, septum thickness, and cardiac fibrosis…….. 112
4.3.6 Cardiomyocyte parameters…… 114
4.4 TAC induced changes in hemodynamic parameters……. 115
4.5 TAC-induced changes in the ECG…… 117
4.6 Conclusion……. 119

5. Abstract…….... 121

6. References……. 125

7. Appendix…...……. 137

8. Declaration……..……. 141

9. Acknowledgements….……. 143

10. Poster and presentations …….. 145

11. Curriculum vitae …… 147

Abbreviations

AC	area composite
ACE	angiotensin converting enzyme
AJs	adherens junctions
Akt	protein kinase B
Ang II	angiotensin 2
AP	action potential
ATP	adenosine triphosphate
AV valves	atrioventricular valves
BW	body weight
$[Ca2^{+}]_i$	cytosolic Ca^{2+}-concentration
CICR	Ca^{2+}-induced Ca^{2+}-release
CMYA1	cardiomyopathy-associated gene 1
CMYA3	cardiomyopathy associated gene 3
CO	cardiac output
DAP	diastolic arterial pressure
EC coupling	electro-mechanical coupling
ECG	electrocardiogram
ECM	extracellular matrix
EDV	end-diastolic volume
ERK-2	extracellular-regulated kinase-2
ESV	end-systolic volume
ET-1	endothelin1
FHL-1	Four-and-a half LIM domain protein-1
FHL-2	Four-and-a half LIM domain protein-2
HF	heart failure
HR	heart rate

HW	heart weight
$I_{Ca,L}$	L-type calcium channels
ICDs	intercalated disks
IGF1	insulin-like growth factor 1
I_{K1}	inward rectifier K^+ current
I_{Ks} and I_{Kr}	K^+-outward currents
IL1β	interleukin-1β
IL6	interleukin-6
I_{to}	transient K^+-outward current
LAD	left anterior descending
LV	left ventricular
LVEDP	left ventricular end diastolic pressure
LVEF	left ventricular ejection fraction
LVH	left ventricular hypertrophy
LVSP	left ventricular systolic pressure
LVW	left ventricular weight
LW	lung weight
MEF2	myocyte enhancer factor 2
MEK2	mitogen activated protein kinase kinase-2
MI	myocardial infarction
MLP	muscle LIM protein
MMPs	matrix metalloproteinases
mTOR	mammalian target of rapamycin
MyBP-C	myosin-binding protein C
N-CAD	N-cadherin
NCX	Na^+- Ca^{2+} exchanger
NE	norepinephrine

I_{Na}	Na^+-inward current
PFA	paraformaldehyde
PI3K	phosphoinositide 3-kinase
PKB	protein kinase B
RAAS	renin angiotensin aldosterone
RAF1	rapid accelerated fibrosarcoma-1
RVW	right ventricular weight
RyR	ryanodine receptor
SAP	systolic arterial pressure
SA node	sinoatrial node
SR	sarcoplasmic reticulum
SV	stroke volume
TAC	transverse aortic constriction
T-cap	titin-cap
TIMPs	tissue inhibitors of metalloproteinases
TGF-β	transforming growth factor-β
TL	tibia length
TNF-α	tumor necrosis factor-α
TPR	total peripheral resistance
VR	venous return
WT	wild-type
XIRPs	Xin repeat-containing proteins
XIRP1	Xin repeat containing protein 1
XIRP2	Xin repeat containing protein 2

1 Introduction

1.1 The heart - an overview

1.1.1 Physiological function of the heart

The function of the heart is to generate and maintain arterial blood pressure necessary to provide adequate perfusion of organs. The contraction of the cardiac walls elevates the blood pressure from the low filling values to the high pressures, at which the blood is ejected through the aortic valve into the aorta (Klabunde, 2011). Cardiac muscle has to contract repetitively for lifetime, and for that purpose it requires a continuous supply of energy. Cardiac muscle is therefore very rich in mitochondria, which regenerate ATP by oxidative phosphorylation of substrates and thus fulfill the myocardial energy requirements. To provide adequate O_2 and substrates for the metabolic machinery, the myocardium is also endowed with a rich capillary network, about one capillary per fiber.

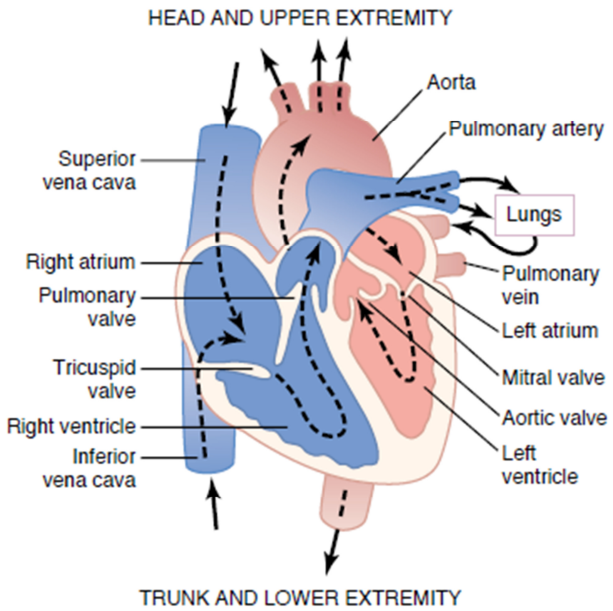

Figure 1.1 Structure of the heart, and course of blood flow through the heart chambers and heart valves. (Guyton & Hall, 2006)

The heart consists actually of two separate pumps, the left heart and the right heart which have different functions. Each side of the heart is divided into two chambers, an atrium and a ventricle, connected by one-way valves, called atrioventricular (AV) valves, designed so that blood can flow only from the atrium into the ventricle. The left heart and the systemic arteries, capillaries, and veins form the systemic circulation. The left ventricle pumps oxygenated blood (in Fig. 1.1 red) to all organs of the body except the lungs. The right heart and the pulmonary arteries, capillaries, and veins build up the pulmonary circulation into which the right ventricle pumps deoxygenated blood (in Fig. 1.1 blue). The blood is pumped sequentially from the left heart into the systemic circulation, flows back to the right heart, which pumps it into the pulmonary circulation, and then back into the left heart (Guyton & Hall, 2006).

The function of the heart is based on the highly coordinated contraction of cardiac muscle cells (cardiomyocytes). Their contraction is elicited by a depolarization of their membrane potential called action potential (AP). The AP is initiated in the sinoatrial node (SA node), which is located near the conjunction of the Vena cava with the right atrium. As the cardiomyocytes are connected by complexes of tight electrical and mechanical junctions, called intercalated discs, the AP is able to propagate rapidly over the heart and thus to elicit synchronized contraction of the cardiomyocytes, which is the pre-condition for the coordinated pumping of the heart. Likewise, refilling of the heart requires synchronized relaxation of the cardiomyocytes (Berne & Levy, 2008).

The volume of blood pumped per minute by each ventricle of the heart is known as cardiac output (CO), which is defined as the product of heart rate (HR) and stroke volume (SV). In addition, further factors such as synchronization of ventricular contraction, ventricular wall integrity, and valvular competence affect CO (Fig. 1.2). SV is influenced by three main factors: (1) preload, which is the end diastolic pressure that stretches the right or left ventricle of the heart to its greatest geometric dimensions depending on the physiologic demand (the amount of myocardial fiber stretch at the end of diastole or the initial stretching of the

cardiomyocytes prior to contraction); (2) afterload, which consists of the resistance that the ventricle has to override to eject blood; and (3) contractility, which is a measure for the contractile performance of the heart independent of pre- or afterload (Kemp and Conte, 2012). As the preload depends on the filling of the respective ventricle this will also exert the stretching stimulus on the cardiac wall and thus the cardiomyocytes. The German physiologist Otto Frank was the first who observed a relationship between the volume present in the frog ventricle before the systole and the pressure developed during the systole (Frank, 1895). Expanding Frank's perceptions, the British physiologist Ernest Starling showed, in an isolated dog heart, that the volume the ventricle ejected during systole was determined by the end-diastolic volume (EDV). The principle underlying this relationship is the length-tension

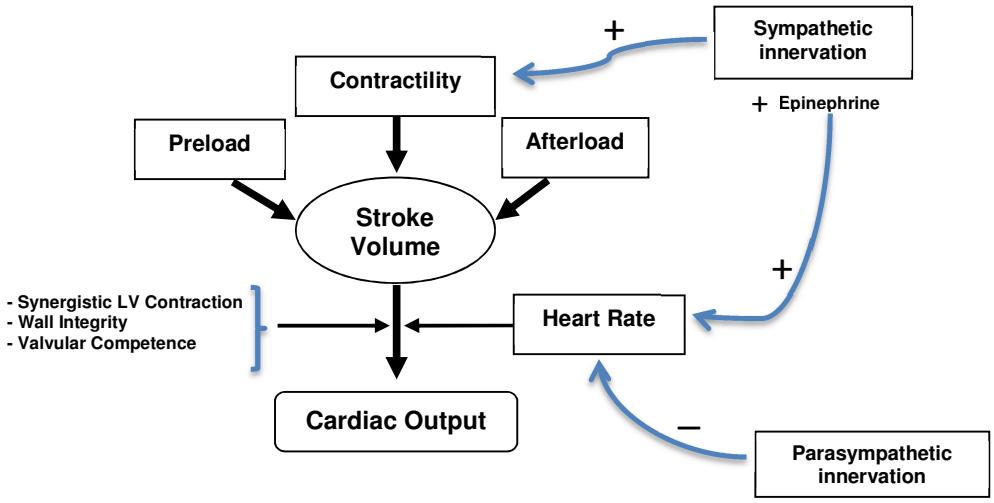

Figure 1.2 Mechanical and humoral factors affecting cardiac output.

relationship in cardiac muscle fibers. The Frank-Starling law or relationship of the heart expresses that the volume of blood ejected by the ventricle depends on the EDV. The EDV itself is set by the volume returned to the heart, the venous return (VR). Hence, SV and CO correlate directly with EDV and VR. The Frank-Starling law ensures that the volume the heart ejects in systole equals VR. Therefore, in steady state CO equals VR (Patterson and Starling, 1914). Increased diastolic filling produces a higher amount of stretch in the heart muscle,

resulting in a larger SV. Furthermore, as the output of one ventricle becomes the VR of the other both must have the same volume.

As mentioned above the third parameter scaling CO is afterload. Afterload is increased when systemic vascular resistance is up-regulated or an aortic valve stenosis occurs. Under the influence of elevated afterload, SV is lowered and end-systolic volume (ESV) rises. This results in a greater EDV, which in turn increases SV due to Starling´s law, and finally ends in a new steady state with higher systolic BP (Klabunde, 2007).

Besides the mechanical regulation, cardiac output is also affected by the activity of the autonomous nervous system. The parasympathetic and the sympathetic component act antagonistically on the SA node. Parasympathetic stimulation leads to a lowering of the HR called negative chronotropic effect. Sympathetic stimulation exerts a positive chronotropic effect by rising the HR. As the CO depends directly on the heart rate, both branches of the autonomous nervous system also influence the CO in opposite directions (Fig. 1.2).

Sympathetic stimulation furthermore increases contractile force (positive inotropic), accelerates relaxation (positive lusitropic), and speeds up excitation conduction (positive dromotropic).

1.1.2 Cellular morphology of the cardiac muscle tissue

The cardiac muscle tissue consists of muscle cells, named cardiomyocytes, fibroblasts and blood vessels. Cardiomyocytes are about ten times as long as wide, branched, and inter-connected end to end by so called intercalated disks (ICDs), which appear as dark lines in light microscopy (Fig. 1.3 A and B).

The intercalated disks contain firstly, gap junctions which connect the myocytes electrically and chemically, secondly, adherens junctions (AJs or fasciae adhaerentes) connecting the myofibrils from neighboring cardiomyocytes transferring the contractile force and finally, desmosomes (maculae adhaerentes) to provide mechanical strength to the ICDs (Forbes and Sperelakis 1985; Fig. 1.3 and 1.4). Later on, it has been reported that the development of the

mammalian ICD junctional system is continued also after birth. Interestingly, the AJs and desmosomes are fused and combined together which is called area composita (AC) (Borrmann et al., 2006: Franke et al., 2006; Pieperhoff and Franke, 2008). Moreover, the review article by Pieperhoff et al (2010) emphasized that the AC get involved in human arrhythmogenic cardiomyopathies (Pieperhoff et al., 2010).

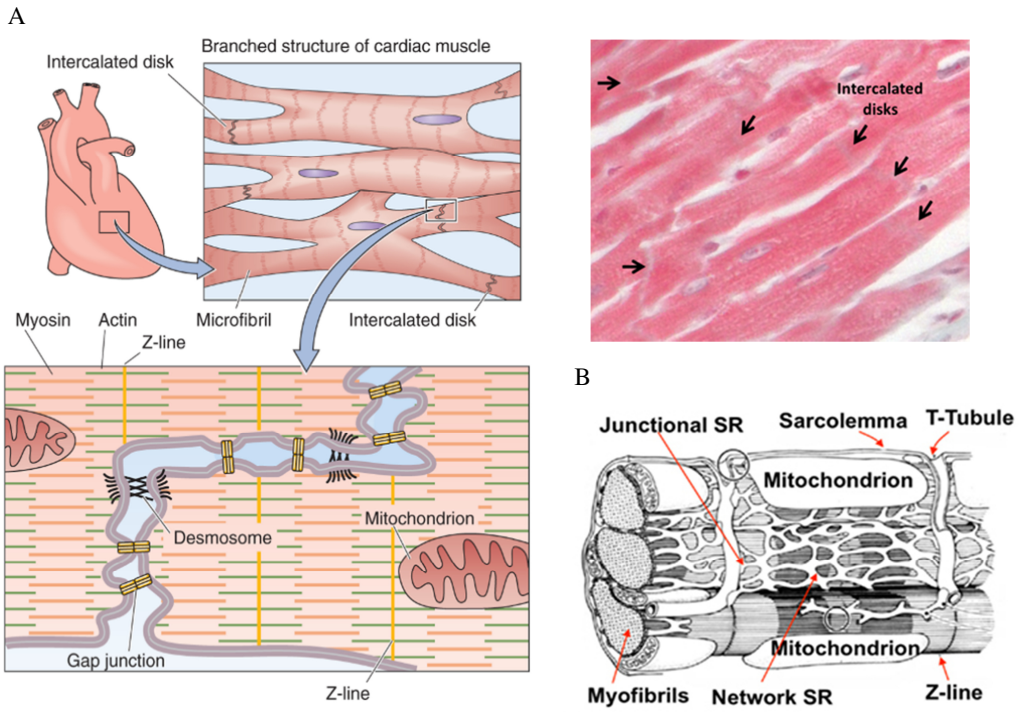

Figure 1.3 The structure of cardiac myocytes.

(Composed of Boron, 2009 (A); Nivala, 2012 (B))

There are three different types of cardiomyocytes: (i) atrial, (ii) ventricular, as well as (iii) pacemaker and conductive cells. All three types of cardiomyocytes are cross-striated muscle cells filled with well-aligned contractile myofibrils already visible at the light microscope level. Cardiomyocytes usually contain one or two nuclei.

Each cardiomyocyte is surrounded by the cell membrane which in case of ventricular cells forms transverse tubular invaginations, T-tubules. The T-tubules pervade the cytoplasm from the cell surface to its center and they are flanked by an internal membraneous tubular network, the sarcoplasmic reticulum (SR), which plays a key role as internal Ca^{2+} stores. To provide the high amount of energy required for both contractions and the pumping of ions, cardiomyocytes contain a high amount of mitochondria situated in rows between the myofibrils (Fig. 1.3B)

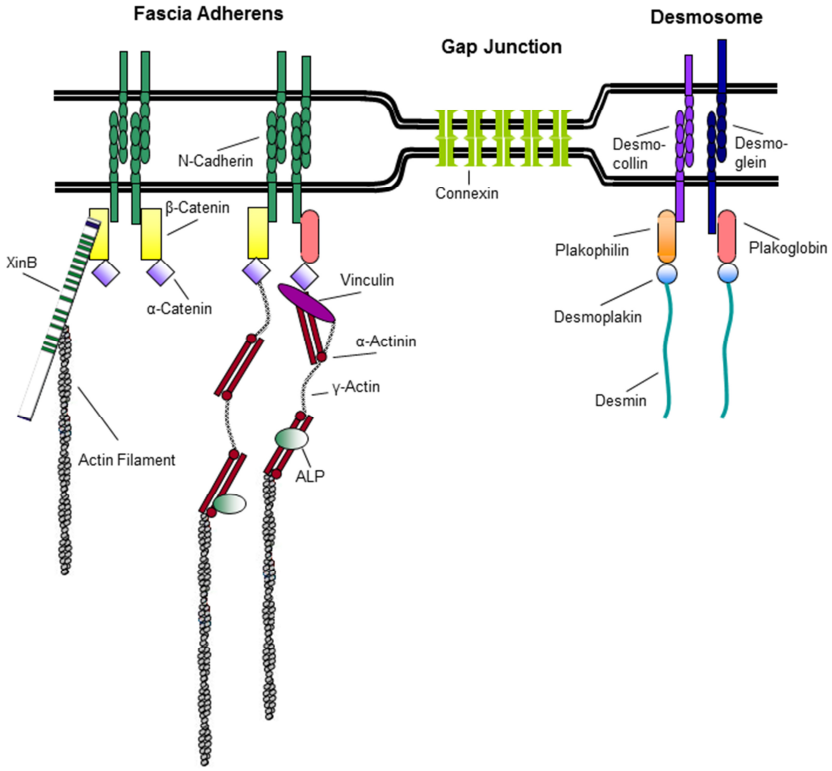

Figure 1.4 Diagrammatic representation of three structural zones of the intercalated disc. Note that the fascia adherens mainly anchors myofibrillar proteins, whilst the desmosome is mainly linked to the cytoskeleton (intermediate filaments and microfilaments). Five connexon channels are shown in the gap junction where each connexon is composed of six subunits, usually comprising connexin 40 and 43. (modified from Jung-Ching Lin et al. (2005) and Molt et al. (2014)).

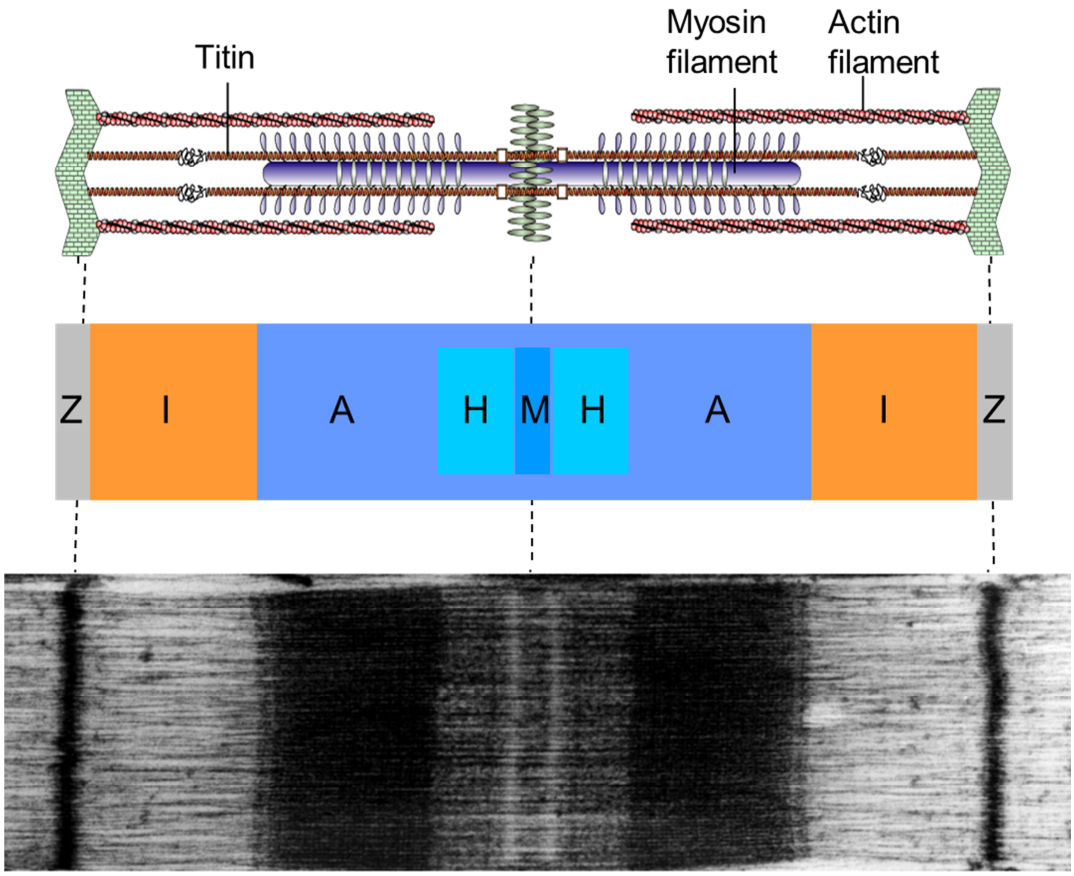

Figure 1.5 Anatomy of the sarcomere.

In the upper sketch a schematic drawing of one sarcomere is demonstrated. Thin filaments mainly consist of F-actin, tropomyosin, and the troponin complex (troponin T, C, and T). They are affixed at the α-actinin of the Z-discs. Thick filaments are based on myosin molecules, whose heads bind to the actin. Due to their ATPase activity the myosin heads are able to change their angle to the neighboring thin filaments and thereby to generate movement and force. Titin is a giant protein which expands from the Z-disc to the M-band. Titin is connected end-to-end in the Z-disc via titin-cap (T-cap) and to α-actinin via so-called Z-repeats. In the middle sketch the bands of the sarcomere are represented. In the A-band (defined by the presence of myosin (A)) titin is attached to the thick filament. In the I-band (region, where the thin filaments are alone (I)) titin has its extensible region, which contributes to the elastic properties of the sarcomere. In the center of the sarcomere the myosin filaments are connected by the proteins of the M-band (M) e.g. myomesin and M-protein. The region in which the thick filaments do not overlap with thin filaments is called the H-zone (H). In an isolated living cardiomyocyte the length of a relaxed sarcomere is 1.8-1.9 µm. Thick filaments also contain further regulatory proteins like myosin-binding protein C (MyBP-C). Lower part consists of an electron microscopic picture of a longitudinal section of a sarcomere. Corresponding bands are located above each other. Figure by courtesy of Prof. Dieter Fürst, Inst. of Cell Biology, Bonn.

The myofibrils are divided into distinct, repetitive microanatomical units, termed sarcomeres, which form the elementary contractile units of the myocyte (Fig. 1.3 B). Each sarcomere is bordered by Z-discs (also called Z-lines), thus the distance between two Z-discs defines the sarcomere length. The sarcomere is mainly composed of the thick myosin- and thin actin-containing filaments, as well as the sarcomeric cytoskeleton (Fig. 1.5). It is subdivided into bands, A-band (anisotropic), I-band (isotropic), which are named according to their refractory properties towards polarized light.

1.1.3 The cytoskeleton of cardiomyocytes

The cytoskeleton is an extensive network of filaments and accessory proteins that enables cardiomyocytes to withstand the extensive mechanical stresses that are developed during each contractile cycle of the heart.

The backbone of the cytoskeleton is composed of three types of filaments: microtubules, intermediate filaments, and microfilaments. These filaments are linked to the myofibrils and to the cell membrane as well as to membranes of cellular organelles via a plethora of associated proteins. In addition, certain transmembrane proteins also connect the cytoskeleton to the extracellular matrix (ECM). In addition, myofibrils contain a specialized cytoskeleton based on the giant protein titin, which spans half sarcomere length and thereby links thick and thin filaments via several titin-binding proteins (Fig. 1.5). Thus the cytoskeleton supports the delicate cell membranes, positions organelles, supports intracellular transport, organizes myofilaments, and provides mechanical strength and structural integrity to the cardiomyocyte. The cytoskeleton of the myocytes is a vital structural network which also forms an interface between the cell and the extracellular environment through specialized transmembrane proteins like integrins and dystroglycans. Especially dystrophin binds to both, intracellular actin and extracellular laminin. Thus, the cytoskeleton enables the cardiomyocytes to form the cardiac tissue and to contract and relax in a coordinated manner. The cytoskeleton

additionally senses biomechanical stress and responds to it by induction of signaling pathways that allow the cell to adapt to these stimuli (Granzier, 2006).

Elements of the cytoskeleton are involved in organizing structures such as costameres in striated muscle cells and in particular ICDs in cardiac muscle (Green et al., 2005). At an ICD, the cell membranes of 2 adjacent cardiomyocytes are extensively intertwined and bound together by gap junctions, adherens junctions and desmosomes (Fig. 1.4, 1.6). With respect to the cytoskeleton it is important to note that adherens junctions directly link the myofibrils mechanically, whereas the desmin intermediate filaments surround the myofibrils and connects them to the desmosomes. These connections help to stabilize the positions of the cells relative to each other and also help to maintain the 3D structural integrity of the tissue. Thus ICDs, as cardiac-specific structures, are responsible for both mechanical and electrical synchronization and are implicated in signal transduction between adjacent cardiomyocytes.

It is worth to mention that the ionic channels like L-type Ca^{2+} channels, which play a key role in cardiac excitation-contraction coupling (c.f. chapter 1.5), are also linked to the cytoskeleton. Accordingly, it has been shown that pharmacological depolymerization of microfilaments by cytochalasin D reduced the Ca^{2+} inward current through L-type calcium channels ($I_{Ca,L}$) dramatically (Rueckschloss and Isenberg, 2001). In agreement with this observation, our group recently found that adult cardiomycytes deficient for gelsolin display a highly increased $I_{Ca,L}$ and consequently also elevated shortening amplitudes (Weisser-Thomas et al., 2015). Gelsolin deficiency shifts the equilibrium of actin polymerization vs. depolymerization to higher degrees of polymerization, leading to more microfilaments in the cytoskeleton. The finding of an up-regulated $I_{Ca,L}$ may also explain the observation that gelsolin-deficient mice are more prone to atrial fibrillation (Schrickel et al., 2009).

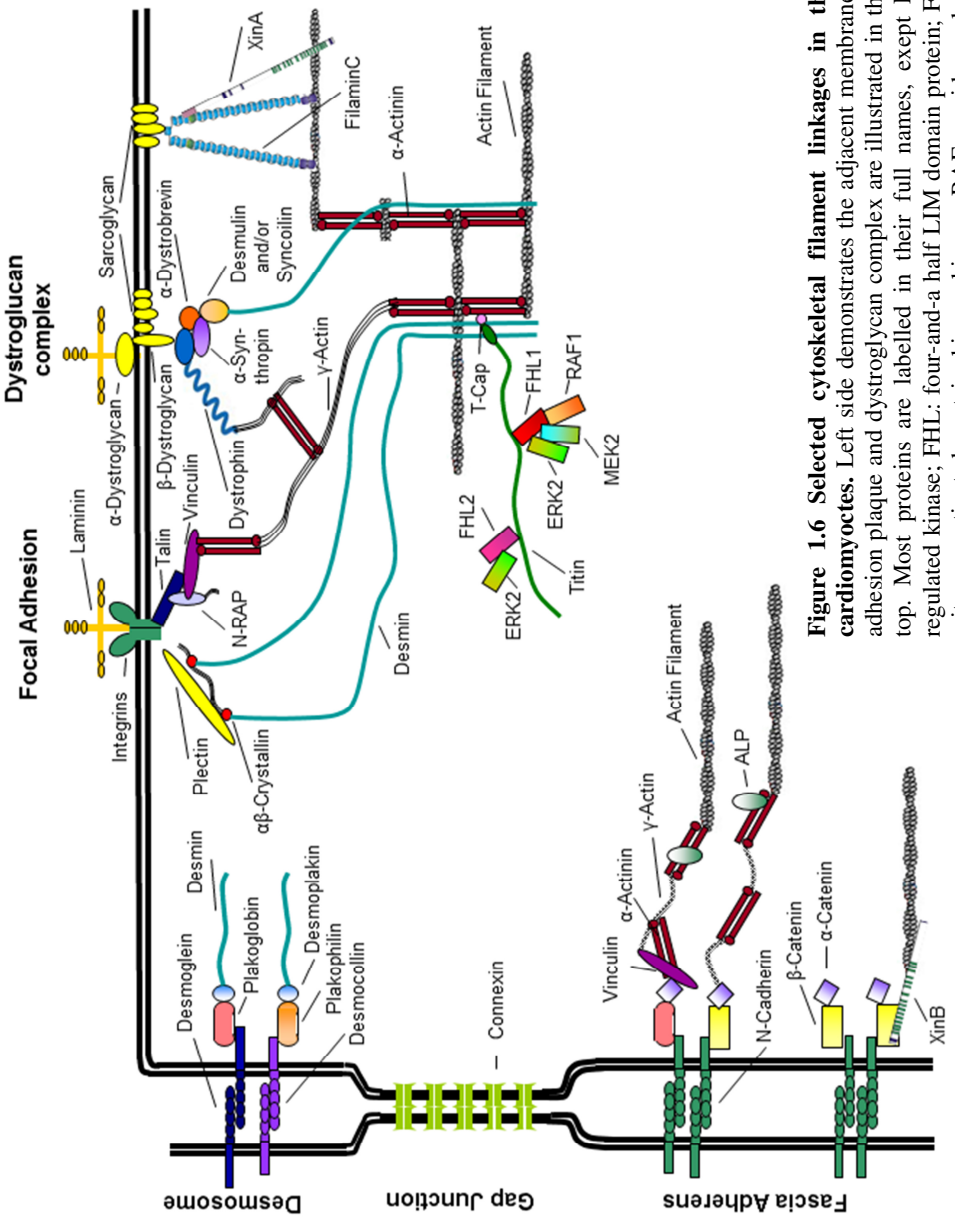

Figure 1.6 Selected cytoskeletal filament linkages in the sarcolemma of cardiomyoctes. Left side demonstrates the adjacent membranes in an ICD. Focal adhesion plaque and dystroglycan complex are illustrated in the membrane on the top. Most proteins are labelled in their full names, exept ERK: extracellular-regulated kinase; FHL: four-and-a half LIM domain protein; FLN: filamin, MEK: mitogen activated protein kinase kinase; RAF: rapid accelerated fibrosarcoma. (modified from Clark et al., 2002, Gontier et al., 2005; Krüger and Linke 2009; Molt et al. 2014; van der Ven et al. 2000)

In general, mutations or deficiencies in elements of the cytoskeleton have been found to be involved in various cardiac diseases. Especially, mutated ICD components cause

cardiomyopathies, arrhythmias and other fatal heart diseases (Li and Radice, 2010; Noorman et al., 2009; Perriard et al., 2003; Severs et al., 2008; Sheikh et al., 2009).

Alterations in the amount and distribution of cytoskeleton elements also occur in cardiomyocytes of hypertrophied and failing myocardium. Furthermore, it has been shown that disruption of genes coding for cytoskeletal proteins such as the muscle LIM protein (MLP), desmin, plakoglobin, and N-cadherin can result in cardiac dilatation and impaired cardiac function (Jane-Lise et al., 2000). In addition, degeneration of cardiomyocytes can be induced by reduction of myofilaments as well as alterations of the cytoskeleton (Hein et al., 2000). Also the heart's participation in several muscular dystrophies has been deduced to mutations and variations in cytoskeletal proteins (Sarantitis et al., 2012; Clemen et al., 2013). Recently, a point mutation in desmin has been demonstrated to cause a myopathy and cardiomyopathy (Clemen et al., 2015).

1.1.4 Xin repeat-containing proteins as part of the cardiac cytoskeleton

As the function of the Xin repeat-containing proteins (XIRPs) in the heart will be in the center of this study, their role in the cytoskeleton of the heart is highlighted in a specific chapter. XIRPs are characterized by a 16 amino acid long conserved molecular motif (Xin repeat) which binds to actin filaments (Cherepanova et al., 2006; Choi et al., 2007; Pacholsky et al., 2004). In mammals XIRPs are encoded by two genes, which originally were thought to be in linked to cardiac diseases and thus named "cardiomyopathy-associated (*CMYA*) genes" *CMYA1* and *CMYA3* (Walker, 2001). Recently, the genes have been renamed to *XIRP1* and *XIRP2*, respectively.

As the gene and protein-naming is inconsistent in different publications, the terminology used in this study is clarified in Table 1.1.

Table 1. 1 The Nomenclature of XIRPs

Protein family	**Gene name**	Alternative gene name	**Species**
XIRP1	*XIRP1*	*hXina, , CMYA1, XIN*	human
XIRP1	*XIRP1*	*mXinα, CMYA1, Cmya, mXin*	mouse
Xin	*Xirp1*	*cXin*	chicken
XIRP2	*XIRP2*	*hXinβ, CMYA3, Cmya3*	human
XIRP2	*XIRP2*	*mXinβ, CMYA3, Cmya3, Myomaxin*	mouse

(Gustafson-Wagner et al., 2007; Huang et al., 2006; Lin et al., 2005; Pacholsky et al., 2004; Sinn et al., 2002; Wang et al., 1999; Wang et al., 2010, 2012; van der Ven et al., 2006), http://www.ncbi.nlm.nih.gov/gene/241431; http://www.ncbi.nlm.nih.gov/gene/22437

The intercalated disk protein Xin was originally discovered in chicken striated muscle and implicated in cardiac morphogenesis (Wang et al., 1999). In contrast to the chicken genome which seems to contain only one *XIRP* gene (Grosskurth et al., 2008), in mammals the mentioned two genes *XIRP1* and *XIRP2* are known (Pacholsky et al., 2004). In zebrafish even three *XIRP* genes have been identified (Otten et al., 2012). In mammals, the *XIRP1* gene encoding XIRP1 consists of two exons, only one of which accounts for the protein-coding region. The situation is even more complicated, because intraexonic splicing of the *XIRP1* mRNA results in the expression of three Xin isoforms: XinA, XinB and XinC (van der Ven et al., 2006). It is quite likely that multiple splice variants exist also of XIRP2, but corresponding analyses still have not yielded a coherent image.

In order to investigate the function of XIRP1, two types of *XIRP1* deficient mice were made. Mice with a total *XIRP1* deficiency (XinABC$^{-/-}$ mice) were bred by our group (Otten et al., 2010), whereas mice lacking only two of the three XIRP1 isoforms (XinAB$^{-/-}$ mice) were introduced by Gustafson-Wagner et al. (2007). Based on the available literature and the splicing pathway, these XinAB$^{-/-}$ mice most likely are still able to synthesize the XinC protein.

In differentiated skeletal muscle XIRPs are mainly found at myotendinous junctions, whereas in the heart they are localized in the ICDs (Wang et al., 2012). Furthermore, inactivation of *Xin* in developing chick embryos was reported to result in a severe disruption of cardiac looping morphogenesis (Wang et al., 1999). This suggests that the Xin gene may have played a key role in the evolution of the vertebrate heart (Wang et al., 2013).

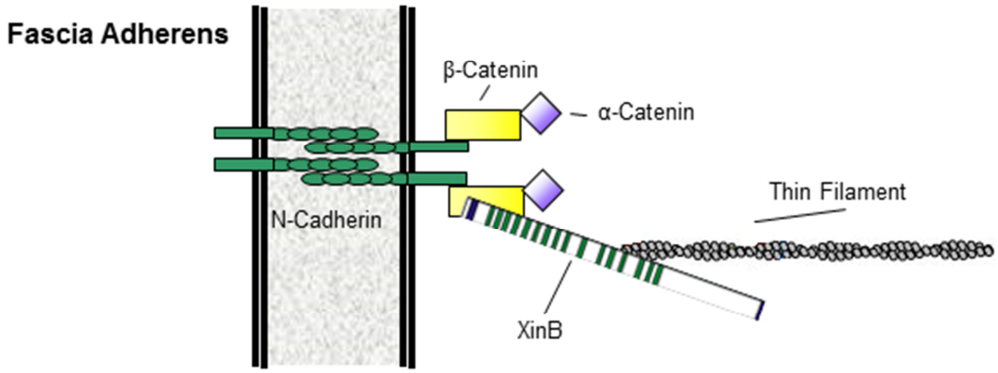

Figure 1.7 Proposed model for XIRP1 (XinB) localization at the adherens junction of the intercalated disk (based on the ideas of Jung-Ching Lin et al. (2005) and Molt et al. (2014).

In the murine heart, XIRP1 has also been demonstrated in ICDs. As shown in Fig. 1.7, XIRP1 is part of the fascia adherens of the ICD. Here β-catenin is bound to the cytoplasmic domain of N-cadherin. Furthermore, β-catenin is connected to α-catenin, which was suggested to either function as a linker between cadherins and thin filaments (Watabe-Uchida, et al., 1998,), or alternatively to compete for the Arp2/3 complex to form an initiation complex for the assembly of actin filaments (Drees, et al., 2005). Free XIRP1 may first be in an auto-inhibited state, during which the C-terminal proline-rich region prevents the Xin repeats from binding to actin filaments. As soon as XIRP1 binds to β-catenin with the respective binding domain, a conformational change could be induced. This may lead to an open conformation of the Xin repeats which are then able to bind with this region to actin filaments (Jung-Ching et al., 2005). Interestingly, XIRP1 has also been detected in the regions of sarcomere repair

in cross-striated muscle together with filamin C and aciculin (Molt et al., 2014). This can be interpreted in the way that XIRP1 is involved in repair and remodeling processes in cross-striated muscle.

In 2004 a second protein with Xin-repeats was described as XIRP2 (Pacholsky et al., 2004). It binds to filamentous actin and α-actinin through the Xin repeat region in a fashion similar to XIRP1. In the heart XIRP2 was localized in ICDs (Gustafson-Wagner et al., 2007). At about the same time, Huang et al. (2006) described a new gene with Xin-repeats, which they called *myomaxin*. This gene was described as the murine ortholog of a partial cDNA named "cardiomyopathy associated gene 3" (*CMYA3*). This gene was shown to be controlled by the transcription factor "myocyte enhancer factor 2" (MEF2). The expressed protein was described to be related to Xin and was detected in the peripheral Z-disc region and costameres (Huang et al., 2006). In a later publication this group described the *CMYA3* gene as *XIRP2* and consequently the expressed protein was called XIRP2 (McCalmon et al., 2010). The transcription factor MEF2 is stimulated by angiotensin II (AngII) a well-known pro-hypertrophic factor. Indeed McCalmon et al. (2010) were able to show that AngII was able to up-regulate XIRP2 expression in cultured rat neonatal cardiomyocytes. Promoter assays in COS cells expressing the putative *XIRP2* promoter and the type I angiotensin receptor provided evidence that the promoter region of the *XIRP2* gene harbors an AngII responsive region. Like XIRP1 also XIRP2 seems to play a role in cardiac development, as loss of XIRP2 in mice led to ICD defects at postnatal day 16.5, a developmental stage when the heart forms ICDs (Wang et al., 2013).

Surprisingly, the described *XIRP1*-deficient mice (XinAB$^{-/-}$ and XinABC$^{-/-}$) exhibit different cardiac phenotypes. The XinAB$^{-/-}$ mice, which still can express XinC, are viable, fertile and display normal cardiac morphogenesis with cardiac hypertrophy, fibrosis conduction defects and signs of cardiomyopathy at higher age (Gustafson-Wagner et al., 2007). A significant up-regulation of XIRP2 likely provides partial compensation and may account for the viability of the XinAB$^{-/-}$ mice (Gustafson-Wagner et al., 2007). Interestingly, XinC has been detected

solely in cardiomyopathic human tissues (Otten et al., 2010). As depicted in Fig. 1.7, mouse XIRP1 is potentially coupling the N-cadherin/β-catenin complexes to the underlying actin cytoskeleton, therefore XIRP1 deficiency may modulate ICD integrity and function. This may lead to the consequence that XinAB$^{-/-}$ hearts develop structural ICD defects and cardiomyopathy with conduction deficits (Wang et al., 2013).

XinABC$^{-/-}$ deficiency, in contrast, leads to topographical ICD alterations, premature fibrosis and subtle changes in contractile behavior, which is a milder cardiac phenotype than that observed in XinAB$^{-/-}$ mice. Furthermore, it indicates that XinC may be dominantly involved in the development of human cardiac hypertrophy (Otten et al., 2010).

Furthermore, McCalmon et al. (2010) generated a XIRP2 hypomorphic mouse, which spontaneously developed a mild type of cardiac hypertrophy. As discussed further down in chapter 2.2, AngII is able to induce and promote the development of cardiac hypertrophy. Interestingly, AngII induced cardiac hypertrophy was attenuated in the XIRP2 hypomorphic mice.

Taken together, these data predict a crucial role for XIRP1 and XIRP2 in cardiac development and disease and it will be of interest to determine the consequences of a disruption of both *XIRP* genes.

1.1.5 The excitation-contraction coupling of cardiomyocytes

Contraction of cardiac muscle cells is not initiated by neurons as in skeletal muscle but by electrical excitation generated by the cardiac pacemaker. This pacemaker consists of specialized cells located in the SA node of the right atrium. The pacemaker cells are able to undergo spontaneous depolarization and generate spontaneous and periodic APs. These APs are then propagated throughout the heart. By the following mechanism: when an AP is initiated in one cell, current flows through the gap junctions and depolarizes neighboring cells. If this depolarization reaches the threshold, then a new AP is elicited in this cell. This AP is again able to depolarize neighboring cardiomyocytes. By this mechanism APs

generated in the SA node can propagate over the whole cardiac muscle. Propagation of APs follows the specialized conduction system of the heart as these cells allow the highest AP-conduction velocity (Boron, 2009).

Function of the AP is to initiate the contraction of cardiomyocytes, this process is called

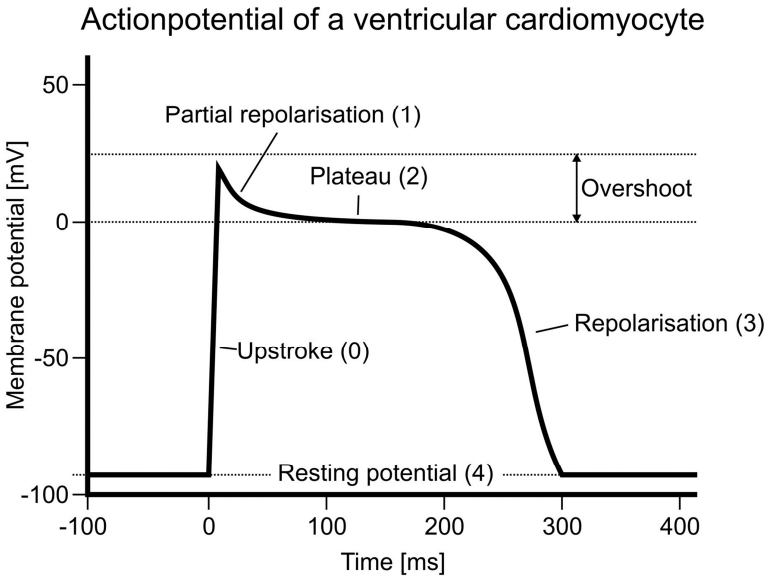

Figure 1.8 Action potential of a ventricular cardiomyocyte. (0) Depolarization due to Na^+-inward current, I_{Na}, through fast voltage activated Na^+-channels. (1) Initial repolarization by a transient K^+-outward current, I_{to}. (2) Plateau maintained by a Ca^{2+}-inward current through L-type channels, $I_{Ca.L}$, and a reduced K^+-conductance. (3) Repolarization depending on the K^+-outward currents I_{Ks} and I_{Kr}. (4) Resting membrane potential stabilized by K^+-current through inward channels, I_{K1}.

electro-mechanical coupling (EC coupling). This function depends highly on the shape of the AP and on the underlying ionic currents. The cardiac AP introduced here, is typical for cardiomyocytes of the left ventricular myocardium of humans and other mammals with low heart rates (HR), i.e. resting rates of 60-80 beats per seconds. The AP is divided into four phases: (0) the depolarization, (1) the partial repolarization, (2) the plateau phase, (3) the repolarization, (4) the resting potential (Fig. 1.8) Phase 0 is depending on a Na^+ inward current through voltage activated Na^+ channels. Phase 1 is evoked by a transient K^+-outward current. The sustained depolarization during the plateau phase (phase 2) is maintained by a Ca^{2+}-inward current through L-type Ca^{2+}-channels and a reduced K^+-conductance. The

repolarization during phase 3 is obtained by K^+-outward currents through rapidly and slowly activating K^+-channels. The main current component for the stabilization of the resting potential is K^+-outward current through inward rectifier K^+-channels. The duration of the AP lasts 200-300 ms. Rodents, which often exhibit higher HRs from 250-350 bpm (rats) or 550-650 (mice), naturally have shorter AP-durations without a distinctive plateau phase.

As the AP depolarizes the sarcolemma of the cardiomyocytes it also depolarizes the attached t-tubules. Here the depolarization opens voltage-gated L-type Ca^{2+} channels through which Ca^{2+} flows into the cytoplasm. This opens ryanodine receptor Ca^{2+} release channels (RyR) in the SR, which is located in direct vicinity of the T-tubular membrane. When the RyR channels open, stored Ca^{2+} is released from the SR into the cytosol, creating a Ca^{2+} "spark" that can be detected by Ca^{2+} sensitive fluorescent dyes like fura-2. Synchronized sparks from different RyR channels raise the cytosolic Ca^{2+}-concentration, $[Ca^{2+}]_i$, sufficiently to elicit a uniform contraction of the cardiomyocyte. The $[Ca^{2+}]_i$ is elevated approximately 10-fold from a resting level of ~100 nM to ~1 µM (Marks, 2003). As the myocardial RyR channels open in response to Ca^{2+} binding the mechanism of EC coupling in the cardiomyocytes has been named *Ca^{2+}-induced Ca^{2+}-release* (CICR; Fabiato,1985). Interestingly, 90% of the $[Ca^{2+}]_i$ rise eliciting the contraction is provided by the SR and only 10% are flowing though L-type Ca^{2+} channels.

1. AP enters the T-tubule.
2. L-type Ca^{2+} channels open, Ca^{2+} flow into the cytoplasm.
3. Ca^{2+} induces Ca^{2+} release from the SR via ryanodine receptor-channels.
4. Local Ca^{2+} release induces Ca^{2+} spark.
5. Synchronously appearing sparks create a Ca^{2+} signal.
6. $[Ca^{2+}]_i$ increases and Ca^{2+} binds to troponin C.
7. Cross bridge cycling starts, contraction develops.
8. Ca^{2+} is pumped back into the SR, $[Ca^{2+}]_i$ is lowered.
9. Ca^{2+} dissolves from troponin C, relaxation develops.
10. Ca^{2+} is pumped out of the cell by the Na^+/Ca^{2+} exchanger.
11. Cytoplasmic Na^+ is maintained by the Na^+ pump in the sarcolemma.

Figure 1.9 Excitation contraction coupling in cardiac muscle. The figure shows the cellular events leading to contraction and relaxation in a cardiac contractile cell.

The Ca^{2+} ions bind to troponin and initiate the cycle of cross-bridge formation and detachment. The resulting mechanism of sliding filament movement is identical to that in skeletal muscle.

Like in skeletal muscle, Ca^{2+} is transported back into the SR with the help of a Ca^{2+}-ATPase. However, in cardiac muscle the Ca^{2+} originating from the extracellular space has to be removed from the cell. Each Ca^{2+} ion transferred out of the cell is transported against its electrochemical gradient in exchange for 3 Na^+ entering the cell down their electrochemical gradient. The transport is via the *Na^+- Ca^{2+} exchanger* (NCX). Sodium that enters the cell during this transfer is removed by the Na^+-K^+-ATPase (Fig. 1.9) (Silverthorn, 2008). Due to the falling $[Ca^{2+}]_i$ the Ca^{2+} ions will dissolve from the troponin C and the cross-bridge cycling will cease allowing relaxation of the cells.

In case of recordings of the contractile activity of the whole heart by intraventricular pressure catheter the time dependent pressure variations are used as contractility index, i.e. the peak of the first temporal derivative of the increasing pressure, dP/dt_{max}, is a well accepted measure of cardiac contractility (Fig. 1.10). The tangents in Fig. 1.10 visualize the differences in dP/dt_{max}

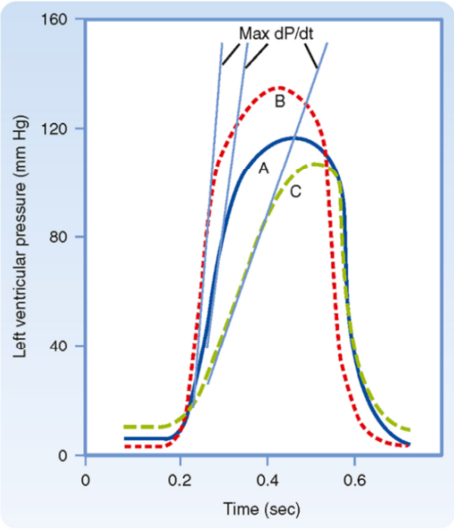

Figure 1.10 The ventricular pressure curves. The slope of the ascending limb is maximal during the isovolumic phase of systole Left ventricular pressure curves with tangents drawn to the steepest portions of the ascending limbs to indicate maximal dP/dt values. A, control; B, hyperdynamic heart induced by administration of norepinephrine; C, hypodynamic heart, as in cardiac failure. (Berne & Levy, 2009)

in a control (A), in hyperdynamic (B) and a hypodynamic (C) heart. The hyperdynamic heart displays a decreased EDP, a steep pressure rise, a high peak (systolic) pressure and a fast pressure fall. In the contrast, the hypodynamic heart has an elevated EDP, a low dP/dt_{max} as well as a delayed and reduced peak pressure (Berne & Levy, 2008).

1.2 Cardiac remodeling and hypertrophy

The heart has to adapt to long lasting changes in pre- or afterload or to damages, which occur after myocardial infarction (MI), by structural changes of the cardiac tissue. This adaptation process is called "remodeling" (Cohn, 2000). A specific form of remodeling is the development of cardiac hypertrophy, which has been mentioned above in the chapter about XIRP. As the investigation of Xin repeat proteins is in the focus of this study, the induction of cardiac remodeling may be an important help to unravel the role of XIRP in the cardiac tissue. Therefore the process of remodeling specifically the development cardiac hypertrophy will be explained in detail in the following chapters.

1.2.1 Adaptive or maladaptive remodeling

The term "remodeling" usually describes processes that lead to variations in size and shape of the left ventricle, but sometimes it also used for the description of comparable conversions in the other cardiac chambers. At the point when the left ventricle is damaged for example by MI, heart attack or by cardiomyopathy changes often occur in the size and shape of the ventricle. Often ventricle becomes enlarged, its general shape is transformed from an elliptical to more spherical pattern, and the integrity of the muscular wall changed either it becomes thicker or thinner. The ventricular remodeling especially the initial remodeling that for instance occurs immediately after a heart attack can help the ventricle to compensate for the damage that has occurred, and may help the heart to continue pumping sufficiently. But if this initial remodeling is reduced after the first conversion phase, or worse, if the remodeling process continues, the changes in the ventricle are not any longer beneficial. They will

hamper cardiac function and finally induce its deterioration and transition to heart failure (HF). Furthermore, arrhythmias and ischemic heart disease may develop which increase the risk of sudden death (Cohn et al., 2000).

In this context it is of interest that the application of inotropic drugs which help the diseased heart to contract more powerful, do not help to cure HF. Even more, despite their benefits on cardiac contractility inotropic drugs have been shown to accelerate death. In contrast, Angiotensin converting enzyme (ACE) inhibitors and β-blockers do significantly improve not only the symptoms but also the survival of patients with HF. These therapies also limit remodeling, and where remodeling has already occurred they can correct the size and shape of the damaged left ventricle. This ability of reverse remodeling is now thought to be extremely important in the therapy of heart failure to reduce symptoms and prolong survival (Cohn et al., 2000). Taken together, remodeling may be classified as adaptive or maladaptive depending on the time course and the degree of conversions in the myocardial tissue (Cohn et al., 2000; Dorn et al., 2003; Opie et al., 2006).

1.2.2 Development of cardiac hypertrophy

The following chapters will concentrate on the development of left ventricular cardiac hypertrophy as other types of remodeling are not relevant for this study. Development of cardiac hypertrophy is an adaptation of the heart to elevated work-load and is thus a very frequent type of cardiac remodeling. Development of cardiac hypertrophy can be induced by physiological as well as by pathological demands to the heart.

Cardiac hypertrophy can be provoked by exercise or pregnancy in healthy individuals and is then characterized as “physiological”. In “physiological” hypertrophy the cardiomyocytes grow in length and diameter. This leads to an enlargement of the wall diameter as well as the volume of the ventricle.

Fibrosis is not induced, but the vascular and capillary networks are in enlarged in proportion to the higher demands (Fig. 1.11). Physiological hypertrophy is often found in athletes after

intensive aerobic training as common in bicycle racing or rowing. This hypertrophy stays in the adaptive state for long time and can be reduced in case of a lowered work-load (Olson, 2004).

In contrast, hypertrophy that depends on pressure or volume overload is named "pathological". Hypertension and aortic stenosis represent two different types of chronic pressure overload, both of which lead to development of left ventricular hypertrophy (LVH) (Gerdts, 2008). Pathological cardiac hypertrophy is associated with ventricular remodeling through alterations in the extracellular matrix that eventually impact cardiac function and energy use, and cause increased rates of myocyte cell death by apoptotic and necrotic mechanisms. Pathological cardiac hypertrophy can produce concentric hypertrophy in which the ventricular wall and septum thicken with a net decrease in ventricular chamber

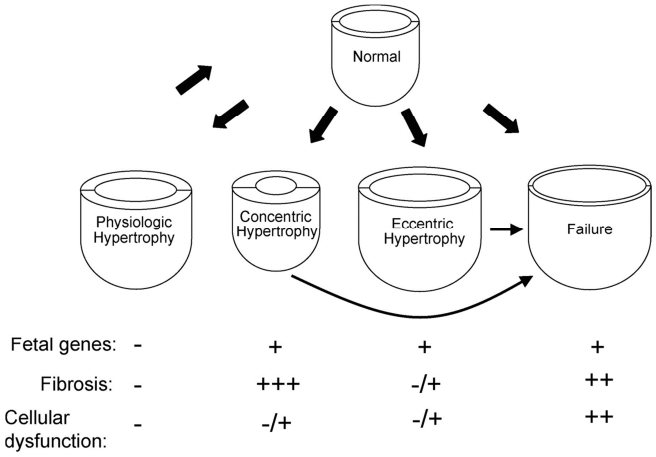

Figure 1.11 Classification of ventricular remodeling patterns

Physiological hypertrophy is characterized by a growth of the chamber lumen and an adequate wall the thickness, neither fetal genes are re-expressed nor is fibrosis induced. Pressure overload is usually compensated by concentric hypertrophy, often accompanied by fibrosis. Volume overload typically results in eccentric hypertrophy which is associated with mild or no fibrosis. Except for physiological hypertrophy, all other types of hypertrophic remodeling can progress to failure and dilation with dysfunctional myocytes (Figure slightly modified after Kehat, 2010: p. 16)

dimensions (Fig. 1.11). This remodeling is associated with a greater increase in cardiac myocyte width than length. Concentric remodeling is associated with incomplete LV

relaxation and increased filling pressures, i.e. increased left ventricular end diastolic pressure (LVEDP).

Development of “pathological” hypertrophy can also form the phenotype of eccentric and dilatory hypertrophy. This usually results from a volume overload. Eccentric hypertrophy is based on elongation of cardiomyocytes. The signaling pathways leading to pure growth in length or to growth in thickness of the cardiomyocytes are not entirely understood. In spite of the name “pathological” this type of hypertrophy also starts with an adaptive phase to compensate increased wall stress and maintain output. This first phase is also named compensated hypertrophy. Eccentric remodeling helps to adjust the large increase in EDV (volume-overload) and maintain left ventricular ejection fraction (LVEF). The cellular alterations decrease wall thickness and dilate the heart, and eventually impair systolic function and reduce LVEF.

Both described pathological forms of hypertrophy can proceed to a decompensated state, characterized by a dilated left ventricle, with relatively thin walls and an enlarged volume. This leads to declining ventricular function and may finally end in HF (Kehat, 2010) (Fig. 1.11). Especially hypertension, which depends on an increase in the total peripheral resistance (TPR) of the vascular system, causes the development of concentric hypertrophy. Catecholamines as well as the renin angiotensin aldosterone (RAAS) system are well known as potent vasoconstrictors. Thus these hormones are often indirectly involved in the development LVH. It has been reported that catecholamines as well as angiotensin 2 (Ang II) also exert direct trophic effects on the heart, i.e. they directly induce cardiac hypertrophy besides their influence via the increased blood pressure.

For the investigation of the development of pressure induced cardiac hypertrophy the model of transverse aortic constriction (TAC) has been introduced by Rockman et al. (1991). It is the commonly used model of pressure-overload in animals performed by constriction the aortic lumen between the brachiocephalic arteries and the left carotid artery. Although TAC initially

leads to compensatory hypertrophy of the heart, over time the response to the chronic hemodynamic overload becomes maladaptive resulting in cardiac dilatation and HF.

1.2.3 Contribution of cardiomyocytes to hypertrophy

Cardiac hypertrophy is based on changes in the cardiomyocytes as well as in the fibroblasts and the extracellular matrix. As cardiomyocytes are not any longer able to proliferate and stem cells like the satellite cells in skeletal muscle have not been proven, growth of the individual cardiomyocytes is necessary for any cardiac hypertrophy. The signaling pathways leading to physiological or pathological cardiac hypertrophy have been reported to be different. The differences in signaling between development of physiological and pathological cardiac hypertrophy have been reviewed extensively in Bernardo et al. (2010) and will be introduced here only briefly.

Development physiological cardiac hypertrophy seems to depend mainly on insulin-like growth factor 1 (IGF1), which is produced in the liver due to increased somatotropin levels in the blood. Cardiomyocytes carry IGF1-receptors on their surface which signals via phosphoinositide 3-kinase (PI3K), Akt (or Protein kinase B (PKB)) and mammalian target of rapamycin (mTOR). Interestingly, IGF1 is also expressed by the cardiomyocytes themselves. Under experimental conditions, IGF1 led to cardiac growth resembling physiological hypertrophy and aerobic exercise induced increased IGF1 levels in the heart. Cardiomyocytes grow in length but also in diameter by increasing the number of myofibrils per cell and by integrating additional sarcomers into the myofibrils. Fibrosis is not induced in this process.

Onset of pathological pathological hypertrophy seems to be started by different processes. The increased workload of the heart in both, pressure or volume-overload, induces sustained wall stress. This may be transferred by different elements of the cytoskeleton to mechano-sensitive ion channels (reviewed in Calaghan et al., 2004) as well as to protein kinases, which start specific signaling cascades (reviewed in Lyon et al., 2015). Mechanotransduction may start at intracellular structures like the Z-lines or at the ICDs, which transmit mechanical force

between neighboring cardiomyocytes, and also contact structures between the ECM and the cells like focal adhesion plaques or dystroglycan complexes.

Very interesting hypotheses about mechanotransduction have been proposed by Lyon et al. (2015) and incorporated in Fig. 1.6. Four-and-a half LIM domain protein1 (FHL1) and 2 (FHL2) is bound to titin near the Z-line (Review: Krüger and Linke, 2009). Titin is involved in the elasticity of the cardiomyocyte and thus is differentially stretched depending on the mechanical load of the cardiomyocyte. The stretch differences may enable FHL1 to activate extracellular-regulated kinase-2 (ERK-2), mitogen activated protein kinase kinase-2 (MEK2), and/or rapid accelerated fibrosarcoma-1 (RAF1). Interestingly, mice deficient of FHL1 have been shown to develop a blunted hypertrophic response to TAC (Review: Chu and Chen, 2011). The role of FHL2 in the development of cardiac hypertrophy is still under discussion. Recently our group found that FHL2 deficiency protects against TAC dependent cardiac hypertrophy in an indirect way (Goltz et al., submitted).Comparable protein-complexes are also involved in transducing the pro-hypertrophic effects of Ang II, norepinephrine (NE) and endothelin1 (ET-1) (c.f. review Bernardo et al., 2010). These pathways induce re-expression of fetal genes leading the typical alterations in the proteins involved in excitation-contraction coupling.

Another aspect of specific interest for this study is reviewed in Lyon et al. (2015). N-cadherin (N-CAD) is part of the fascia adherens and allows to transmit mechanical forces between adjacent myofibrils (Fig. 1.6, 1.7). These adherens structures have to be rebuilt due to increased wall stress under pressure or volume-overload. Here also XIRPs have been located. Chopra et al. (2011) found that N-CAD containing adherence structures were able to induce cardiomyocyte remodeling in response mechanical stress.

Concentric remodeling of the heart is associated with duplication of sarcomeres in parallel and cardiomyocyte thickening, and is the direct result of sustained pressure increase. Eccentric remodeling of the heart is associated with duplication of sarcomeres in arrangement and lengthening of cardiomyocytes in order to increase the chamber volume. Furthermore, the

density of desmin filaments increases during remodeling to compensate pressure overload (Wang et al. 1999). In agreement with this finding desmin-deficient mice develop cardiac hypertrophy (Milner et al., 1999). The degree of desmin remodeling has even been demonstrated to be a very precise predictor for the transition from compensated to decompensated hypertrophy (Monreal et al. 2008). Pressure induced cardiac hypertrophy also induces the amount cytoskeletal microtubules (Tagawa et al., 1996). Also the stiffness of titin changes during development of cardiac hypertrophy due to an isoform switch (Hutchinson et al., 2015). This switch also varies the signaling characteristics of this molecule which have been discussed above. Also XIRP proteins have been shown to be involved in the development of cardiac hypertrophy as explained in chapter 1.4. Taken together, modifications of cytoskeletal proteins are both a cause and consequence of contractile dysfunction and cardiac remodeling (Sequeira et al., 2013).

1.2.4 Mechanisms of fibrosis

The organization of the ECM is very important for the arrangement cardiomyocytes within the ventricular wall and fibroblast proliferation and fibrosis play an important role during the formation of cardiac hypertrophy Therefore, the following section will introduce the mechanisms of fibrosis.

Collagen type I and type III constitute the majority of the fibrillar collagen content of the myocardium. The collagen network within the LV is highly organized. Alterations in this network influence structure and function of the LV. In response to pressure overload the collagen expression is increased. This in turn elevates stiffness of the ventricular walls and makes the LV less compliant and leads to abnormalities in diastolic function. In contrast, a degradation of collagen results in an increasing compliance and dilatation of the LV (Deschamps and Spinale, 2006).

In a healthy heart turnover of collagen is relatively low and deposition and degradation are in steady state. Under pathological conditions collagen turnover is up-regulated. Collagen

turnover depends on the balance of matrix metalloproteinases (MMPs) and the tissue inhibitors of metalloproteinases (TIMPs).

Dysregulation of this balance can be brought about by a number of factors (Siwik and Colucci, 2004). In cardiac fibroblasts, the inflammatory cytokines such as interleukin-1β (IL-1β), interleukin-6 (IL-6) and tumor necrosis factor-α (TNF-α) decrease collagen synthesis, increase MMP expression and decrease TIMP expression (Li et al., 1999; Siwik et al., 2000). Inflammatory cytokines are tightly linked to tissue stress and their production is induced following biological stimuli such as pressure overload and myocardial injury. Transforming growth factor-β (TGF-β) is an anti-inflammatory cytokine and a potent stimulator of collagen synthesis. It mediates collagen accumulation through increasing transcription, stabilizing procollagen mRNA, and decreasing collagen degradation via enhanced TIMP or reduced MMP expression. Sustained production of TGF-β underlies the development of myocardial fibrosis (Kassiri and Khokha, 2005). TGF-β is secreted in an inactive form and proteolytically activated by proteases like MMPs. Its activation is supported by tissue damage and cellular stress (Annes et al., 2003). TGF-β induces secretion of several ECM components by fibroblasts (Desmouliere et al., 1993). The ECM has a major influence on cell migration, proliferation, adhesion, and cell-to-cell signaling (Geiger et al., 2001; Weber et al., 1994). TGF-β antagonism lowers fibrosis and thereby also the symptoms of HF (Lars et al., 2013).

The development of LV dilation has been shown to be associated with discontinuity and disruption of the supporting fibrillar collagen network, abnormalities in the degree of collagen crosslinking and defects in basement membrane structure and function (Baicu et al., 2003; Candido et al., 2003; Factor, 1994; Spinale et al., 1991; Spinale et al., 1996; Weber et al., 1992).

1.3. Aim of the study

In chapter 1.1.3 the importance and the functions of the cytoskeleton of cardiomyocytes have been described. Furthermore, mutations in different proteins of the cytoskeleton have been shown to cause or to be associated with the pathogenesis of cardiomyopathies and the cardiac symptoms in several muscular dystrophies. In addition, cardiac arrhythmias have been attributed to such mutations (Fatkin et al., 2010; Ho, 2010; Marian, 2010; Modica-Napolitano and Singh, 2002; Nerbonne and Kass, 2005).

Previously, our group found that ablation of all XIRP1 isoforms (XinABC$^{-/-}$ mice) under normal conditions resulted in a milder phenotype than that observed in XinAB$^{-/-}$ mice, which still can express XinC (Otten et al., 2010). Based on this study, we hypothesized that complete XIRP1 deficiency may have more drastic consequences, if development of pathological hypertrophy is induced by TAC. During this remodeling process changes in the ICD become evident. As XIRP1 is an element of the fascia adherens (c.f. Fig. 1.7), its deficiency may leads to alterations during the remodeling of the ICDs. However, we found that the extent of cardiac hypertrophy did not differ between wild type and XinABC$^{-/-}$ TAC mice (Kebir et al., in preparation). A possible explanation could be that XIRP2 may be up-regulated in XIRP1 deficiency and thus substitute for XIRP1 in these cardiomyocytes. Thus we hypothesized that an additional knock-down of XIRP2 may help to unravel the functions of both XIRPs in the murine heart. To investigate this, XinABC$^{-/-}$ mice (Otten et al. 2010) were crossed with XIRP2 hypomorphic mice (McCalmon et al., 2010) and the resulting animals referred to in the following as XIRP1XIRP2 dko. The cardiac phenotype of the XIRP1XIRP2 dko mice was investigated under physiological conditions and after induction of cardiac hypertrophy by TAC.

2 Material and Methods

2.1 Experimental animals

To generate the mouse model, XinABC$^{-/-}$ mice (Otten et al. 2010) were crossed with XIRP2 hypomorphic mice (McCalmon et al., 2010) and the resulting animals referred to in the following as XIRP1XIRP2 dko). XIRP wild-type (XIRP WT) female, XIRP1XIRP2 dko female mice from the "Institut für Zellbiologie were used for this study. After delivery, the mice were housed individually ventilated in polycarbonate transparent pathogen-free cages (365x207x140 mm) with animal bedding (ASBE-wood GmbH, Ahrensfelde, Germany) at a room temperature of 20-22 °C, 50% humidity and 12 hours day-night cycle. The mice were given free access to standard rodent chow (ssniff Spezialdiäten GmbH, Seost, Germany) and water *ad libitum*. All mice were handled according to the principles of laboratory animal care (NIH publication no: 85-23, revised 1996) and experimental procedures followed the rules of the German Protection of Animal Acts from 18th of May, 2006; changed on 7th of August 2013 (Animal rights 18th May 2006, changed 7th August 2013)

2.2 Experimental protocols

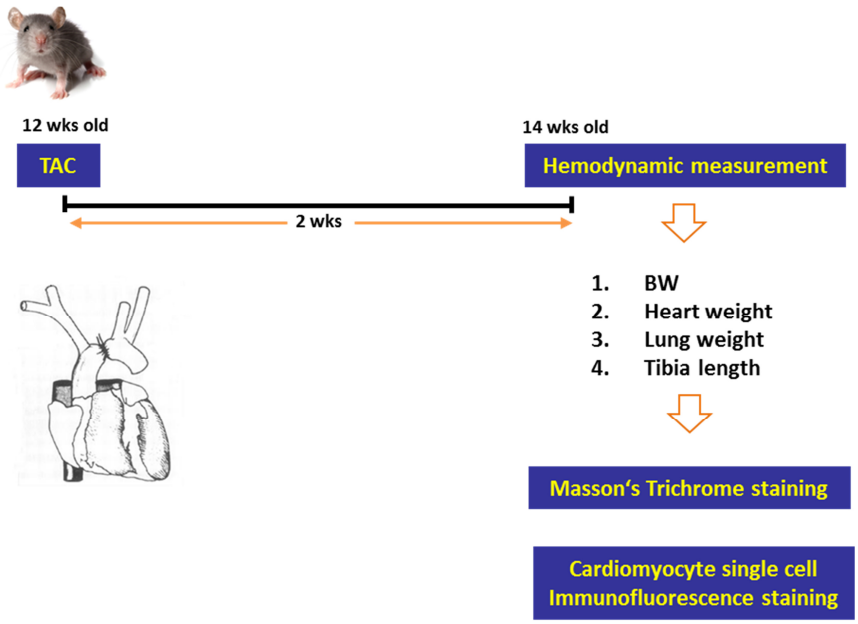

Figure 2.1 An overview of experimental protocols.

The 11-13 week-old adult mice were divided into 4 groups.

1. XIRP WT sham
2. XIRP WT TAC
3. XIRP1XIRP2 dko sham
4. XIRP1XIRP2 dko TAC

Half of them underwent to the Transverse aortic constriction (TAC) operation whereas the sham groups were operated without aortic ligation. The purpose of TAC is to reduce the diameter of the aorta to one third (Fig. 2.2). TAC is a model of pressure overload induced cardiac hypertrophy and heart failure (Rockman et al., 1991). The mice were allowed to develop hypertrophy for 14 days.

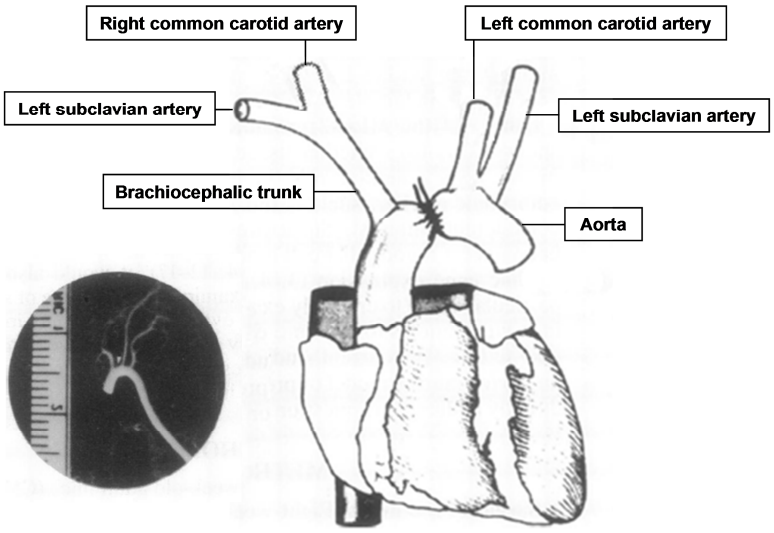

Figure 2.2 Transverse aortic constriction. To induce pressure overload, the aortic is tied between the brachiocephalic trunk and the left common carotid artery (Slightly modified from Rockman et al., 1991).

(1) TAC surgery in mice causes chronic left ventricular (LV) pressure overload, progressive left ventricular hypertrophy (LVH), and subsequent cardiac failure, providing an experimental model for human cardiac response to systemic hypertension. Since its development, the TAC model has been used extensively on genetically engineered mice to investigate the role of specific genes

during the development of LVH and cardiac failure in *vivo* (Barrick et al., 2006). The murine TAC model (Rockman et al., 1991) was proven to be a valuable tool to mimic human cardiovascular diseases and elucidate fundamental signaling processes involved in the cardiac hypertrophic response and heart failure development. When compared to other experimental models of heart failure, such as complete occlusion of the left anterior descending (LAD) coronary artery, TAC provides a more reproducible model of cardiac hypertrophy and a more gradual time course in the development of heart failure (Angela et al., 2010). To standardize the degree of aortic constriction a 27-gauge needle was used as a placeholder to pass a suture underneath the aortic arch (Baumgarten et al., 2002). In this study mice were allowed to develop hypertrophy for 14 days after the initial surgery (Harada et al., 1998) (see chapter 2.3.1).

(2) For the hemodynamic measurement (an invasive pressure measurement), the hemodynamic parameters heart rate (HR), systolic arterial pressure (SAP), diastolic arterial pressure (DAP), left ventricular systolic pressure (LVSP), left ventricular end-diastolic pressure (LVEDP), were recorded using an Ultra-Miniature Pressure Catheter (Scisense advancing micro-sensor technology™, USA/CAN). All mice independent of TAC or sham operation were monitored 14 days later. Following induction of anesthesia, the ultra-miniature pressure catheter was retrogradely inserted through the right common carotid artery into the LV. After stabilization, hemodynamic parameters were recorded while anesthesia was maintained at 1 vol % isoflurane (see chapter 2.3.2). Euthanasia was performed by deep anesthesia (4% isoflurane) then hearts and lungs were excised immediately. Both were weighted, the heart was prepared further by cutting off both atria and then dividing LV and RV which were weighted separately. Finally, all organs were snap frozen in liquid nitrogen and stored at −80◦C for molecular analysis. Some of the hearts after excision were fixed by 4% Paraformaldehyde (PFA) (4 g of PFA powder and 100 ml of PBS (0.137 M NaCl, 0.05 M NaH_2PO_4, pH 7.4)) for histological studies.

(3) Besides the morphometric parameters, body weight (BW), heart weight (HW), left ventricular weight (LVW), right ventricular weight (RVW), lung weight (LW), which were weighted, tibia

length (TL) was measured by a caliper to calculate individual BW/TL, HW/TL, LVW/TL, RVW/TL, LW/TL ratios (see chapter 2.4.2).

(4) For histology, hearts were excised after blood pressure and Electrocardiogram (ECG) recordings and perfused in a Langendorff apparatus with Ca^{2+}-free Tyrode solution (in mM: 135 NaCl, 4 KCl, 1 $MgCl_2$, 2 HEPES, and 2.6 EGTA; pH 7.4) for 5 min then perfused with 4% PFA 8-10 min, fixation and embedding were performed consecutively. Paraffin embedded hearts were cut into 5 µm sections and submitted to Masson trichrome staining. Interstitial fibrosis and LV diameter were quantified using Image J analysis software (Version 1.47; Wayne Rasband, National Institutes of Health, USA) (see chapter 2.4.1).

(5) In immunohistochemistry staining of isolated cardiomyocytes, hearts were excised and isolated ventricular cardiomyocytes were prepared by perfusing excised hearts in a Langendorff apparatus. The isolated cardiomyocytes which were attached to laminin-coated microscope slides were then fixed with cold (–20°C) methanol (5 min) and acetone (0.5 min). Cell width and length of 56-100 cells of each animal were measured using an ocular micrometer. Cardiomyocytes were stained with antibodies to localize intercalated disk (ID) proteins using standard procedures. The localization of IDs was evaluated statistically. The following antibodies were used for primary antibody: anti-FLNC RR90 antibody (Van der ven et al., 2000), specific for Filamin A and C d1-2, respectively; T12 antibody (Fürst et al., 1988) specific for Titin Z-band epitope; CX43 antibody (AG Willecke) specific for gap junction; CDH antibody (Sigma, Munich) specific for cadherin; myosin heavy chain 20 antibody (Mf20) (Developmental studies hybridoma bank, Iowa, USA) 34C-s antibody (Developmental studies hybridoma bank, Iowa) specific for Rryanodine receptors; FlnC antibody (AG Fürst) specific for filaminC d16-20; BB78.8 antibody (Vinkemeier et al., 1993) specific for Myomesin, M-Band. For secondary antibody, the following antibodies were used; Goat anti mouse IgG1 Alexa 594 (SouthernBiotech, Alabama, USA); Goat anti mouse IgA FITC (Invitrogen, Darmstadt); Goat anti rabbit-Alexa 647 (Jackson, Darmstadt); Goat anti mouse IgG1 Cy2 (Invitrogen); Goat anti mouse IgG2b-Alexa 594 (Molecular probes); Goat anti rabbit Alexa 647; Goat anti mouse IgG1 Cy2; Goat anti mouse IgG2A-Alexa 594; Goat anti rabbit-

Alexa 647. Dapi (Invitrogen) blue fluorescent nuclear stain was used to visualize nuclei. The cardiomyocyte slides were examined and pictures were acquired using an inverted microscope equipped with fluorescence optics (Nikon Eclipse TE-2000-E) and a cooled CCD camera (DVC company, Texas, USA) and Image Pro Plus software (Media Cybernetics, Surrey, Canada) (see chapter 2.4.3). Cell isolations and fixations were performed by the author. Antibody binding and immunofluorescence microscopy was performed by J. Schuld Institute of Cell Biology.

2.3 In *vivo* experiments

2.3.1 Transverse aortic constriction

TAC was performed to induce increased afterload in the heart which leads to heart failure. The method was adopted by Rockman et al (1991) and slightly modified. TAC was performed in 11-13 week-old adult female XIRP1XIRP2 WT, XIRP1XIRP2 dko mice.

2.3.1.1 The operating field

The operating field was disinfected with 70% ethanol. The operation stage (Fig. 2.3 a) was connected to the water bath (Fig. 2.3 b) to let the water circulate under the animal to maintain the temperature at 37 °C ± 1 °C. It is very important to maintain the normal body temperature during surgery to avoid a rapid decrease in heart rate. The surgical tools were sterilized by the autoclave before surgery. The surgical instruments used were: curved scissor, mosquito clamp, fine curve forceps x 2, cubic curve forceps x 2, chest retractor x 2, and needle holder (Fig. 2.4).

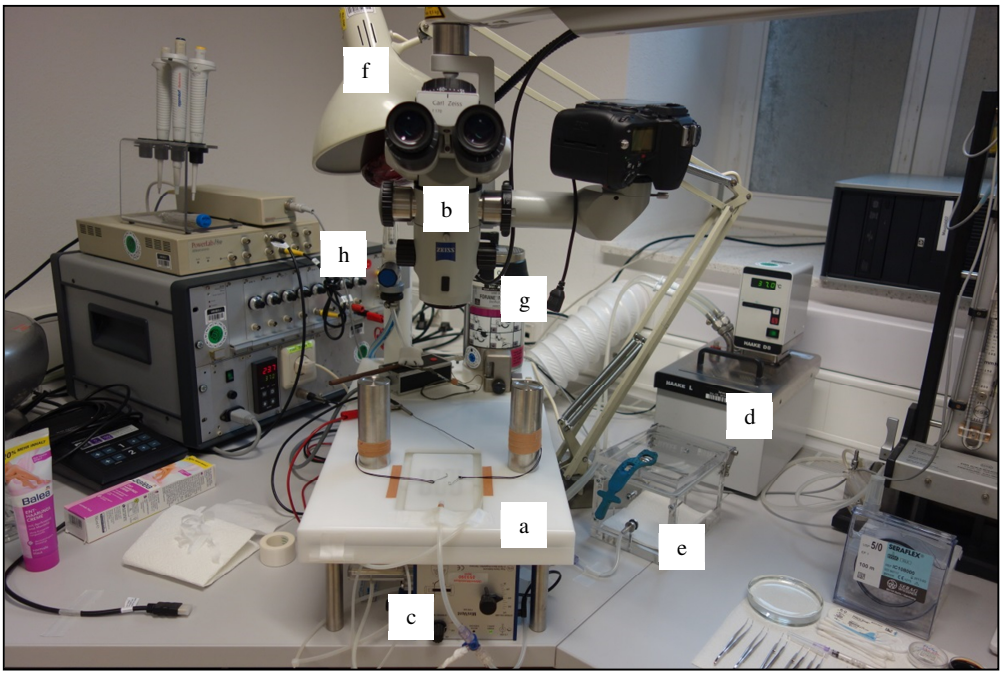

Figure 2.3 The setup for small animal surgeries. (**a**) The operation stage, (**b**) the stereo microscope with electrical focus and camera, (**c**) the mini ventilator, (**d**) the water bath, (**e**) the anesthesia induction chamber, (**f**) the infrared lamp, (**g**) the isoflurane vaporizer, (**h**) the oxygen flow meter.

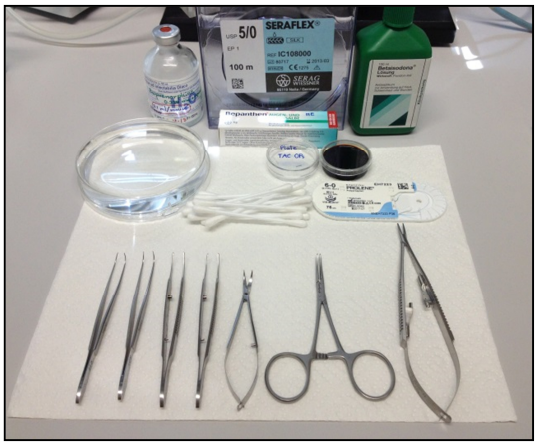

Figure 2.4 The surgical instruments. Include; fine curve forceps x 2, cubic curve forceps x 2, scissor, mosquito clamp, and needle holder (from left to right).

2.3.1.2 Endotracheal intubation

The mouse was weighed on a digital scale (Kern EMB 500-1, Precision balance, KERN & SOHN, Balingen) then was anesthetized in a transparent induction chamber (Fig. 2.3 e) which was pre-filled with 2% isoflurane mixed with 0.5 - 1.0 l/min 100% O_2 for anesthesia induction. When muscle relaxation was obvious, the mouse was removed from the transparent induction chamber placed in a supine position with paws and tail taped to the heated operation stage. Anesthesia was maintained by continuous inhalation of 2% isoflurane. The eyes of the mouse were painted by eye ointment (Bepanthen®, Bayer vital GmbH, Leverkusen, Germany) to prevent air irritation to the eyes. The mouse's nose was put into the wide side of a pipette tip that was connected to the plastic tube, which was ended in a Y-branch. By the Y-branch the 2% isoflurane flow from the isoflurane vaporizer (Fig 2.3 g) was combined with a flow of 100% O_2 (0.5% - 1.0% l/min) from an O_2 flow meter (Fig 2.3 h) to provide a continuous supply of 2% isoflurane. A temperature probe that was connected to a temperature controller was inserted into the mouse rectum to measure the body temperature. If the mouse body temperature was lower than 37 °C an infrared lamp was switched on until 37 °C was restored. A thread was placed around the animal's front upper teeth to extend the neck. The tongue was carefully pulled out using a cubic curved forceps. A hair removing cream was used to remove the fur from the neckline to mid chest level (Fig. 2.5 a and b). A middle skin longitudinal incision was made on the neck and extended down to the xiphoid by using a curve scissor. The submandibular salivary glands and sternothyroid muscles were separated respectively, and then the trachea and larynx were exposed. The cubic curve forceps was held in the left hand to fix the larynx and the endotracheal tube was inserted advanced towards to the larynx, and then pushed into the trachea by the right hand at the same time. Finally the mouse was attached to a Harvard volume-cycled rodent ventilator (MiniVent 845, Hugo Sachs Elektronik, March-Hugstetten, Germany) (Fig 2.3 c) cycling at 110 breaths/minute and a tidal volume of 0.2 ml. During the surgical procedure, anesthesia was maintained at 2.5% isoflurane with 0.5 - 1.0 l/min 100% O_2.for anesthesia. The mouse was

injected with buprenorphine (0.1 mg/kg) (Buprenorphine hydrochloride 0.3 mg in 1 ml, Reckitt Benckiser Pharmaceuticals Inc, Richmond) intraperitoneally.

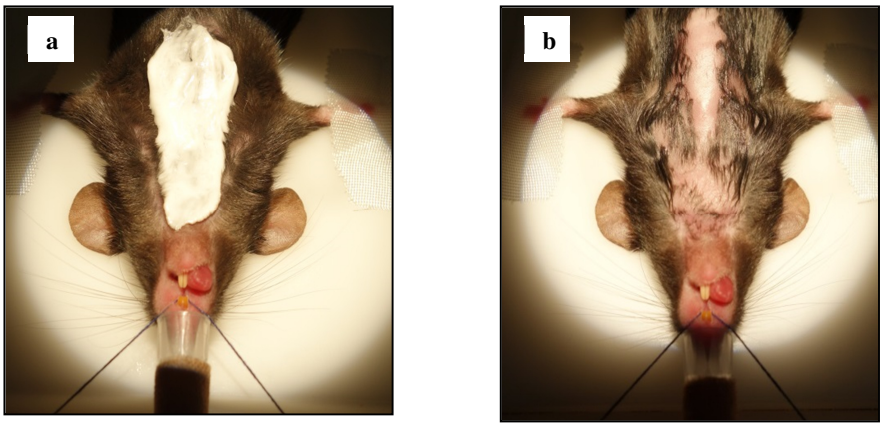

Figure 2.5 Hair removing. (**a**) Before use hair removing cream and (**b**).after used hair removing cream.

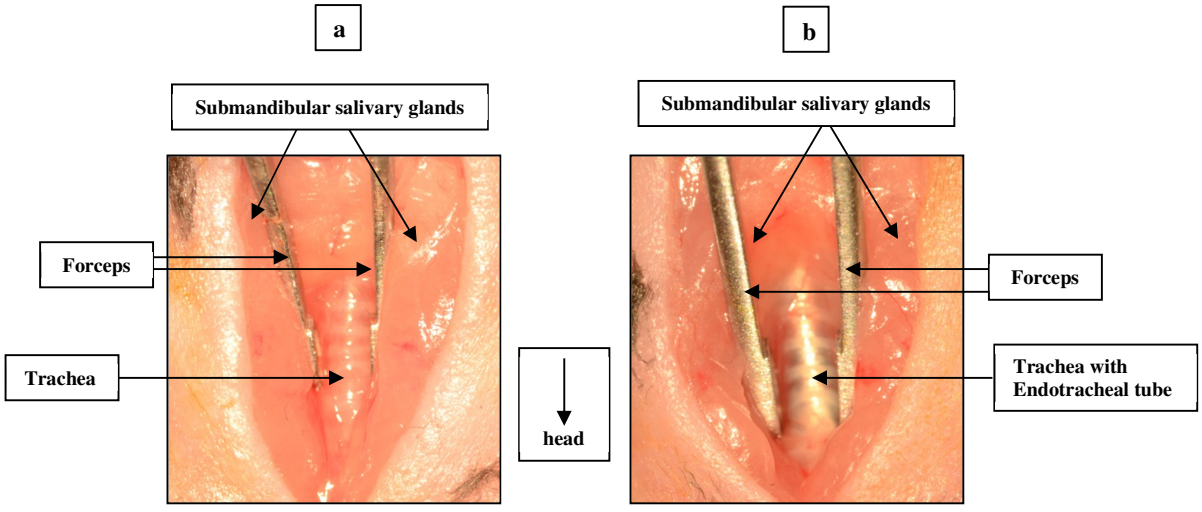

Figure 2.6 Endotracheal intubation. The inserted cannula can be confirmed with direct vision through the exposed trachea. (**a**) The arrows indicate the direction of inserted cannula, (**b**) exposed trachea before intubation and after intubation

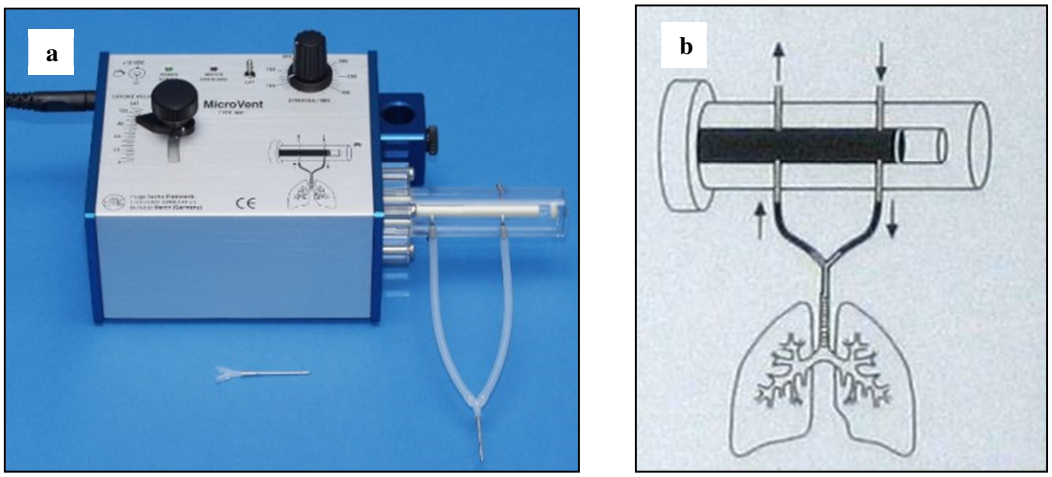

Figure 2.7 Mini-ventilator and the endotracheal tube connection (**a** and **b**)
Available from http://www.hugo-sachs.de [7 January 2015].

2.3.1.3 Ligation of the transverse aorta

Under a surgical microscope, the skin was disinfected with povidone-iodine solution (Betaisodona Lösung®, Mundiphama GmbH, D-limburg) and opened consecutively. The left pectoralis major and minor muscle were bluntly dissociated until the rib was exposed (Fig. 2.8 a). A parasternal incision was made to open the chest by cutting the left second and third ribs with the curved scissor. The chest retractors were used to open the thorax and to stop bleeding at the same time (Fig. 2.8 b). Fine curved forceps were used to gently separate the thymus and fat tissue from the aortic arch. The aortic arch was visualized (Fig. 2.8 c). The 5–0 silk suture was passed underneath the aortic arch between the brachiocephalic trunk and left common carotid artery (Fig. 2.8 d). Two loose knots were tied around the transverse aorta and a small piece of a 27½ gauge blunt needle was placed parallel aortic arch between the aorta and a first knot (Fig. 2.8 e). The first knot was quickly tied against the needle, followed by a second one, then the needle was promptly removed (Fig. 2.8 f). In sham control mice, the entire procedure was identical except for the ligation of the aorta. The chest retractors were removed and the thorax was closed then the skin was sutured with a continuous suture pattern by using a 6.0 prolene suture (Nahtmaterial 6-0

Prolene®, Ethicon GmbH, D-Norderstedt) (Fig. 2.8 h). Finally, the wound was disinfected with povidone-iodine solution.

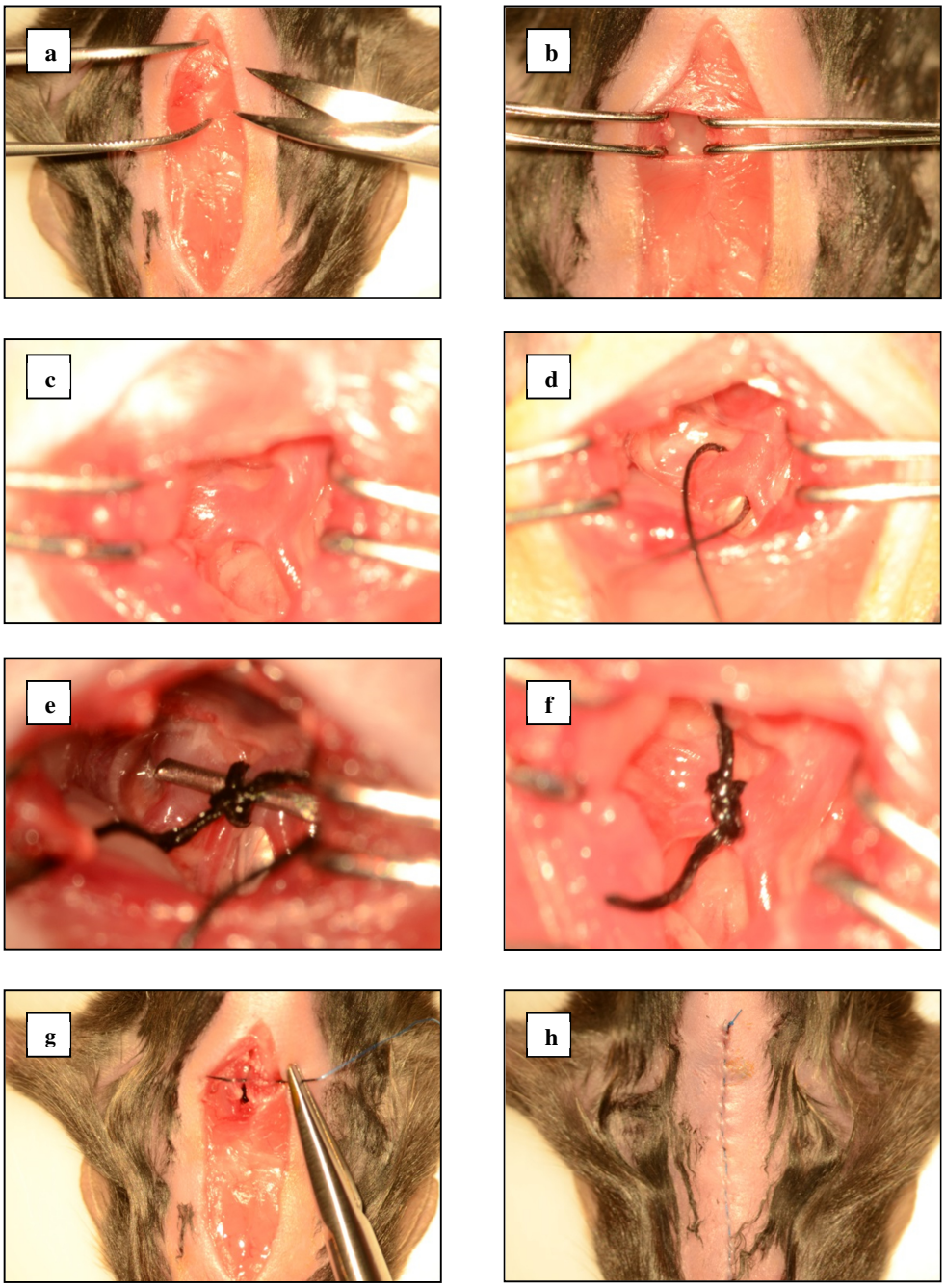

Figure 2.8 The transverse aortic constriction. (**a**) The left pectoralis major and minor muscle dissection, (**b**) the thorax cavity was opened by the retractors, (**c**) the aortic arch, (**d**) the thread was passed underneath the aortic arch between the brachiocephalic arteries and left common carotid arteries, (**e**) the small piece of a 27½ gauge blunt needle was placed parallel aortic arch between the aortic artery and the first knot, (**f**) the aortic ligation, (**g**) the thorax was closed, (**h**) the skin suture.

2.3.1.4 Post-operative recovery

Anesthesia was gradually decreased from 2.5% to 1% and then turned off. The outflow of the ventilator was pinched off for 2 seconds to re-inflate the lungs. Then endotracheal tube was removed when signs of spontaneous breathing occurred. The mouse was moved to the prone position and allowed to recover under the infrared heating lamp. After the mouse had woken up, it was placed in a cage under infrared light and observed for 20 minute. Finally, the mouse was transferred back to the housing cage.

2.3.2 Hemodynamic measurement

Two weeks after TAC, the mouse was re-anesthetized with isoflurane as described in 2.3.2.3 to determine the degree of pressure overload induced by ligation of the transverse aorta. This evaluation was based on invasive blood pressure recording.

2.3.2.1 The catheter preparation

2.3.2.1.1 The equipments

1. Ultra-miniature pressure catheter (Transonic System Inc, NW Maastricht, Netherlands) (Fig. 2.9 a)
2. FP095B-Dual channel pressure control unit version 095B-01 (Transonic System Inc, NW Maastricht, Netherlands) (Fig. 2.9 b and c)
3. Powerlab/8SP (ADInstruments Ltd, Spechbach, Germany) (Fig. 2.9 d)
4. Computer (Hewlett-Packard GmbH, Böblingen, Germany) running LabChart v6.0 for Windows (ADInstruments Ltd, Spechbach, Germany)

2.3.2.1.2 Calibration method

An ultra-miniature pressure catheter was plugged into the FP095B-Dual channel pressure control unit that was connected to the Powerlab /8SP data acquisition system and the computer consecutively. The complete measuring system was turned on. The labChart program was run at a

sampling rater of 1 kHz. Then the purple *0 mmHg* button was pressed in order to enable the LabChart program to digitize the voltage referring to *0 mmHg*. In the next step the *100 mmHg* button was pressed to transfer the voltage for this pressure into the LabChart program. In the LabChart program we have to choose set up 2 point calibration and unit conversion. Finally, both voltages are now combined with the referring pressures (Fig. 2.11).

Figure 2.9 The calibration equipment. (**a**) The pressure catheter, (**b**) the dual pressure control box, (**c and d**) the front and back panel of the dual pressure control box. Scisense System Inc., (2010). *Pressure measurement system use and care*. Ontario, Canada.

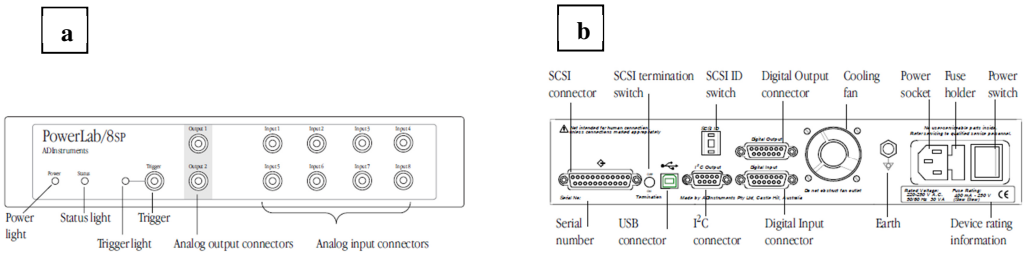

Figure 2.10 The PowerLab/8SP. The front and the back panel of the PowerLab/8SP (**a** and **b**) ADInstruments Pty Ltd, (2001). *PowerLab SP owner's guide*. NSW, Australia.

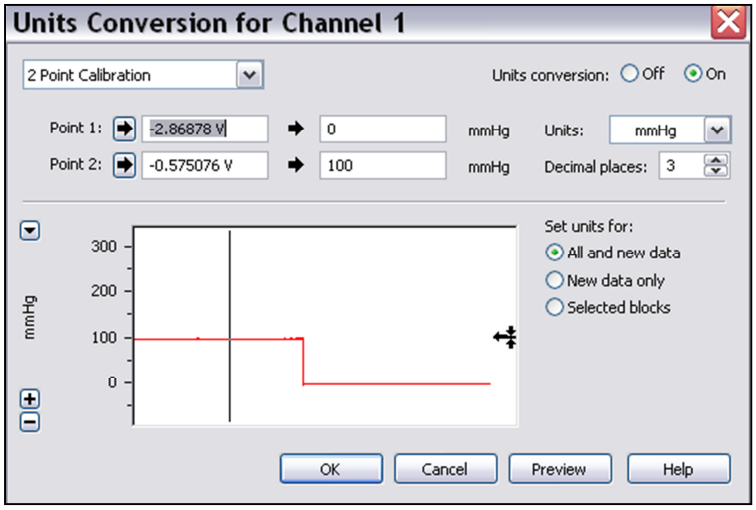

Figure 2.11 Screen shot of units conversion.

2.3.2.2 Running the experiment

The data acquisition system has to be calibrated as described in the previous section. The sensing tip of the pressure catheter was pre-soaked in a saline solution for at least 20 minutes to allow the sensor to hydrate properly before use and to minimize baseline pressure drift during the experiment. After removing the catheter from the saline solution, the pressure signal (s) had to be set to zero by using the *Coarse* and *Fine* button controls on the dual channel pressure control unit before catheter insertion. Then the *cath on* button on the pressure box was pressed on and the catheter was ready to be advanced into the blood vessel.

2.3.2.3 Preparing the Mouse

The mouse was anesthetized in the transparent induction chamber with 2% isoflurane mixed with 0.5 - 1.0 l/min 100% O_2. The mouse body temperature was maintained at 37°C by the described feedback loop between rectal probe and infrared lamp. The skin above the neck on the right side was cut and the cube forceps were used to separate left and right submandibular salivary glands. Then a blunt cotton bud was used to gently access the area right to the trachea to visualize the right common carotid artery. Three 6-0 prolene sutures were passed underneath the right common

carotid artery by a fine forceps and arranged to be proximal middle and distal. The proximal suture was placed as proximal as possible and tied. The middle suture was done up in a loose knot and the distal suture was fixed by a small curve clamp (Fig. 2.12 a). A small incision was cut into the artery by the fine vannas scissors just above the proximal knot through which the pressure catheter was inserted (Fig. 2.12 b). The middle knot was fastened and the small curve clamp that fixed the distal suture was loosed then the pressure catheter was advanced. Before the recording started the isoflurane concentration was decreased to 1% keep the HR above 500 beat/min (bpm) (Fig. 2.12 c). After 5-10 minutes, when the blood pressure was stabilized, and the pressures catheter was advanced into the LV. To conform the correct position of the pressure catheter tip in the LV, the dramatically decreased DAP and the changed in the waveform of ventricular pressure recording were considered (Fig. 2.14 a). The LVP was recorded for approximately 10 minutes. Afterwards, the isoflurane concentration was increased to 4 % and the whole heart and lung were explanted and weighted, LV and RV were separated and then weighed. Finally, the tibia was performed and its length was measured.

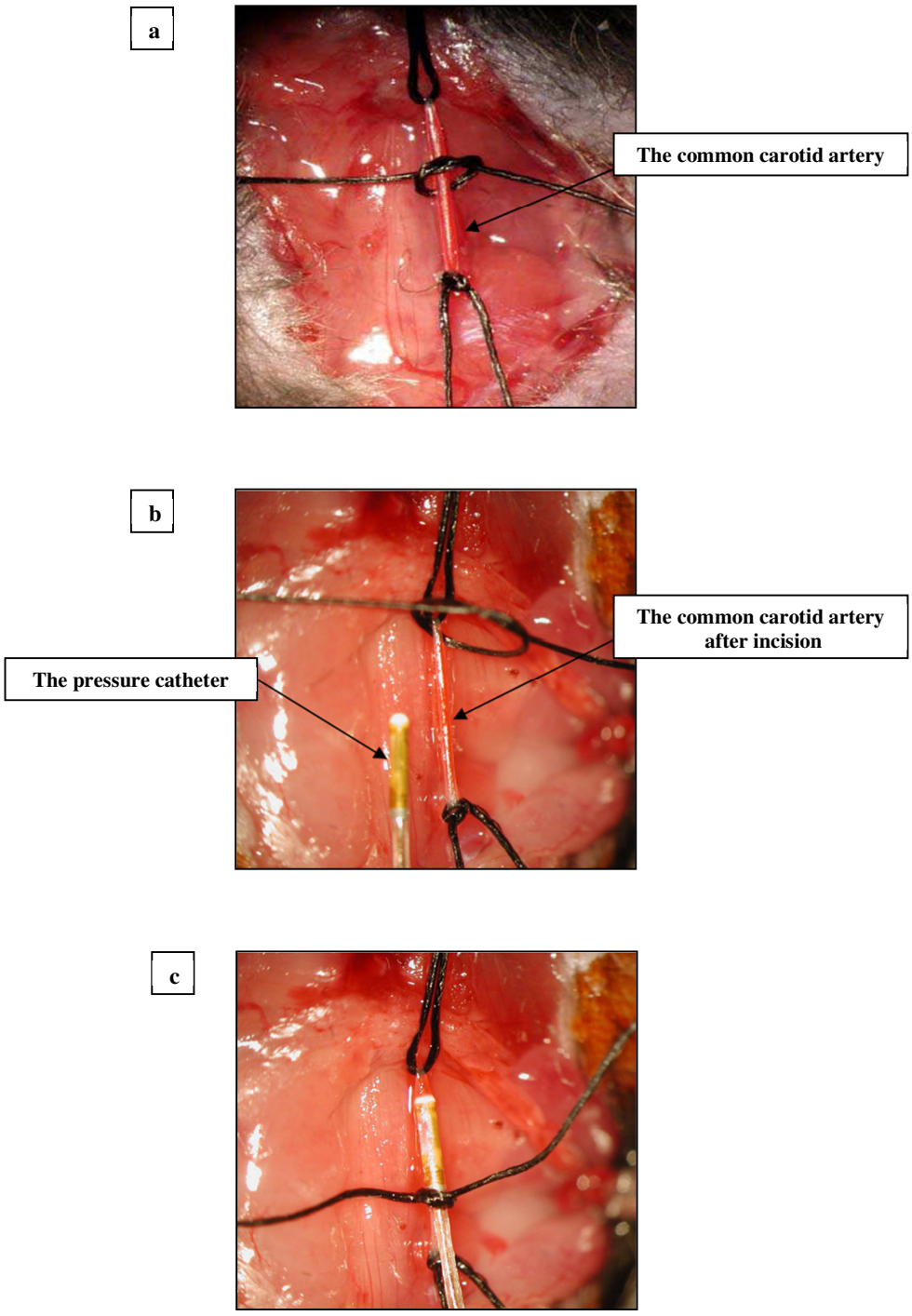

Figure 2.12 Pressure catheter insertion. (**a**) Ventral view on to the neck region of a mouse; common carotid artery after preparation and fixation with silk threads, 10x magnification (Bittig, 2005), (**b**) ventral view of the neck region of a mouse after insertion of the catheter in the carotid artery, 16-fold magnification (Vervölgyi, 2007), (**c**) ventral view of the neck region of a mouse after incision of the vessel, next to it is the pressure catheter, 10-fold magnification (Vervölgyi, 2007).

2.3.3 Hemodynamic data analysis

The data of the hemodynamic measurements were analyzed offline using the Chart 6 for Windows ® program (ADInstruments). For analysis and display of display of cycle-by-cycle parameters from arterial or ventricular pressure recordings the Blood Pressure Module was applied for analysis of arterial and ventricular pressure recordings and to calculate a variety of parameters (Fig. 2.13)

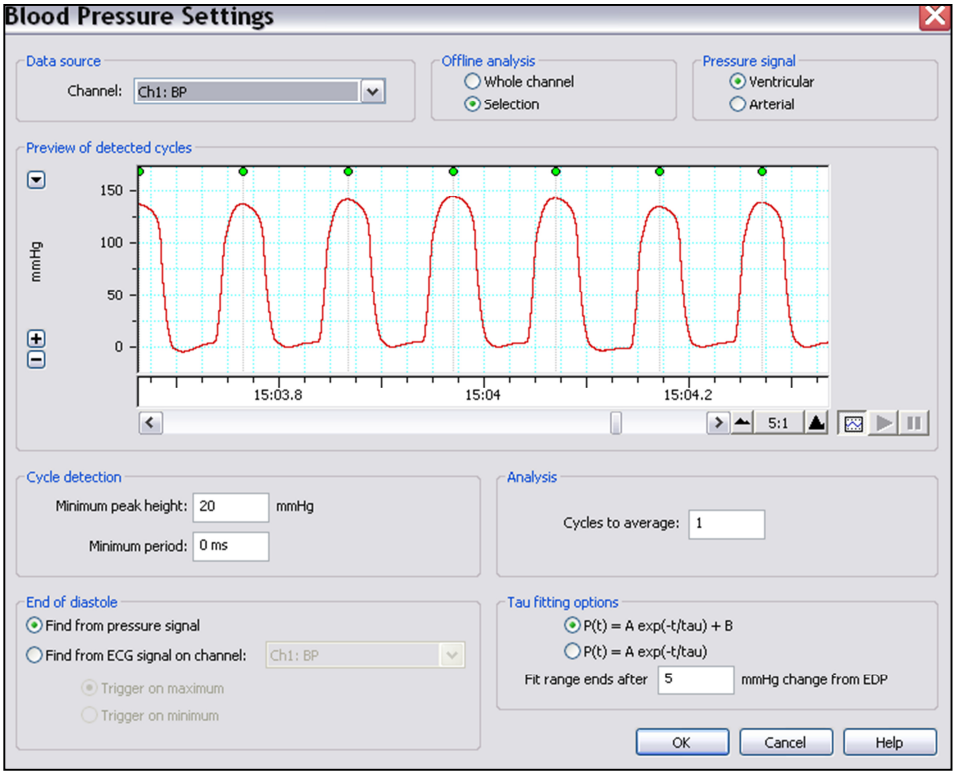

Figure 2.13 The blood pressure setting dialog.

2.3.3.1 Setting the module to analyze the data

For offline analysis labChart was opened and a file was chosen. Then the blood pressure setting dialog was loaded. Parameters for cycle detection and Tau fitting options were set as shown in Fig 2.13. In the Data source pane, the channel 1 exhibiting MAP was used to select 3-5 minutes of stable arterial blood pressure for further evaluation. This selected time was marked and then all data of this time window including SAP, DAP, MAP, and HR were exported as text file to excel.

Further averaging and evaluation were performed in excel. Left ventricular pressure was evaluated in the same manner but further derived parameters EDP, dP/dt_{max} (the steepest slope during the rising pressure curve) and dP/dt_{min} (the steepest slope during the declining pressure curve) were also exported and evaluated in excel.

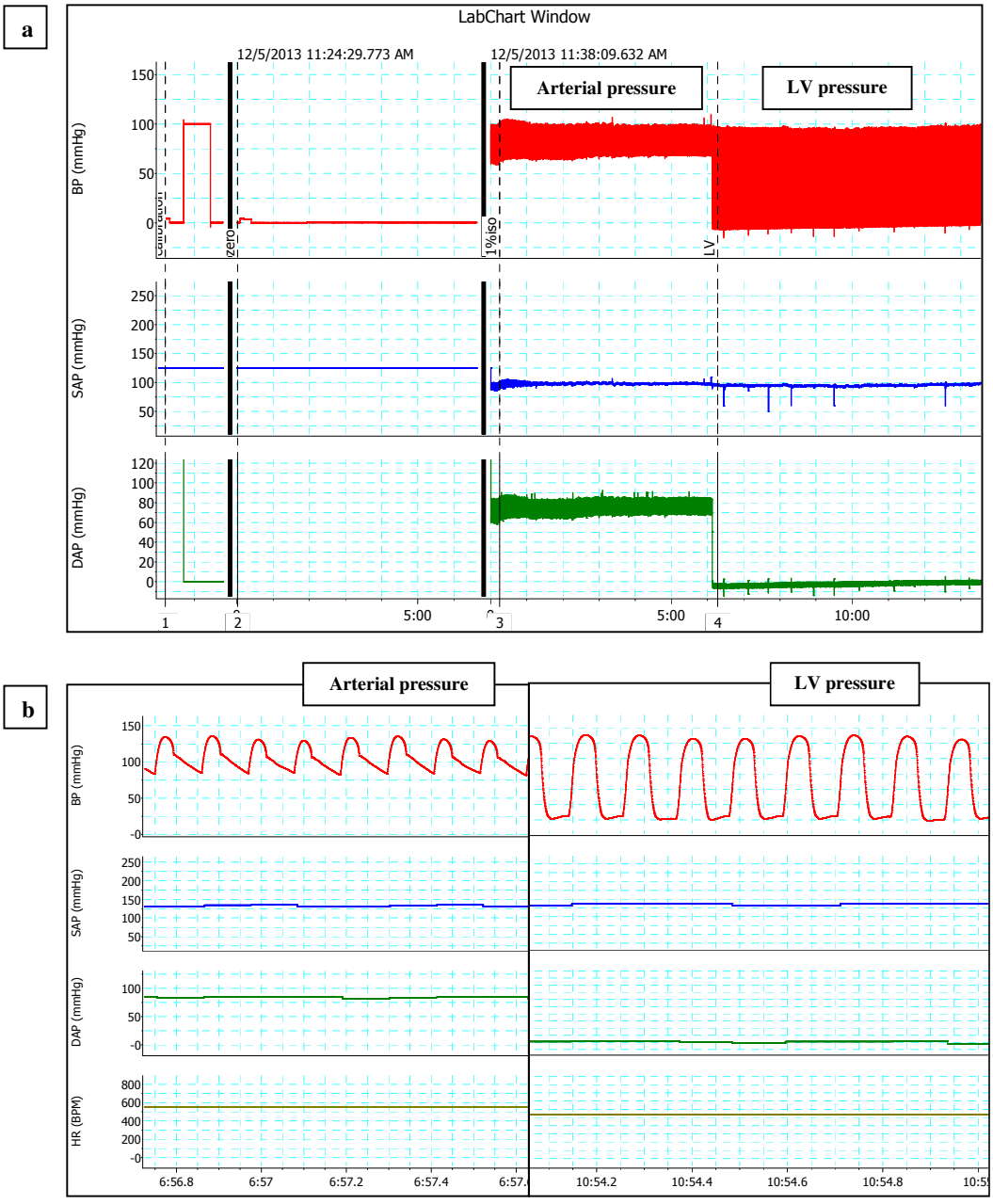

Figure 2.14 Labchart window sheet. (**a**) The arterial and LV pressure data, (**b**) the arterial and the ventricular cycle.

2.4 Light microscopy

2.4.1.Histology

2.4.1.1 PFA Fixation

2.4.1.1.1 Heart cannulation

A petri dish was filled up with the Tyrode's solution with EGTA (EGTA-Tyrode's solution in mM: 135 NaCl, 4 KCl, 1 $MgCl_2$, 2HEPES, 2.6 EGTA, and 10 glucose and 1 mg/ml BSA; pH 7.4 (NaOH)) and then a glass rod was fixed with clay at the edge of the petri dish. A loose tie was placed around the cannula close to the clay. The cannula was filled up with EGTA-Tyrode's solution and any small air bubbles were removed. After hemodynamic measurement, the mouse was euthanized with 4% isoflurane. The sternum was cut and the ribs were cut to open the thorax. Then the heart was excised from the thorax and transfered to the EGTA-Tyrode's solution in the prepared petri dish. Under the microscope the aorta was visualized.

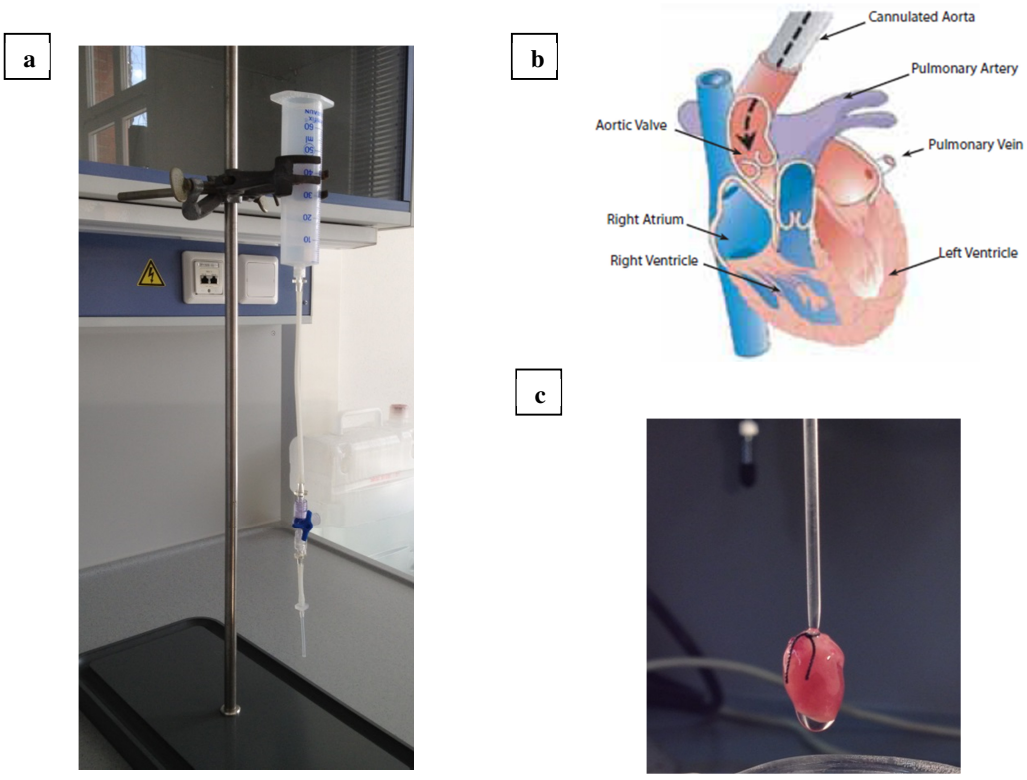

Figure 2.15 The heart perfusion. In the Langendorff perfusion system the perfusate flows in a retrograde fashion into the aorta. (**a**) The Langedorff heart perfusion system, (**b**) schematic drawing of the heart and the cannula, (**c**) the cannulated heart.

Two fine curve forceps were used to grab the edge of aorta and to pull the aorta over the cannula. The thread was tied around the aorta two times to fix the aorta firmly at the cannula. Finally, the cannula with the heart was immediately connected to a Langendorff perfusion system (Fig. 2.15).

2.4.1.1.2 Perfusion of the heart

The heart was retrogradely perfused with the above described Tyrode solution with EGTA for 5 min and then with 4% PFA for 8-10 min. After that the perfused heart was taken off the perfusion system and transferred in a 15 ml test tube that was filled up with 4% PFA solution. The heart was fixed with the 4% PFA for 24 hours. The heart was dehydrated in a graded series of ethanol (30%, 50%, and 70%) each step lasted 24 hr.

2.4.1.2 Automated tissue processor

The perfused heart was taken out of the test tube and transferred into a labelled cassette. These cassettes were mounted in an automated tissue processor (Tissue-Tek®VIPTM 5 Jr, Sakura Finetek GmbH, Staufen, Germany). The tissue processor is designed to infiltrate tissue specimen with a sequence of differnet solvents melted paraffin wax being the last. In brief, the heart was in 70% ethanol in the begining (water-based) and passed through multiple changes of dehydration and and xylene ending with paraffin.

2.4.1.3 Paraffin embedding

The tissue embedding station (Medax GmbH & Co. KG, Neumünster, Germany) was turned on at least 1 hour before use. On the heated area, the disposable embedding vessel was filled with melted paraffin from a paraffin dispenser. Then vessel was positioned on the cold area of the heated plate of the tissue embedding station (Fig. 2.16) in order to produce a small layer of solid paraffin at the botom of the the embedding vessel. The heart was picked up in the cassette of the automated tissue processor with fine forceps and submersed in the melted paraffin in the embedding vessel. It was oriented with the aorta on the top and the apex of heart on the bottom.The paraffin block was allowed to solidify in a cold area and then stored at room temperature.

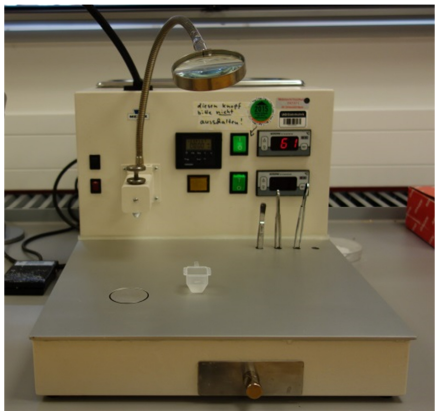

Figure 2.16 Tissue embedding station.

2.4.1.4 Sectioning with a microtome

The Microme HM 355 (Microm GmbH, Walldorf, Germany) (Fig. 2.17) was prepared and the water bath was set to 42 °C (Fig. 2.17 a). The heart in the paraffin block was taken off the embedment vessel and trimmed by a knife (Microm international GmbH, Walldorf, Germany). The knife was heated in the flame of a Bunsen burner. The trimmed block was placed on the heated knife and glued to a piece of hardwood by the surface with the melted paraffin. Then the paraffin block was secured by melting some small paraffin shavings. Finally the paraffin block was allowed to cool down completely (Fig. 2.18). The paraffin block with the heart was mounted on the microtome (block holder Fig. 2.17 b) and approached to the knife (Fig 2.17 c). The paraffin block was trimmed by cutting off 20 µm sections until the desired level was reached. The section thickness was then changed to 5 µm. The ribbon of sections moved a descnding slope to the surface of the wather bath. The ribbon of sections floated on water for about 15-30 seconds to stretch and to eliminate folds and wrinkles. A microscope slide was then gently immersed into the water and the sections were placed on the slide gently to prevent trapping of air bubbles. The microscope slides with sections were placed in an oven with 62°C for 6 hours to attach firmly to the slides. After that the slides were transferred into a slide box and stored at room temperature.

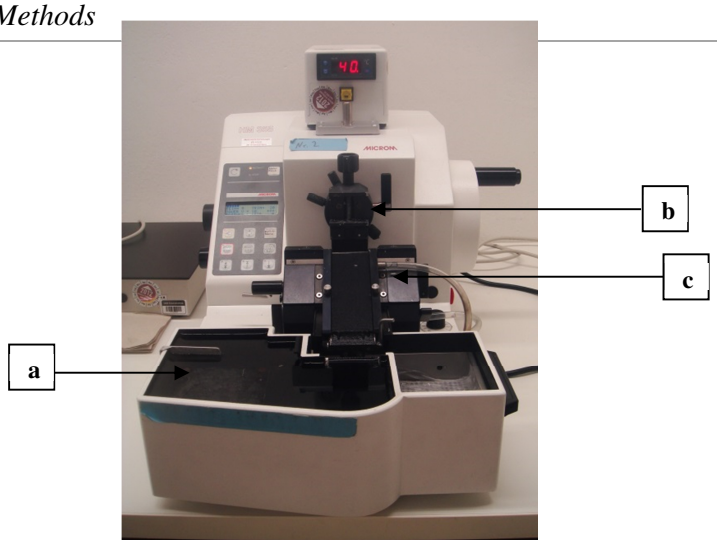

Figure 2.17 Microtome. (**a**) The water bath, (**b**) the block holder, (**c**) the knife.

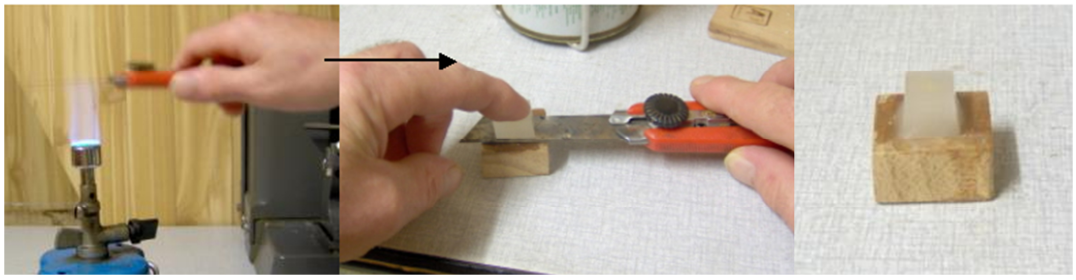

Figure 2.18 Mounting the paraffin block on a piece of hardwood using a heated knife
Yvan Lindekens. (2007) Making your own paraffin section @home (part2). Weblog. (online) available from http://www.microscopy-uk.org.uk/mag/indexmag.html?http://ww.microscopy-uk.org.uk/mag/artfeb07/yl-para2.html (accessed 6th April 2014).

2.4.1.5 Masson's Trichrome Staining

For investigation of the development of cardiac hypertrophy, it is important to differentiate between cardiomyocytes and connective tissue in the heart. Therefore it is important to apply a staining procedure which stains both tissues in different colors. Masson´s trichrome method (Masson-Goldner staining kit, Merck KGaA, Darmstadt, Germany) stains muscle cell red, connective tissue green, and cell nuclei black. Therfore we decided for Masson trichrome staining to differentiated between the different tissues.

First, the microscope slide was placed in the 65 ^{o}C oven for 20 min and was allowed to cool down for 10 min. Under the hood, the paraffin heart slide was put into Xylene for 5 min two times to deparaffinize and then it was rehydrated in a descending series of ethanol (100% for 30 s, 90%, 80% and 60% each for 3 min). After that the slide was washed in distilled water for 30 s and stained in Hematoxylin for 5 min. The slide was taken off from the Hematoxylin and washed in ddH_2O for 30 s and washed further under running tap water for 5 min. In the next step the slide was transferred into 1% acetic acid solution for 30 s, and then was stained in Azophloxin solution for 5 min. The slide was then differentiated in 1% acetic acid solution for 30 s. This was followed by 1 min in Tungstophosphoric acid orange G solution and a differentiation step of 30 s in 1% acetic acid solution. It was then stained in Light green for 4 min and again differentiated in 1% acetic acid solution for 30 s. The slide was dehydrated in an ascending series of ethanol (60%, 80%, 90% and 100% each for 30 s). The slide was put in Isopropanol for 1 min and was cleared with Xylene for 1 min. Finally, a drop of Entellan was placed on the slide and a cover slide was positioned on the section. This was done by pressing gently onto the cover slide with a pair of small forceps to squeeze air bubbles out. The slide was allowed to dry under the hood overnight and then stored in a slide box at room temperature.

2.4.1.6 Image analysis and quantification

2.4.1.6.1 LV Thickness

For quantification of LV thickness the stained heart section was photographed at 10-fold magnification. The Image J software was used to analyze LV thickness. In the Image J program the scale file was opened. A straight was chosen and used to measure 1 mm length from the scale picture. The analyze tab was opened and in the set scale dialog the value from the scale measurement was transformed into pixels as demonstrated in Fig 2.19).

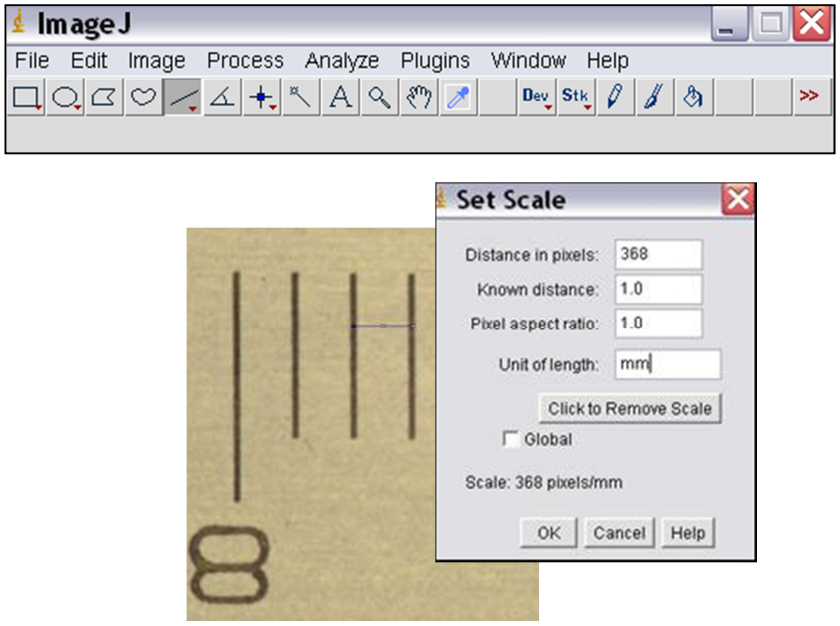

Figure 2.19 The image J setting scale.

With these settings a straight was selected in an image file was used to measure the LV thickness (Fig. 2.20). To do this the analyze tab opened and measure was chosen. The results were displayed automatically and exported to an excel sheet.

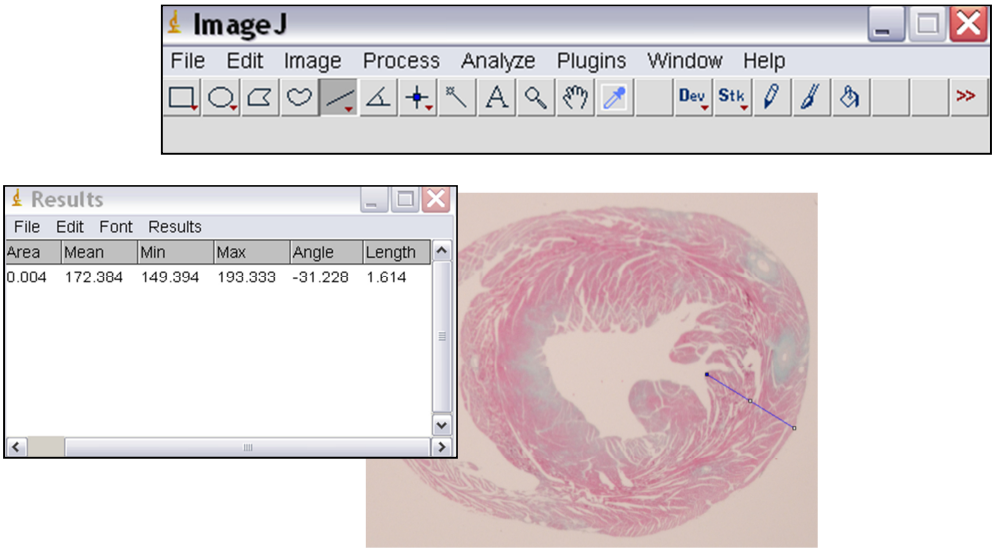

Figure 2.20 The left ventricular thickness measurement by Image J.

2.4.2 Morphometric mesurements

The morphometric parameters, body weight (BW), heart weight (HW), left ventricular weight (LVW), right ventricular weight (RVW) were evaluated by a KERN accurate scale (KERN & SOHN GmbH, Ziegelei 1, 72336 Balingen – Germany) whereas tibia length (TL) was measured by a caliper (Fig. 2.21).

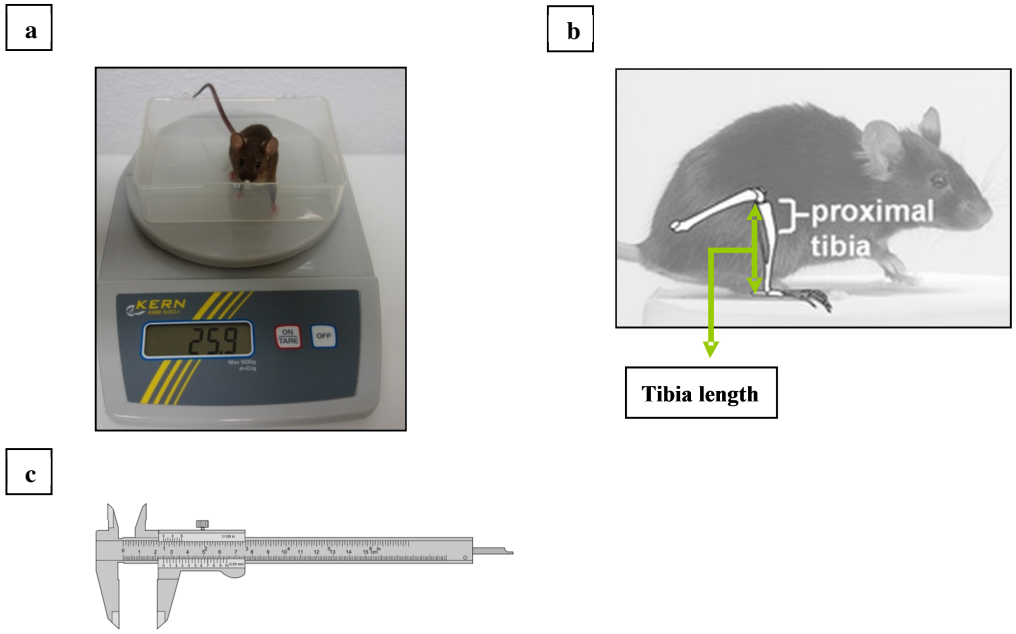

Figure 2.21 The scale and the tibia length measurement.

(a) The scale, (**b**) the tibia length, (**c**) the caliper

2.4.3 Immunohistochemical staining of isolated cardiomyocytes

2.4.3.1 Isolation of ventricular cardiomyocytes

The mouse was weighed and set into the induction chamber, which had been prepared with a tissue paper soaked with 2-3 drops of isoflurane. When the mouse had lost consciousness, it was taken out of the induction chamber and killed by cervical dislocation. The abdomen was opened and then the liver was gently pulled down and the diaphram was cut to open the thoracic cavity and expose the heart. Then the heart was excised from the thorax and transferred into the EGTA-Tyrode's solution. It was then attached to a Langendorff perfusion system as described in chapter

2.4.1.1.1. The pressure was adjusted to 0.05 bar. The heart was perfused with EGTA-Tyrode's solution for 5-7 min, subsequently, with high-potassium solution (in mM: 4 NaCl, 10 KCl, 130 K-glutamate, 1 $MgCl_2$, 0.05 $CaCl_2$, 2HEPES, and 10 glucose and 1 mg/ml BSA; pH 7.4 (KOH)) for 5-6 min. In the next step the perfusion was switched to a high potassium solution supplemented with trypsin (0.33 mg/ml trypsin from bovine pancreas (S93610) from Sigma-Aldrich®, Steinheim, Germany) for 5 min, followed by pure high-potassium solution for 4-5 min. The last perfusing solution was high potassium supplemented with collagenase (0.4 mg/ml; collagenase from *Clostridium histolyticum* Sigma Blend Type L (C8176) from Sigma-Aldrich®, Steinheim, Germany). Throughout the procedure, the temperature of the heart was maintained between 35-36.5°C. After the perfusion the heart was cut into small pieces by scissors and cells were liberated from the tissue by mechanical shearing in Tyrode's solution (in mM: 135 NaCl, 4 KCl, 1.8 $CaCl_2$, 1 $MgCl_2$, 2HEPES, and 11 glucose and 1 mg/ml BSA; pH 7.4 plus trypsin inhibitor 0.0167 mg/ml all from Sigma-Aldrich®, Steinheim, Germany) and then filtered through a nylon mesh (width 125 μm) into test tubes in order to separate the cells from the debris. After a short spin, the supernatant was removed and the pellet was resuspended in 2.5 ml of Tyrode's solution and allowed to settle for 10 minutes at 37°C. After that, the supernatant was removed and cells remaining in the pellet were resuspended in ~2.5-3.5 ml of Tyrode's solution according to the amount of cells. Ventricular cardiomyocytes prepared from mice of different genotypes were attached to laminin-coated microscope slides and fixed with cold -20°C methanol (5 min) and acetone (0.5 min).

2.4.3.2 Immunofluorescence staining of ventricular cardiomyocytes

The cardiomyocytes were stained with antibodies to localize ICD proteins using standard procedures. The cardiomyocyte slides were rehydrated, fixed, and frozen in phosphate buffered saline (PBS) as usual for 10 minutes. Then the slides were blocked with 10% normal goat serum (NGS) in 1%BSA in PBS for 45 minutes at 37°C. After that the blocking solution was removed from the slides by tapping. Later the slides were incubated with primary antibody mix at 4°C

overnight. The following mixed primary antibodies were used (primary antibodies were diluted in 1%BSA in PBS):

1. RR90 10x (Filamin A and C d1-2); 1:5; mouse IgA
   T12 (Titin Z-band epitope); 1:10; mouse IgG1
   CX43 (gap junction); 1:1000; rabbit
2. CDH (Cadherin); 1:100, rabbit
   T12 (Titin Z-band epitope); 1:10; mouse IgG1
   Mf20 (Myosin HC, all); 1:20, mouse IgG2b
3. 34C-s (Ryanodine receptors); 1:5; mouse IgG1
   FlnC (FilaminC d16-20); 1:1000, rabbit
   BB78.8 (Myomesin, M-Band); 1:2: mouse IgG2b

Next, the slides were washed with PBST (PBS with 0.5% Tween) 2 times and then washed in PBS 1 time for 5 minutes each. Afterwards, the slides were incubated with mixed secondary antibody at 37°C for 2 ½ hours. The following mixed antibodies were used (the secondary antibodies were diluted in 1%BSA in PBS):

1. Goat anti mouse IgG1 Alexa 594,; 1:300
   Goat anti mouse IgA FITC; 1:60
   Goat anti rabbit-Alexa 647; 1.200
2. Goat anti mouse IgG1 Cy2,; 1:300
   Goat anti mouse IgG2b-Alexa 594; 1:1000
   Goat anti rabbit Alexa 647; 1.200
3. Goat anti mouse IgG1 Cy2,; 1:300
   Goat anti mouse IgG2A-Alexa 594; 1:1000
   Goat anti rabbit-Alexa 647; 1.200

Dapi1:40000 were added to mixed secondary antibody. Later on, the slides were washed with PBST 2 time and then washed in PBS 1 time for 5 minutes each, respectively. After that, the slides were washed with deionized water (ddH_2O). Finally, the slides were mounted with a drop

of mounting medium (Mowiol with N-propylgalat (1:10) and stored in the dark. Specimens were examined and pictures were acquired using an inverted microscope equipped with fluorescence optics (Nikon Eclipse TE-2000-E) and a cooled CCD camera (DVC Company) and Image Pro Plus software (Media Cybernetics).

2.5 Statistics

For statistical analysis, all data were expressed as mean (Mean) and standard error of the mean (SEM) was calculated. The computer program Prism 5.0 from GraphPad Software, San Diego, USA, system enabled the rapid determination of statistical significance by one-way ANOVA and subsequent post hoc Newmann-Keuls Multiple comparison test. Differences with a level of $p < 0.05$ were considered significant. In addition, bar graphs were created displaying the arithmetic mean ± SEM.

2.6 Equipments and materials

2.6.1 Animals and materials for animal husbandry

Products	Company
Animal XIRP WT XIRP1XIRP2 dko	Institut für Zellbiologie, Bonn University, Germany
Bedding Espen Einstreu ani–bedding 14 PA animal bedding	AsBe-wood GmbH, Buxtehude, Germany
Cages Makrolon, type II L	Charles River Germany GmbH, Sulzfeld, Germany
Food Standard rodent chow V1534-300	Ssniff Spezialdiäten GmbH, Soest, Germany

2.6.2 Equipment and materials for the operation

Products	Company
Equipments	
Body temperature probe	Hand-made from an electrical workshop of the Physiological Institute II
Chest retractors	Hand-made from a mechanical workshop of the Physiological Institute II
EKG	Hand-made from an electrical workshop of the Physiological Institute II
Endotracheal tube Diameter 1.0 mm and 1.2 mm	Hugo Sachs Elektronik, March , Hugstetten, Germany
6-0 Ethicon Prolene	Ethicon, Johnson & Johnson Medical GmbH, Norderstedt, Germany
Infrared heating bulb Infraphil 150w 230v PAR 38E	Phillips, Holland
Isoflurane vaporizer Isoflurane Vapor 19.3	Dräger, Medizintechnik GmbH, Lübeck, Germany
Mouse ventilator MiniVent Type 845	Hugo Sachs Elektronik
Operation stage Water circulation system	Hand-made from a mechanical workshop of the Physiological Institute II
Surgical instruments curve scissor, mosquito clamp, fine curve forceps, cubic curve forceps, and needle holder	Allgaier instrumente GmbH, Frittlingen/Tuttlingen, Germany
Surgical microscope OPMI 1FR pro	Carl Zeiss Surgical GmbH, Oberkochen, Germany
USP 5/0 Seraflex®	Serag-Wiessner KG, Naila, Germany
Water bath Haake Model L Waterbath with D8 Circulator	Haake, Germany

Products	Company
Chemical	
Analgesic Buprenorphine Temgesic® (Buprenorphine hydrochloride 0.324mg/ml)	Reckitt Benckiser (Deutschland) GmbH, Mannheim, Gremany
Anesthesia Isofluran: Forene®	Abbott GmbH & Co. KG, Wiesbaden, Germany
Ethanol 70%	Otto Fischar GmbH & Co. KG, Saarbrüchen, Germany
Eye ointment Bepanthen®	Bayer vital GmbH, Leverkusen, Germany
Povidone-iodine Betaisodona Lösung®	Mundipharma GmbH, Limburg, Germany

2.6.3 Equipment and materials for the hemodynamic measurement

Products	Company
Computer	HP Compaq dc 7900, Hewlett-Packard Development Company, Germany
LabChart Chart v6.0 for Windows	ADInstruments Ltd, Spechbach, United Kingdom
Pressure catheter Ultra-Miniature Pressure Catheter	Transonic System Inc, NW Maastricht, Netherlands
Pressure Control Unit FP095B – Dual channel Pressure Control Unit Version 095B-01	Transonic System Inc
Power lab 8SP	ADInstruments Ltd, Spechbach, Germany
Surgical instruments curve scissor, mosquito clamp, fine curve forceps, cubic curve forceps, and fine vannas scissor	Allgaier Instrumente GmbH, Frittlingen/Tuttlingen, Germany

2.6.4 Equipment for histology

Products	Company
Equipments	
Blade Einwegklinge SEC 35 (152200)	Microm international GmbH, Walldorf, Germany
Cassette Einbettkassetten Macro E478.1	Karl Roth GmbH Co. KG, Karlsruhe, Germany
Cover slips 24 x 60 mm	Gerhard Menzel GmbH, Braunschweig, Germany
Disposable paraffin molds Peel-A-Way® Embedding Mold (Square – S22)	Polysciences Europe GmbH, Eppelheim, Germany
Image J V 1,47	Wayne Rasband , National Institutes of Health , USA
Microscope slide SuperFrost® Plus	Gerhard Menzel GmbH, Braunschweig, Germany
Microtome The Microme HM 355	Microm GmbH, Walldorf, Germany
Paraffin dispenser	Medax GmbH & Co. KG, Neumünster, Germany
The automated tissue processor	Tissue-Tek®VIPTM 5 Jr, Sakura Finetek GmbH, Staufen, Germany
Chemical	
Hematoxynlin solution HHS32-1L	Sigma-Aldrich®, Missouri, UAS
Masson-Goldner staining kit 100485	Merck KGaA, Darmstadt, Germany
Paraformaldehyde	Sigma-Aldrich®, Missouri, UAS
2-Propanol	Merck KGaA
Rapid mounting medium for microscopy Entellan®	Merck KGaA
Xylene	VWR®, Lueven, Belgium

2.6.5 Immunohistochemistry staining

Products	Company
Equipments	
Langendorff heart perfusion system	Hand-made from a mechanical workshop of the Physiological Institute II
Mowiol	Sigma-Aldrich®, Steinheim, Germany
Chemical	
Antibody	
RR90 (Filamin A and C domain 1-2)	Van der ven et al., 2000
Cx43 (Connexin43)	AG Willecke
T12 (Titin, z-band)	Fürst et al., 1988
Mf20 (Myosin HC)	
FlnC 16-20	dshb
(FilaminC d16-20)	AG Fürst
BB78	
(Myomesin domain 12 (m-band))	Vinkemeier et al., 1993
34C-s	
(α,β ryanodine receptors)	dshb
CDH (cadherin)	Sigma, Germany
Alexa Dy 594en	SBA
DAPI	Invitrogen
Alexa 647	Jackson
IgA-FITC GAM	Invitrogen
IgG2a-Alexa 594	Molecular probes
IgA-FITC GAM	Invitrogen
IgG2b-Alexa 594	Molecular probes
IgG1-Cy2	Invitrogen
BSA	
Bovine Serum Albumin	Sigma-Aldrich®, Steinheim, Germany
$CaCl_2$ * 2 H_2O	
Calcium chloride dihydrate	Merck KGaA
Collagenase	
(from *Clostiridium histolyticum*, Sigma Blend Type L, ≤1.0 FALGPA units/mg solid)	Sigma-Aldrich®

Products	Company
Chemical	
D(+)-Glucose monohydrate	Merck KGaA
HCl Hydrochloric acid solution (1 mol/ l)	Merck KGaA
HEPES 2-(4-(2-Hydroxyethyl)-1-piperazinyl)- ethanesulfonic acid, buffer substance	Merck KGaA
KCl Potassium chloride	Merck KGaA
KOH Potassium hydroxide solution (1 mol/ l)	Merck KGaA
Laminin	Sigma-Aldrich®
L-glutamate Potassium	Sigma-Aldrich®
$MgCl_2$ * 6 H_2O Magnesium chloride hexahydrate	Merck KGaA
NaCl Sodium chloride	Merck KGaA
NaOH Sodium hydroxide solution (1 mol/ l)	Merck KGaA
Trypsin (from bovine pancreas, essentially salt free, lyophilized, ~9000 U/mg)	Sigma-Aldrich®
Trypsin inhibitor (from *Glycine* max (soybean), powder, BioReagent, suitable for cell culture)	Sigma-Aldrich®

2.6.6 Others

Products	Company
Caliper	Mauser , St. Denis , France
Scale 1. The coarse digital scale 2. The fine digital scale	Kern EMB 500-1, Precision balance, KERN & SOHN, Balingen, Germany Faust GmbH, Germany
Terg-A-Zyme protease enzyme for presoaking proteinaceous soils and hard-to-remove stains	Alconox Inc., New York, USA
GraphPad Prism 5	Graphpad Inc., La Jolla, CA, USA
Ultra-Tiefkühlschrank (-80C°)	Doubaras GmbH, Düsseldorf, Germany

3 Results

3.1 Animals

3.1.1 Animal numbers

A total of XIRP female 135 animals were examined. 39 XIRP WT mice (17 Sham and 22 TAC), which served as control animals for XIRP1XIRP2dko mice, were compared to 96 XIRP1XIRP2 dko mice (40 Sham and 56 TAC).

3.1.2 Mortality rate

In this study the mortality from immediately after TAC or sham surgery until the end of the experiments 14 days later - depending on the group - amounted to 0% in both sham groups, 10% in the XIRP WT, 16.2 % in XIRP1XIRP2 dko, The low mortality rates in these groups show that the surgeries were performed in a professional manner.

3.1.3 Age of the mice

The mice were age matched and there was no statistically significant difference between the groups at the day of the surgery (XIRP WT 13.5 ± 0.2 weeks old; XIRP1XIRP2 dko 13.0 ± 0.2 weeks old). In addition to the 13 weeks old mice, a group of 1 year old mice was investigated (XIRP WT 13.1 ± 0.1 months old; XIRP1XIRP2 dko 12.0 ± 0.3 months old).

3.1.4 Characterization of protein expression of the mouse model

As mentioned above, in the center of this investigation are mice, which are *XIRP1* deficient and do not express any of the three XinABC$^{-/-}$ isoforms and which are hypomorphic for *XIRP2*. In order to define the genetic status of these mice, the expression of the *XIRP1* and *XIRP2* genes was investigated by Western blot. The proteins XIRP2, XinA, XinB and myomesin were monitored on protein extracts from whole hearts of WT and XIRP1XIRP2 dko mice Fig 3.1.

In WT mice the three Xin-repeat proteins as well as myomesin could be detected. In XIRP1XIRP2 dko mice the three Xin-repeat proteins could not be demonstrated, but myomesin was present in comparable amount as in WT-mice.

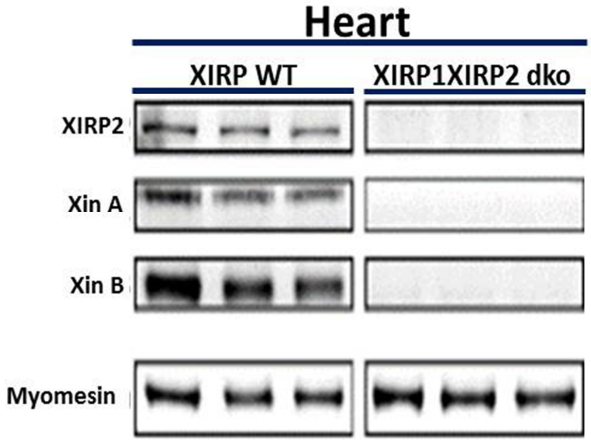

Figure 3.1 Western-blot analysis of whole hearts from WT and XIRP1XIRP2 dko mice. Each lane represents one animal.

Subsequently, cryosections of myocardial tissue from XIRP WT and XIRP1XIRP2 dko were investigated by immunofluorescence microscopy. In first series, antibodies against the proteins XIRP2, filamin A and C as well as vinculin were applied together. In WT mice the four proteins could be demonstrated in the ICDs, where they all co-localized (Fig. 3.2). In a second series, antibodies against XIRP1, filamin A and C as well as α-actinin were incubated on the

cryosections of WT hearts. XIRP1 and the filamins were shown on the ICDs, whereas the α-actinin antibody appeared in the typical cross-striation pattern of cardiac muscle. The merged pictures showed a common localization of the proteins in the Z-disks as well as in the ICDs (Fig. 3.2).

Application of antibodies against XIRP1 and XIRP2 and filamin A and C to cryosections of XIRP1XIRP2 dko hearts did only lead to binding of the filamin antibodies at the ICDs.

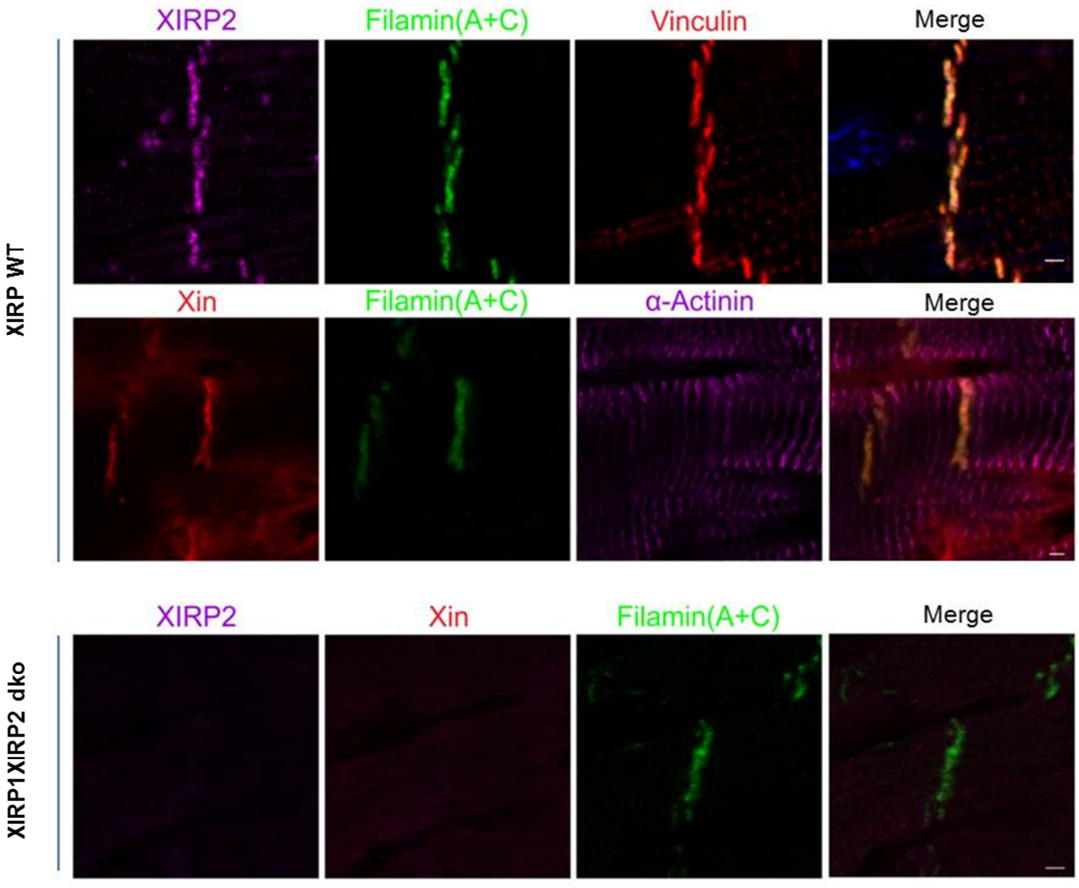

Figure 3.2 Fluorescence microscopic visualization of immunofluorescence stainings in cryosections of hearts from XIRP WT and XIRP1XIRP2 dko mice (scale 2µm).

3.1.5 Body weight of the mice

The body weight (BW) of XIRP WT and XIRP1XIRP2 dko mice did not differ significantly at 13 weeks of age (23.2 ± 0.6 g; n = 10 vs 22.8 ± 0.4 g; n = 23). For comparison, a group of age matched C57BL/6 mice (the most widely used mice for experiments) was added to the bar graph (average age 13.2 ± 0.1-weeks, BW 20.6 ± 0.5 g, n= 17). The C57BL/6 mice were significantly more lightweight.

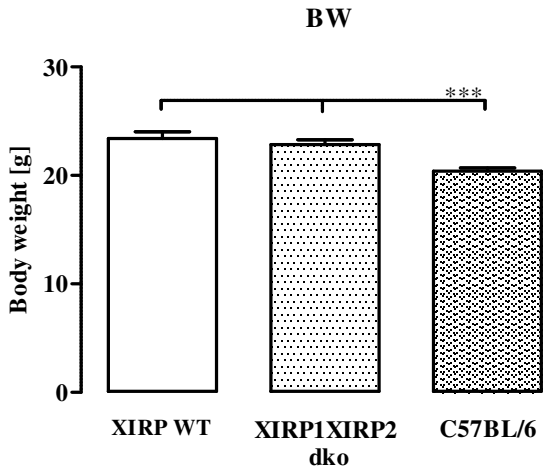

Figure 3.3 Body weight (BW) of the mice of all genotypes. The BW did not differ between the XIRP WT and the XIRP1XIRP2 dko, but age matched C57BL/6 mice were significantly more lightweight. The data are represented as mean ± SEM; n= 10-23 /group, ****P*< 0.001.

3.1.6 Tibia length of the mice

The tibia length (TL) of XIRP1XIRP2 dko mice was significantly longer than that of XIRP WT mice 13 weeks of age (16.42 ± 0.06 mm; n = 52 vs 15.77 ± 0.1 g; n = 27). For comparison a group of age matched C57BL/6 mice was added to the bar graph (average age 13.2 ± 0.1-weeks, TL 16.05 ± 0.08 mm, n= 36).

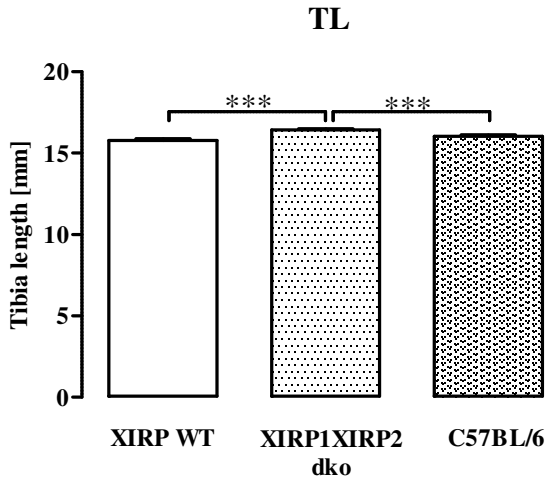

Figure 3.4 The tibia length (TL) of the mice of all genotypes, the TL of XIRP1XIRP2 dko were significantly longer than Xin WT and C57BL/6 mice. The data are represented as mean ± SEM; n= 27-53/ group, ****P*< 0.001.

3.1.7 HW, HW/BW ratio, and HW/TL ratio

Like in the case of BW, also the heart weights (HW) of the two genotypes of mice did not differ significantly (XIRP WT 130.9 ± 3.6 g n = 11 vs XIRP1XIRP2 dko 127.1 ± 3.5 g n = 23). Also the normalized ratios of heart weight/body weight (HW/BW ratio; XIRP WT 5.64 ± 0.08 mg/g n = 11 vs XIRP1XIRP2 dko 5.57 ± 0.11 mg/g n = 23) and heart weight/tibia length (HW/TL ratio; XIRP WT 8.23 ± 0.19 mg/mm n = 11 vs XIRP1XIRP2 dko 7.7 ± 0.2 mg/mm n = 23) were statistically not different.

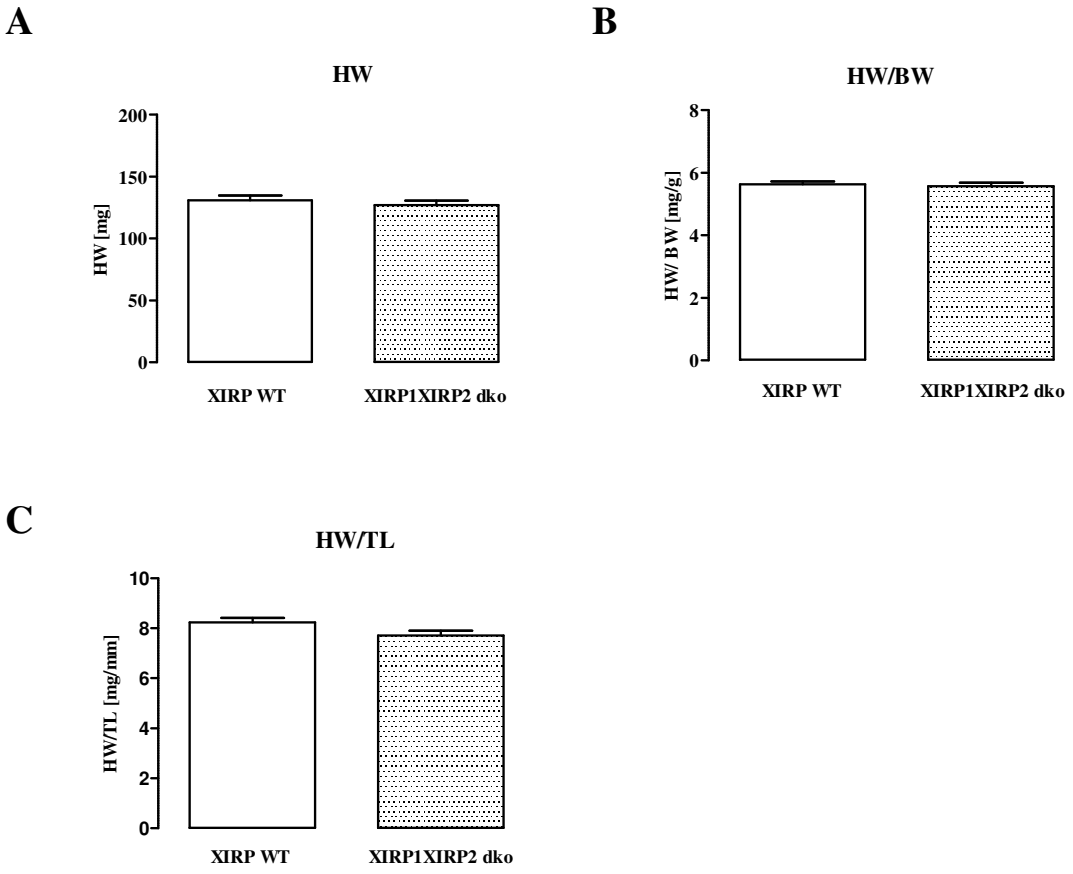

Figure 3.5 HW, HW/BW ratio and HW/TL ratio of XIRP WT and XIRP1XIRP2 dko mice**.** Both genotypes did not differ significantly in HW, HW/BW ratio, and HW/TL ratio. The data are represented as mean ± SEM; n= 11-30 /group.

3.1.8 LVW, LVW/BW ratio, and LVW/TL ratio

In case of differences in the systemic circulation between the two genotypes a comparison of left ventricular weights is more meaningful, therefore these data are demonstrated here. Neither left ventricular weight (LVW) nor the LVW/BW ratio nor the LVW/TL ratio differed significantly between the genotypes, but LVW/TL was with $P = 0.054$ close to the level of significance (XIRP WT n = 6 vs XIRP1XIRP2 dko n = 9: LVW 96.5 ± 3.19 g vs 90.3 ± 4.17 g; LVW/BW ratio 4.27 ± 01.19 mg/g vs 3. 94 ± 0.13mg/g; LVW/TL ratio 6.19 ± 0.22 mg/mm vs. 5.5 ± 0.22 mg/mm).

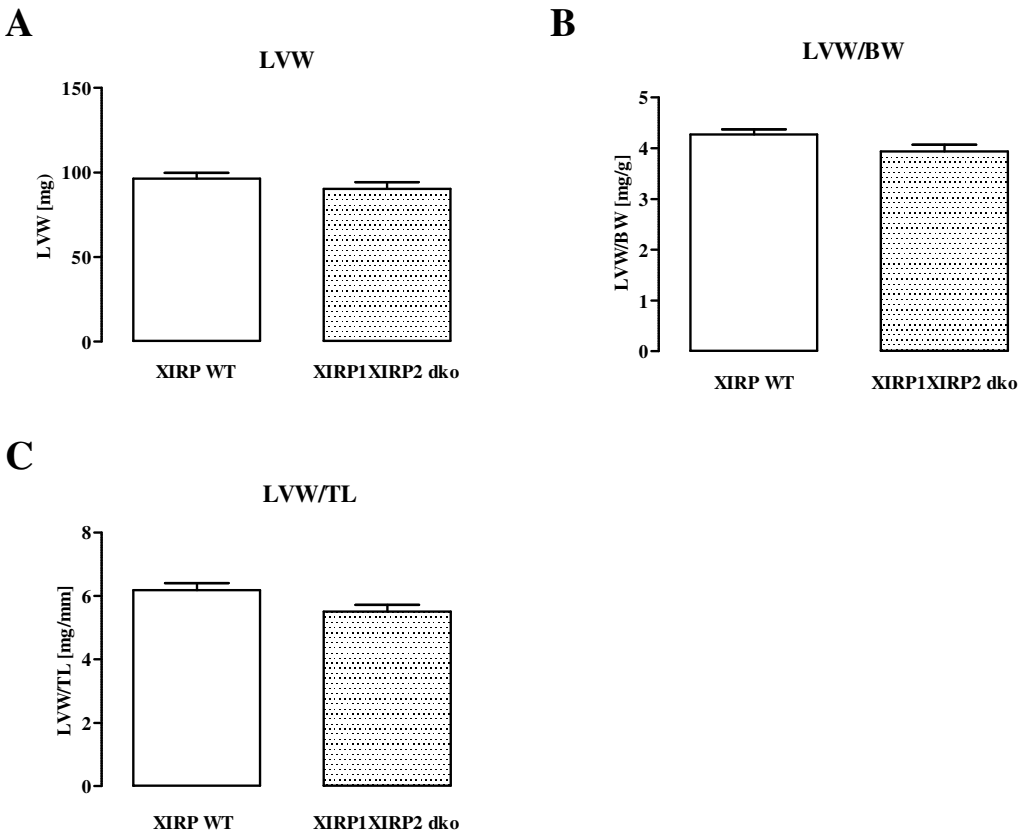

Figure 3.6 LVW, LVW/BW ratio, LVW/TL ratio of XIRP WT and XIRP1XIRP2 dko mice**.** LVW, LVW/BW ratio, and LVW/TL ratio did not differ significantly between both genotypes. The data are represented as mean ± SEM; n= 6-9 /group.

3.1.9 LW, LW/BW ratio, and LW/TL ratio

The lung weight (LW) is an important parameter which may differ in case of increased EDP in the left ventricle. This leads to a congestion of blood in the lungs. Therefore the lung weight was detected in both genotypes. Neither LW nor the LW/BW ratio were significantly different between the genotypes, but the LW/TL ratio was with $P = 0.034$ significantly different (XIRP WT n = 11 vs XIRP1XIRP2 dko n = 23: LW 150.8 ± 3.04 g vs 144.4 ± 3.89 g; LVW/BW ratio 6.53 ± 0.17 mg/g vs 6.32 ± 0.11 mg/g; LVW/TL ratio 9.5 ± 0.23 mg/mm vs. 8.75 ± 0.21 mg/mm).

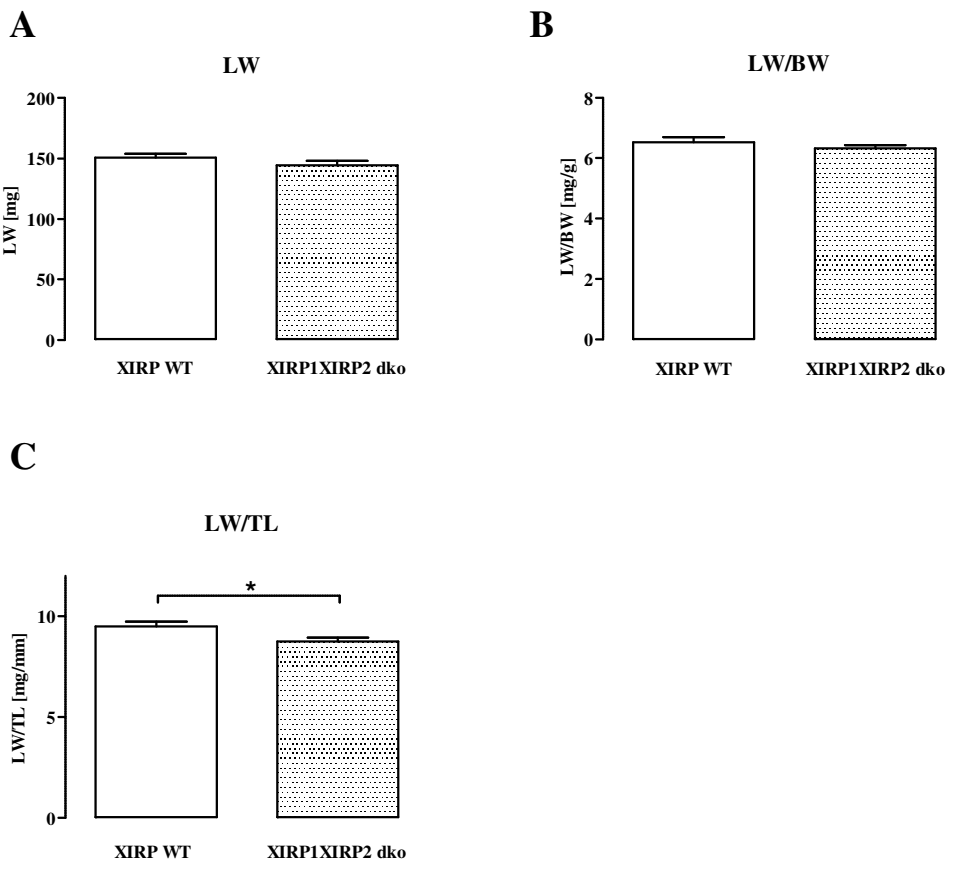

Figure 3.7 LW, LW/BW ratio, LW/TL ratio of XIRP WT and XIRP1XIRP2 dko mice**.** LW/TL ratio was significantly smaller in XIRP1XIRP2 dko than in XIRP WT, whereas LW and LW/BW ratio were equal. The data are represented as mean ± SEM; n= 11-23 /group.

Taken together, in the macroscopic anatomic parameters there were only minor differences between both genotypes compared in this study. In the following chapters all investigated parameters will be demonstrated in conjunction with the results of the TAC surgery.

3.2 The effect of TAC surgery

3.2.1 The effect of surgery on BW

To evaluate the influence of the surgery on the BW, it was measured at the date of surgery and sacrifice. Subsequently the BW-difference was calculated. This development of body weight is demonstrated in table 3.1. Except in the XIRP1XIRP2 dko sham group, in which the weight stayed nearly stable, all other groups gained a small amount of weight, which did not reach the level of significance.

Table 3.1 Development of BW from the operation to the measurement day

Genotype	Treatment	*n*	BW-OP	BW-ME	BW-difference
XIRP WT	Sham 14d	10	23.1 ± 0.6	23.4 ± 0.6	0.3 ± 0.4
XIRP WT	TAC 14d	13	23.0 ± 0.8	23.3 ± 0.7	0.4 ± 0.3
XIRP1XIRP2 dko	Sham 14d	23	22.9 ± 0.6	22.8 ± 0.5	-0.0 ± 0.3
XIRP1XIRP2 dko	TAC 14d	30	23.4 ± 0.5	24.1 ± 0.4	0.7 ± 0.3

Results are means ± SEM; *n,* number of animals. BW-OP: body weight on the day of the surgery BW-ME: body weight on the day sacrifice, BW-difference: (BW-ME)-(BW-OP), statistically non-significant difference ($P < 0.05$) by all groups comparison.

3.2.2 HW, HW/BW ratio, and HW/TL ratio

14 days of TAC induced a significant increase in all three heart weight parameters HW, HW/BW ratio, and HW/TL ratio in both genotypes (Fig. 3.8 A, B, and C). However, differences between the genotypes could not be detected (XIRP WT: sham HW 130.9 ± 3.7 mg vs TAC HW 163.7 ± 6.1 mg; sham HW/BW ratio 5.6 ± 0.1 mg/g vs. TAC HW/BW ratio 6.8 ± 0.2 mg/g; sham HW/TL ratio 8.2 ± 0.2 mg/mm vs. TAC HW/TL ratio 10.4 ± 0.3 mg/mm; XIRP1XIRP2 dko: sham HW 127.1 ± 3.5 mg vs. TAC HW 171.0 ± 3.9 mg; sham HW/BW ratio 5.6 ± 0.1 mg/g vs. TAC HW/BW ratio 7.1 ± 0.2 mg/g; sham HW/TL ratio 7.7 ± 0.2 mg/mm vs TAC HW/TL ratio 10.5 ± 0.3 mg/mm).

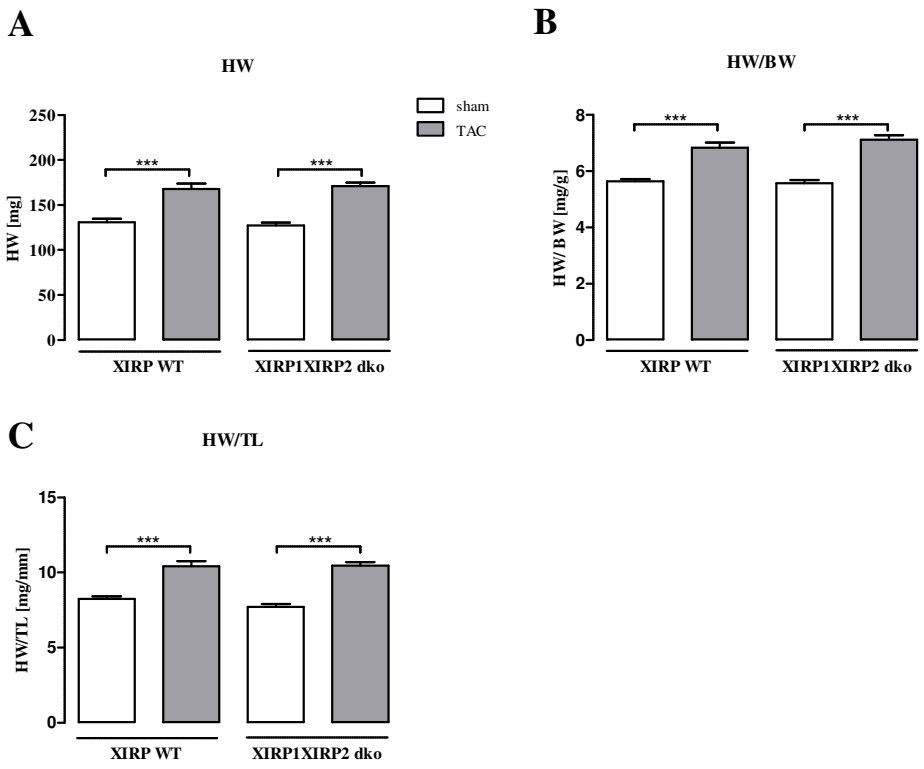

Figure 3.8 HW, HW/BW ratio, HW/TL ratio of XIRP WT and XIRP1XIRP2 dko mice. HW, HW/BW ratio, and HW/TL ratio were significantly increased in TAC group of both genotypes. The data are represented as mean ± SEM; n= 11-30 /group, **P*< 0.05 was considered statistically significant.

3.2.3 LVW, LVW/BW ratio, and LVW/TL ratio

As shown already for the HW parameters, also the LVW parameters were significantly increased by TAC (Fig. 3.9 A, B, C). But again the influence of TAC did not differ between both genotypes (XIRP WT: sham LVW 96.5 ± 3.2 mg vs TAC LVW = 117.7 ± 4.9 mg; sham LVW/BW ratio 4.3 ± 0.1 mg/g vs TAC LVW/BW ratio 5.0 ± 0.1 mg/g; sham LVW/TL ratio 6.2 ± 0.2 mg/mm vs. TAC LVW/TL ratio = 7.6 ± 0.3 mg/mm; XIRP1XIRP2 dko: sham LVW = 90.3 ± 4.2 mg vs. TAC LVW = 126.4 ± 5.1 mg; sham LVW/BW ratio = 4.0 ± 0.1 mg/g vs TAC LVW/BW ratio = 5.1 ± 0.2 mg/g; sham LVW/TL ratio = 5.5 ± 0.2 mg/mm vs TAC LVW/TL ratio = 7.8 ± 0.3 mg/mm).

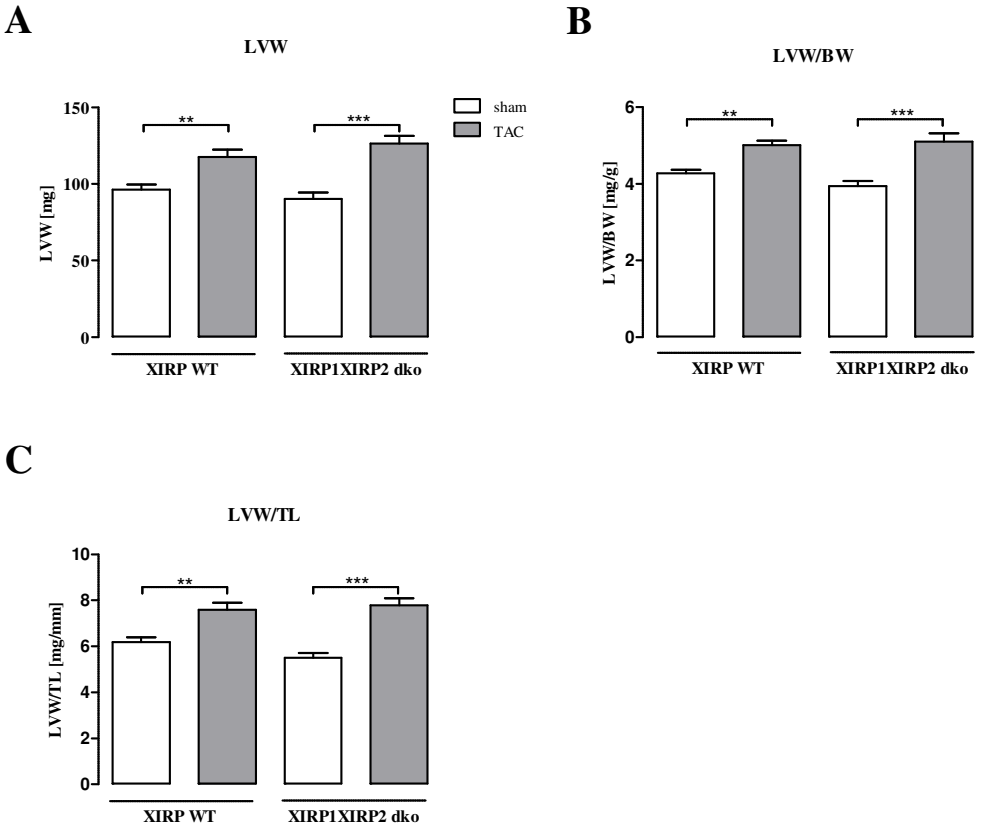

Figure 3.9 LVW, LVW/BW ratio, LVW/TL ratio of XIRP WT and XIRP1XIRP2 dko mice. LVW, LVW/BW ratio, and LVW/TL ratio were significantly increased in the TAC groups to the same level in both genotypes. The data are represented as mean ± SEM; n= 6-9 /group, *P< 0.05 was considered statistically significant.

3.2.4 LW, LW/BW ratio, and LW/TL ratio

14 days of TAC also significantly increased the lung weight parameters in both genotypes. However, in this case all lung weight parameters of XIRP1XIRP2 dko exhibited a tendency to lower values after TAC, reaching the level of significance only in case of LW/TL ratios (Fig. 3.10 A, B, C) (XIRP WT: sham LW 150.8 ± 3.0 mg vs TAC LW 176.3 ± 7.3 mg; sham LW/BW ratio 6.5 ± 0.2 mg/g vs TAC, LW/BW ratio 7.3 ± 0.2 mg/g; sham LW/TL ratio 9.5 ± 0.2 mg/mm vs. TAC LW/TL ratio 11.2 ± 0.4 mg/mm; XIRP1XIRP2 dko: sham LW 144.4 ± 3.9 mg vs TAC LW 166.1 ± 4.8 mg; sham LW/BW ratio 6.3 ± 0.1 mg/g vs TAC LW/BW ratio 6.9 ± 0.2 mg/g; sham LW/TL ratio 8.8 ± 0.2 mg/mm vs TAC LVW/TL ratio 10.1 ± 0.3 mg/mm).

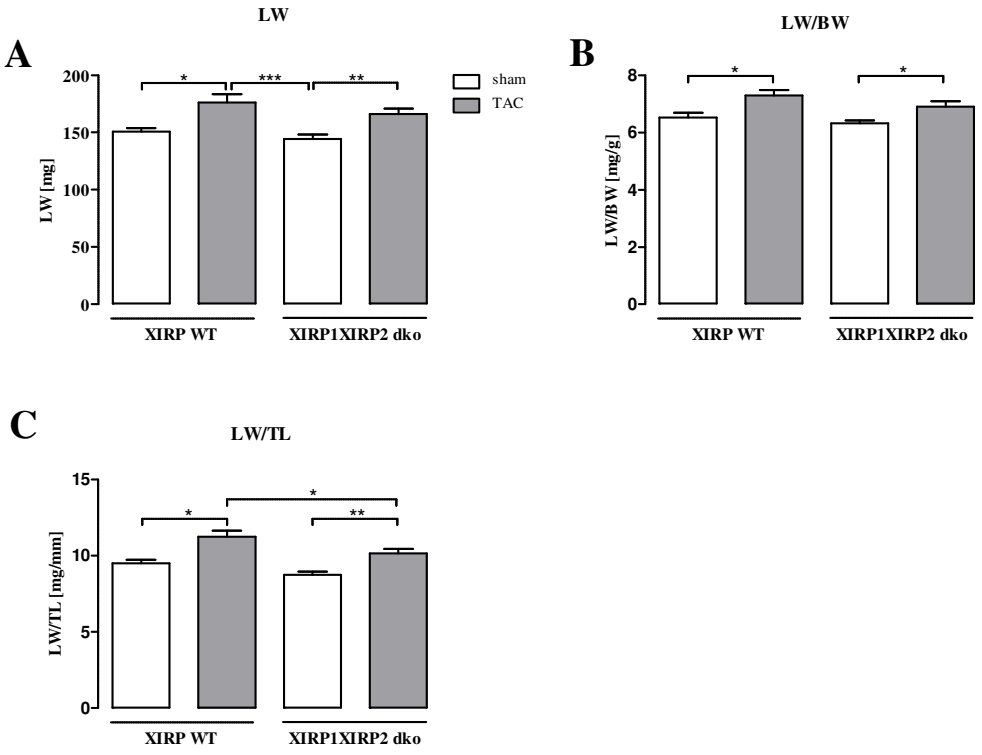

Figure 3.10 LW, LW/BW ratio, LW/TL ratio of XIRP WT and XIRP1XIRP2 dko. TAC increased all LW parameters in both genotypes. But LW/TL ratio was increased in XIRP WT to a higher level than in XIRP1XIRP2 dko mice. The data are represented as mean ± SEM; n= 11-30 /group, **P*< 0.05 was considered statistically significant

3.2.5 Left ventricular and septum thickness

To investigate the influence of the genotype and the TAC on cardiac morphology, sections of the heart were analyzed for left ventricular thickness and thickness of the septum. LV and septum thickness did not differ between sham mice of both genotypes (Fig. 3.11, 3.12). Furthermore TAC induced a significant growth of LV and septum thickness in both mouse strains But did not reveal any differences between the two genotypes in these parameters (LV thickness: XIRP WT sham 0.56 ± 0.03 mm vs. TAC 0.98 ± 0.11 mm; XIRP1XIRP2 dko sham; 0.63 ± 0.03 mm vs. TAC 0.99 ± 0.08 mm; septum thickness: XIRP WT sham 0.57 ± 0.03 mm; XIRP WT TAC 1.0 ± 0.1 mm; XIRP1XIRP2 dko sham 0.65 ± 0.06 mm; XIRP1XIRP2 dko TAC 0.98 ± 0.08 mm).

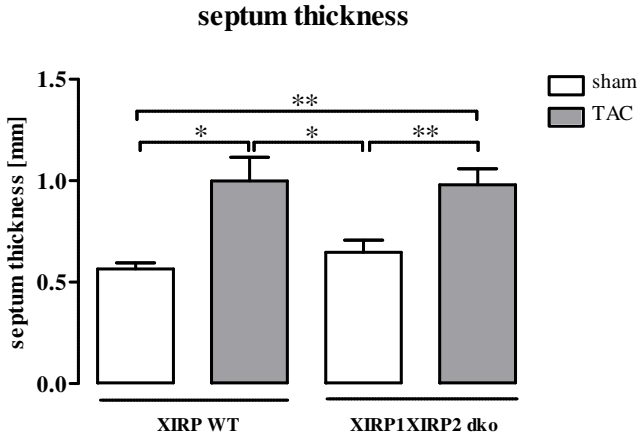

Figure 3.11 Comparison of septum thickness between XIRP1XIRP2 dko and XIRP WT. TAC induced a significant increase in septum thickness reaching the same level in both genotypes. The data are represented as mean ± SEM; n= 6-11 /group, **P*< 0.05 was considered statistically significant.

3.2.6 Fibrosis

Fibrosis was analyzed on cross sections of the cardiac ventricles which were stained by Masson's trichrome. A set of photographs at different magnifications of sham and TAC mice is demonstrated in Fig. 3.12. The pictures were chosen to give an impression of the interstitial fibrosis.

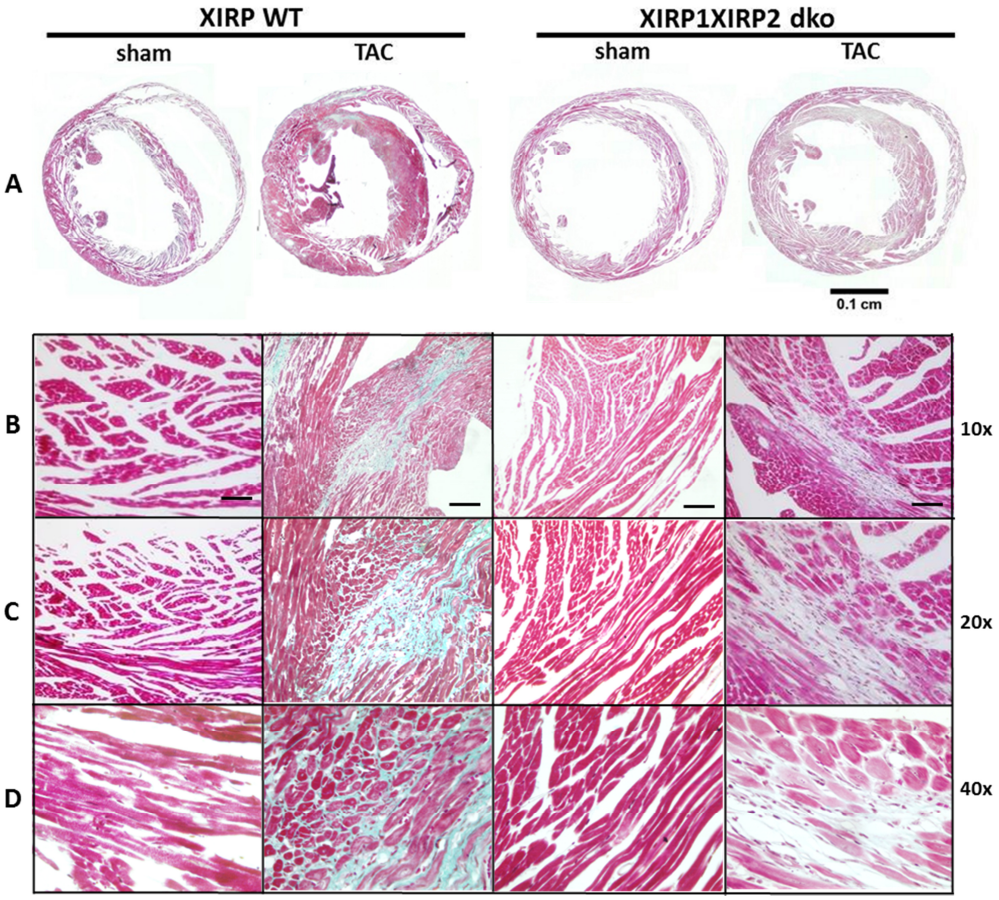

Figure 3.12 Light microscopic photographs of transverse sections of hearts trichrome stained according to Masson from the four groups. **(A)** Low magnification exhibiting the complete sections. **(B-D)** Representative photographs demonstrating the interstitial fibrosis visualized by Masson's trichrome staining in increasing magnifications (scale bar is 500 µm).

In Figure 3.13 the aspect of perivascular fibrosis is emphasized. Perivascular fibrosis was mainly found in TAC mice.

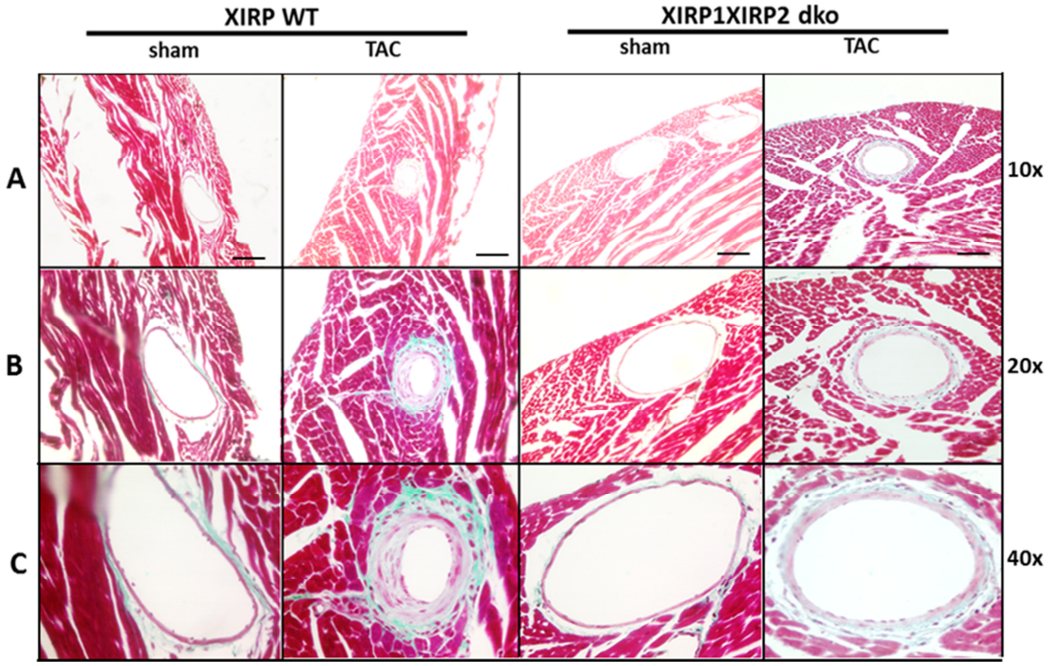

Figure 3.13 Light microscopic photographs of transverse sections of hearts trichrome stained according to Masson from the four groups. **(A-C)** Representative photos of perivascular fibrosis in increasing magnifications (scale bar is 500 µm).

In order to quantify the influence of the TAC and the genotype on the development of fibrosis, photographs demonstrated in Figs. 3.12 and 3.13 were evaluated for the area of fibrosis. This quantification revealed that TAC increased fibrosis in XIRP WT hearts significantly (from 0.17 ± 0.09 % to 4.0 ± 1.1 %). Although an increase of fibrosis was also visible in the XIRP1XIRP2 dko TAC group, this did not reach the level of significance, which is obviously due to a relatively high variation in this group. This high variation also prevented to demonstrate a significant difference between the two TAC groups, which seemed to be visible.

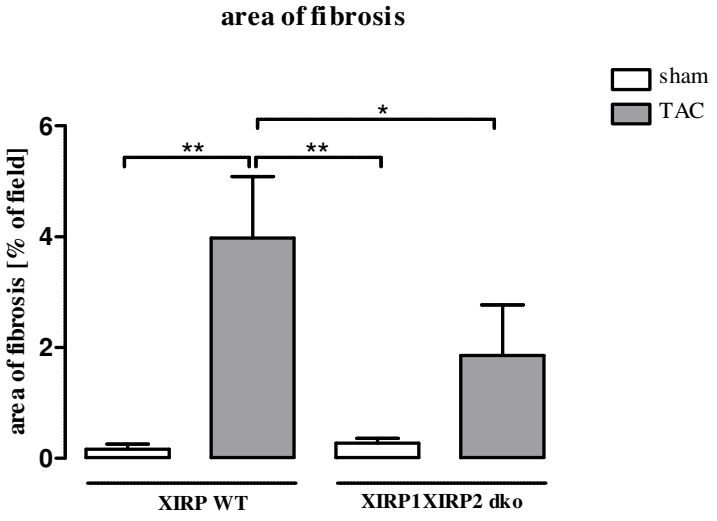

Figure 3.14 Quantified area of fibrosis in sham and TAC hearts of both genotypes. The cardiac interstitial fibrotic area was significantly increased in XIRP WT TAC vs. sham hearts of both genotypes. The data are represented as mean ± SEM; n= 4-7 /group, *P< 0.05 was considered statistically significant.

3.3 Studies on isolated cardiomyocytes

3.3.1 Immunolocalization of different proteins

According to the published role of XIRPs as proteins of the cytoskeleton, the deficiency of these proteins might cause mislocalization of other cytoskeletal proteins. Therefore, a selection of proteins was visualized in isolated cardiomyocytes by immunofluorescence microscopy (performed by Julia Schuld). Cardiomyocytes isolated from XIRP WT sham and TAC and from XIRP1XIRP2 dko sham and TAC hearts were investigated. The cells were stained with antibodies of proteins found in ICDs (connexin43, cadherin) or in Z bands (titin) and M bands (myomesin). The cytoskeletal proteins filamin (Fln) A and C were localized with antibodies binding to both (A/C, Ig-like domains 1-2) and to filamin C exclusively (C, Ig-like domains 16-20) 3.16, and 3.17). Furthermore, the ryanodine receptors (RyRs) were stained as indicators for the triads and the nuclei were marked with Dapi. In the first series myomesin, RyRs, Fln C and nuclei were

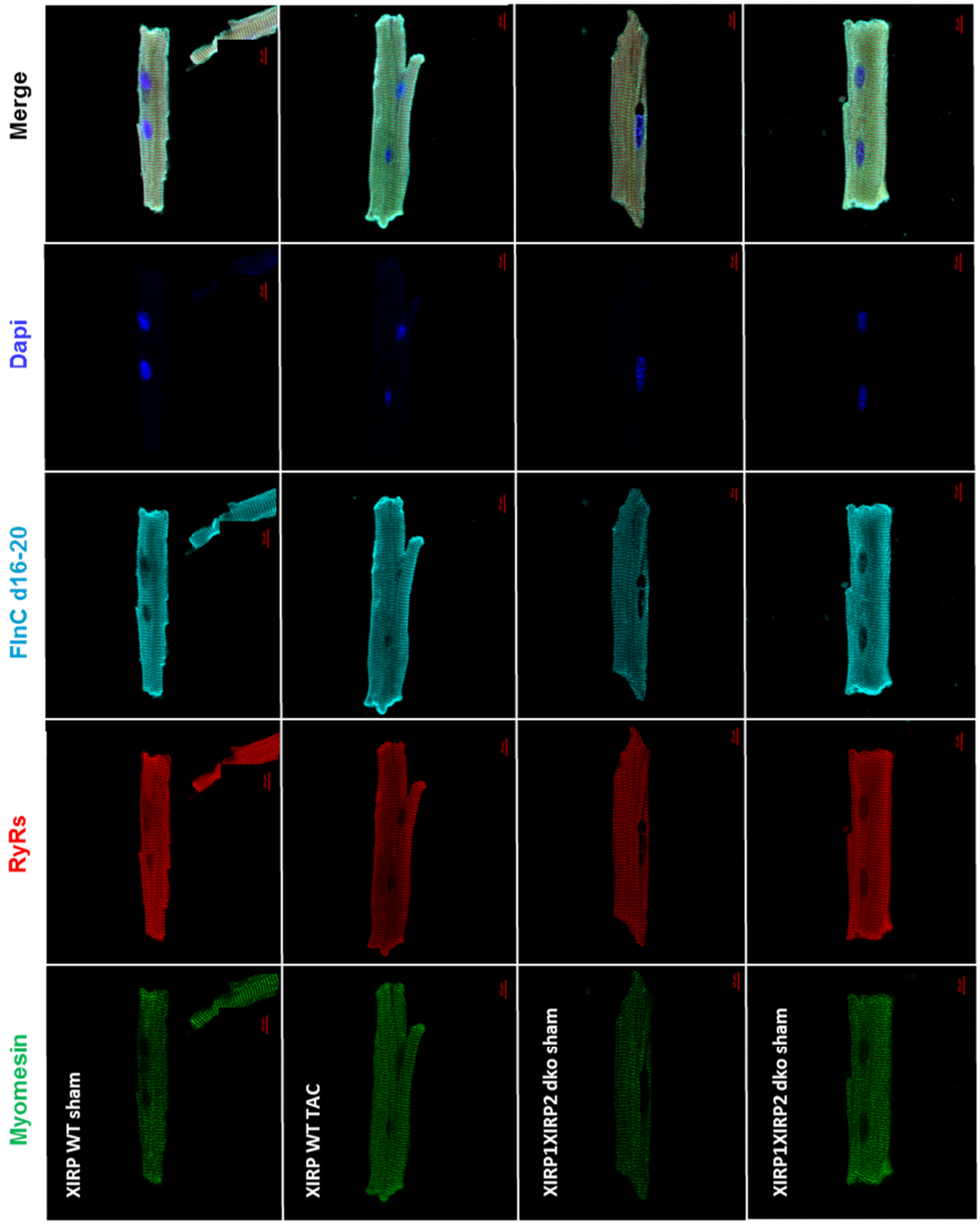

Figure 3.15 Microscopic evaluation and immunolocalization of myomesin, RyRs , and filaminC d16-20 in isolated cardiomyocytes.

stained (Fig. 3.15). Myomesin, RyRs and FlnC display a striation pattern in the cytoplasm and the area of the nuclei appears dark.

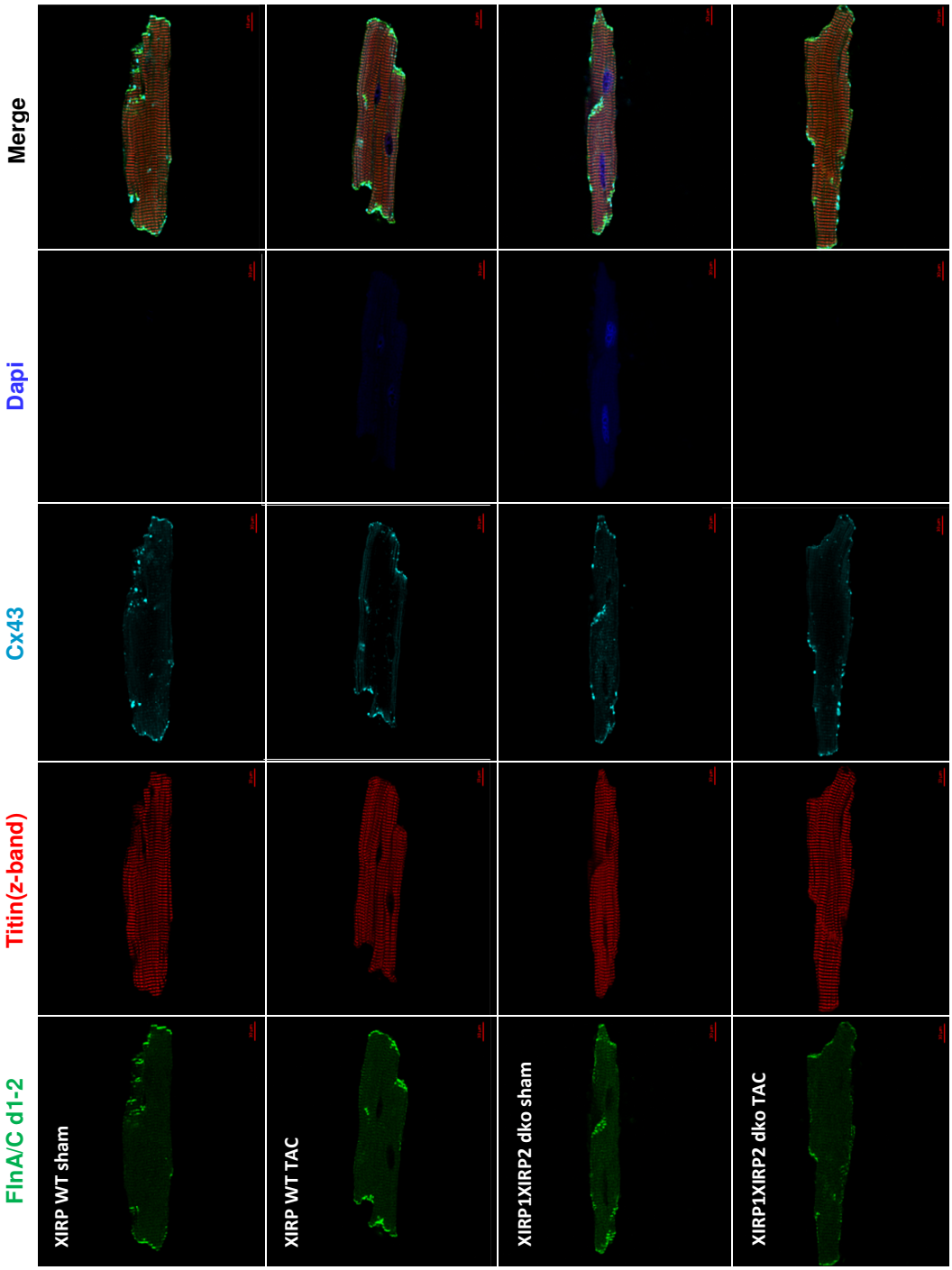

Figure 3.16 Microscopic evaluation and immunolocalization of filaminA/C d1-2, titin, andconnexin43 in isolated cardiomyocytes

Fln C is also detected in the regions of the ICDs. Myomesin and Fln C seem to co-localize in their striation pattern and at the ICDs, whereas RyRs are found in the gaps between these stripes. A basic difference between the four groups could not be detected.

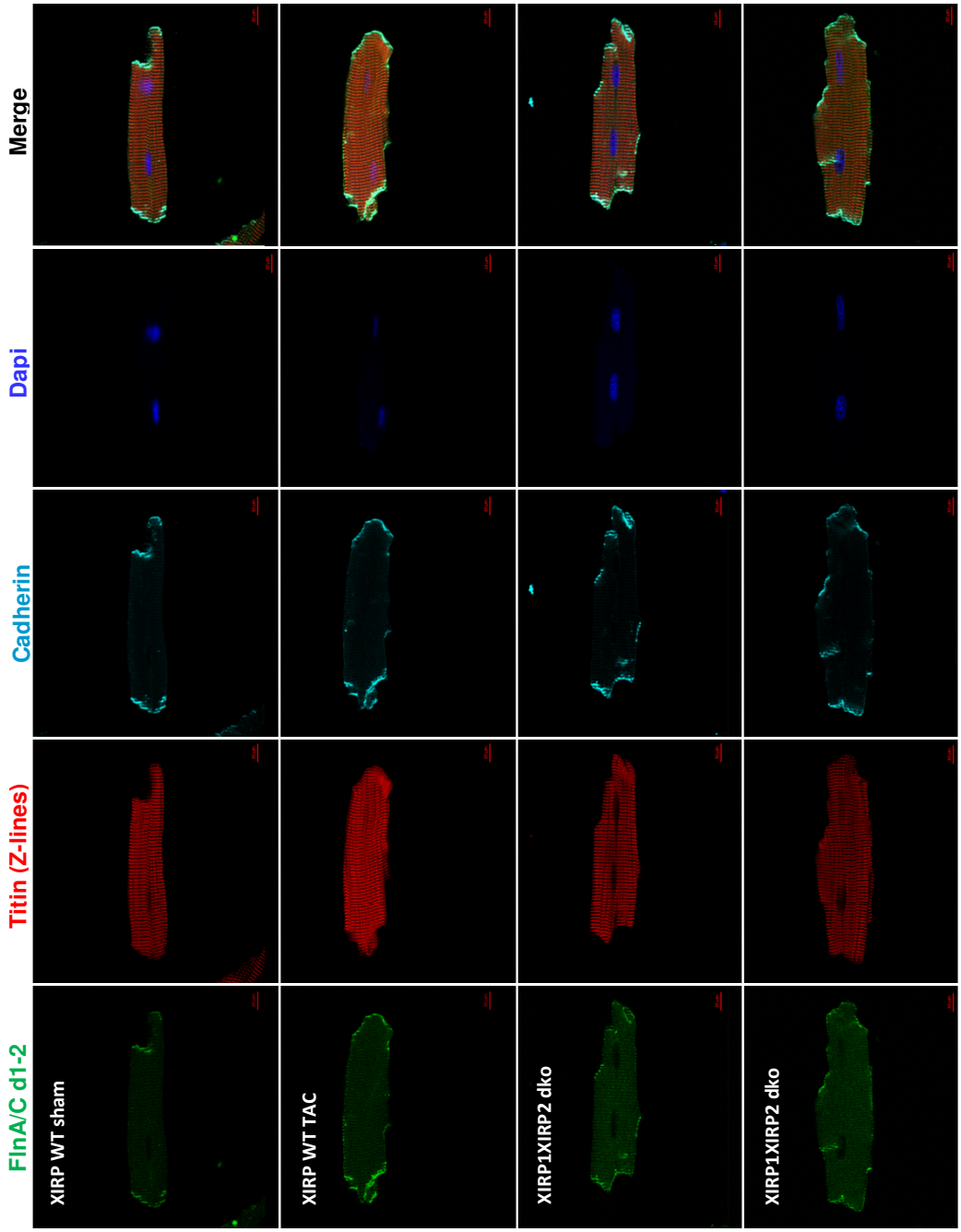

Figure 3.17 Microscopic evaluation and immunolocalization of filaminA/C d1-2, titin, andcadherin in isolated cardiomyocytes.

In a second set of stainings, antibodies (ABs) against Fln A/C, titin (Z-lines) and connexin (Cx) 43 were applied. The Fln A/C and the Cx 43 ABs were concentrated in the regions of the ICDs, where they co-localized. The titin AB exhibited the regular striation pattern of the Z lines. Again an obvious influence of the genotype and the treatment (sham or TAC) could not be detected. In a

third series, ABs against Fln A/C, titin (Z-line) and cadherin were tested. Cadherin was detected in the same regions as the Cx 43 ABs in the experiment before. Also in the experiments with cadherin ABs, neither the genotypes nor the treatments caused an obvious difference in the distribution of the investigated proteins.

3.3.2 Cell size of cardiomyocytes

To check the influence of cardiac hypertrophy, the length and width of isolated cardiomyocytes were measured. XIRP WT sham (n=100), XIRP WT TAC (n=56), XIRP1XIRP2 dko sham (n=52), and XIRP1XIRP2 dko TAC (n=74). The length of the cells did not differ in XIRP WT groups. Interestingly XIRP1XIRP2 dko sham exhibited a significantly higher length than XIRP1XIRP2 dko TAC cells. Moreover, the XIRP1XIRP2 dko sham also were significantly longer than XIRP WT sham cells (cell length; XIRP WT sham 122.1 ± 2.5 µm, TAC 114.7 ± 3.4 µm; XIRP1XIRP2 dko sham 134.3 ± 3.0 µm, TAC 123.4 ± 2.8 µm). The width of the

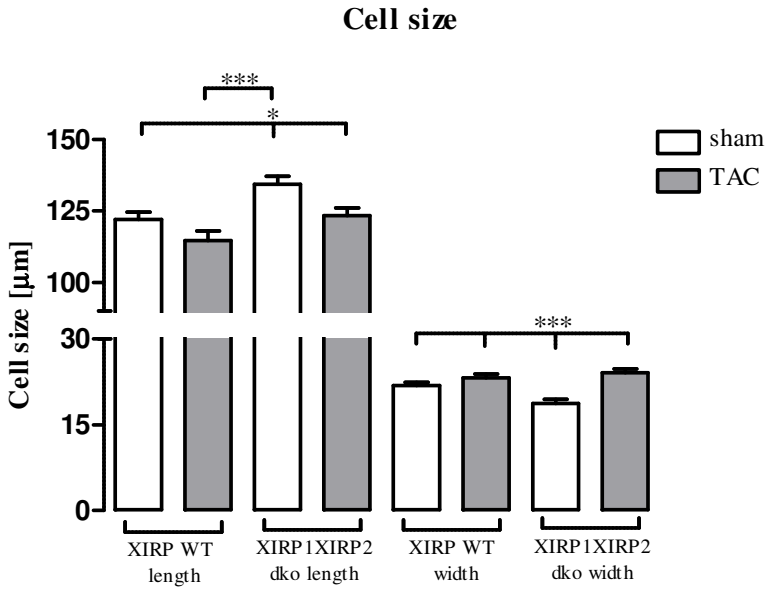

Figure 3.18 Cardiomyocyte length and width.

XIRP1XIRP2 dko cardiomyocytes reached significantly higher values after TAC, whereas the XIRP WT cardiomyocytes exhibited only a trend to transversal growth (XIRP WT sham 22.2 ± 0.7 µm, TAC 23.2 ± 0.7 µm; XIRP1XIRP2 dko sham 18.8 ± 0.7 µm; XIRP1XIRP2 dko TAC 24.1 ± 0.7 µm) (Fig. 3.18).

3.3.3 The distribution of ICDs

ICD-associated proteins were analysed by immunofluorescence microscopy. Staining for cadherin and connexin43 demonstrated that XIRP WT and XIRP1XIRP2 dko cells contained same amounts of terminal ICDs, while the number of non- terminal ICDs was significantly increased in XIRP WT sham and XIRP WT TAC cells (terminal ICDs; XIRP WT sham 3.0 ± 0.1; XIRP WT TAC 2.8 ± 0.1; XIRP1XIRP2 dko sham 3.3 ± 0.2; XIRP1XIRP2 dko TAC 3.1 ± 0.1 and non-terminal ICDs; XIRP WT sham 4.7 ± 0.3; XIRP WT TAC 5.1 ± 0.3; XIRP1XIRP2 dko sham 3.4 ± 0.2; XIRP1XIRP2 dko TAC 3.36 ± 0.2) (Fig. 3.19).

A

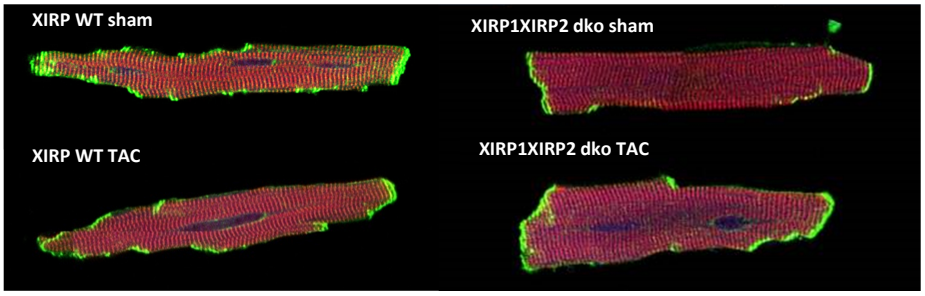

B

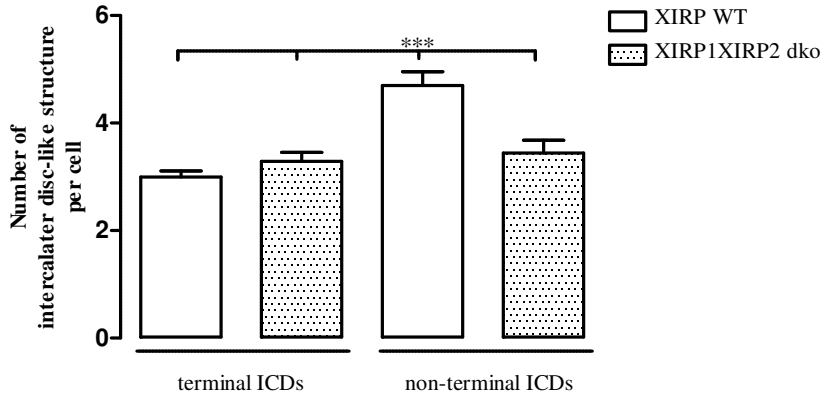

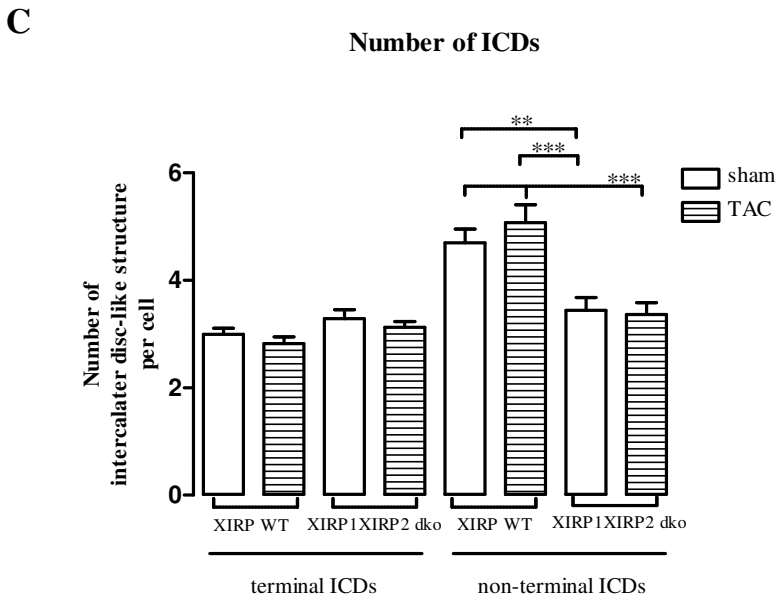

Figure 3.19 The single cardiomyocyte and number of terminal and non-terminal ICDs.

A) The single cardiomyocytes in all groups

B) The number of terminal and non-terminal ICDs of XIRP WT and XIRP1XIRP2 dko

C) The number of terminal and non-terminal ICDs of XIRP WT and XIRP1XIRP2 dko after 14 days TAC

3.4 Hemodynamic parameters

3.4.1 Hemodynamic data after 14 days TAC

TAC surgery significantly increased systolic arterial pressure (SAP) and left ventricular systolic pressure (LVSP) by 50-60 mmHg, which reached comparable levels in mice of both genotypes. DAP was not increased XIRP WT mice. This indicates successful aortic banding In XIRP1XIRP2 dko mice DAP even showed a trend to decrease. The end-diastolic pressure (EDP) showed a trend to increase in TAC mice and reached the level of significance in XIRP1XIRP2 dko mice. The dP/dt $_{max}$ as well as dP/dt $_{min}$ became faster in both genotypes due to TAC, and dP/dt $_{max}$ rose significantly more in XIRP WT than XIRP1XIRP2 dko mice. This may be taken as a sign for a compensated hypertrophy. Heart rate (HR) was also significantly increased in both TAC groups by 16% in XIRP WT and by 8% in XIRP1XIRP2 dko (Fig. 3.20 A, B, C, D, E, F and Table. 3.2).

Table 3.2 The hemodynamic data of XIRP WT and XIRP1XIRP2 dko mice

	XIRP WT		**XIRP1XIRP2 dko**	
	Sham	*TAC*	*Sham*	*TAC*
n (number of the mice)	7	11	23	27
SAP (mm Hg)	107.5 ± 2.0	160.3 ± 4.5 [a]	104.1 ± 2.0	156.8 ± 2.2 [a]
DAP (mm Hg)	78.7 ± 2.5	83.0 ± 1.1 [b]	78.1 ± 1.8	73.9 ± 1.2
MAP (mm Hg)	90.2 ± 2.4	113.8 ± 1.9 [a]	88.5 ± 1.5	108.7 ± 1.2 [a]
LVSP (mm Hg)	106.8 ± 3.6	158.8 ± 5.1 [a]	99.3 ± 2.6	156.6 ± 1.8 [a]
EDP (mm Hg)	8.8 ± 1.6	12.1 ± 2.1	6.7 ± 1.0	13.2 ± 0.1 [a]
LV dP/dt $_{max}$ (mm Hg/s)	9470.7 ± 583.8	11739.5 ± 610.1 [a]	8570.8 ± 248.8	9729.2 ± 349.3 [a]
LV dP/dt $_{min}$ (mm Hg/s)	-10525.1 ± 535.2	-12255.7 ± 767.6 [a]	-9651.5 ± 382.5	-11044.2 ± 381.0 [a]
HR (beat/min)	509.3 ± 11.6	590.3 ± 12.6 [a]	535.7 ± 11.8	576.1 ± 6.5 [a]

All values are shown as means ± SEM for *n* mice. SAP (systolic arterial pressure), DAP (diastolic arterial pressure), MAP (mean arterial pressure), LVSP (left ventricular systolic pressure), EDP (end diastolic pressure), dP/dt $_{max}$ (maximum left ventricular dP/dt$_{max}$, dP/dt$_{min}$ (the minimum left ventricular dP/dt), HR (heart rate). [a]; $P< 0.05$ vs sham [b]; $P< 0.05$ vs XIRP1XIRP2 dko TAC

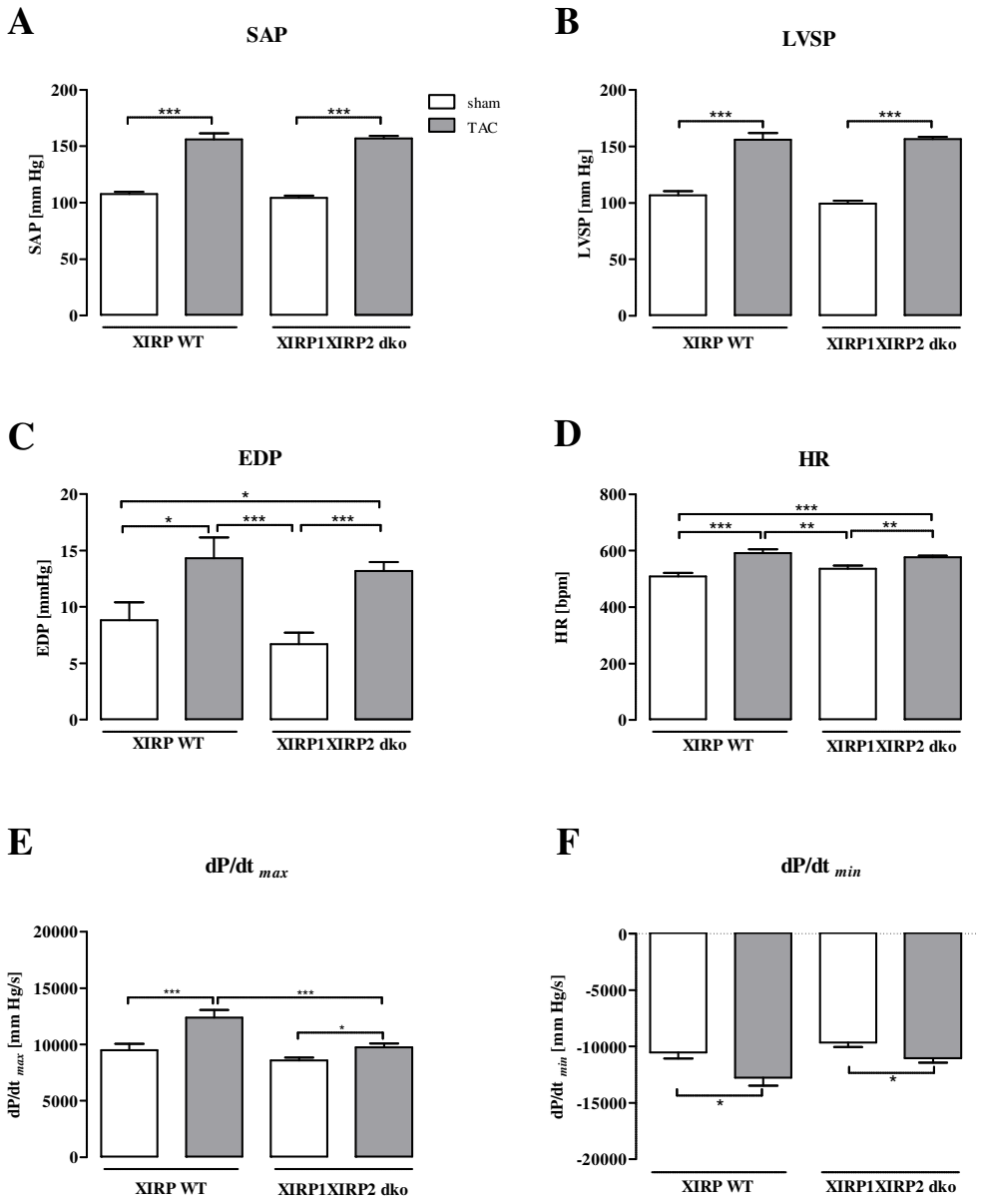

Figure 3.20 Hemodynamic data of XIRP WT and XIRP1XIRP2 dko female after TAC. (**A, B**) TAC surgery increased SAP and LVSP in both genotypes by about the same degree. **(C)** EDP was also increased in TAC mice of both genotypes. **(D)** HR was significantly elevated in both TAC groups. **(E, F)** dP/dt_{max} as well as dP/dt_{min} became faster in both genotypes due to TAC. dP/dt_{max} of XIRP WT TAC mice reached significantly higher level than that of XIRP1XIRP2 dko TAC mice. The data are represented as mean ± SEM; n= 8-29 /group, **P*< 0.05 was considered statistically significant.

3.5 Electrocardiogram

An electrocardiogram (ECG) allows detection of the electrical excitation of the heart. In this study, the surface ECG lead II according to Einthoven was recorded. In Fig 3.21 the coupling of the electrodes is presented in man and mouse. Lead II means that the voltage difference between the right arm and the left leg is monitored. The typical recordings from man and mouse are shown in Fig. 3.21 B. Due to the high heart rates and the small size of the mice, the shape of both ECG differs remarkably. The ECGs were recorded under anesthesia (1% isoflurane) in sham and TAC mice of both genotypes.

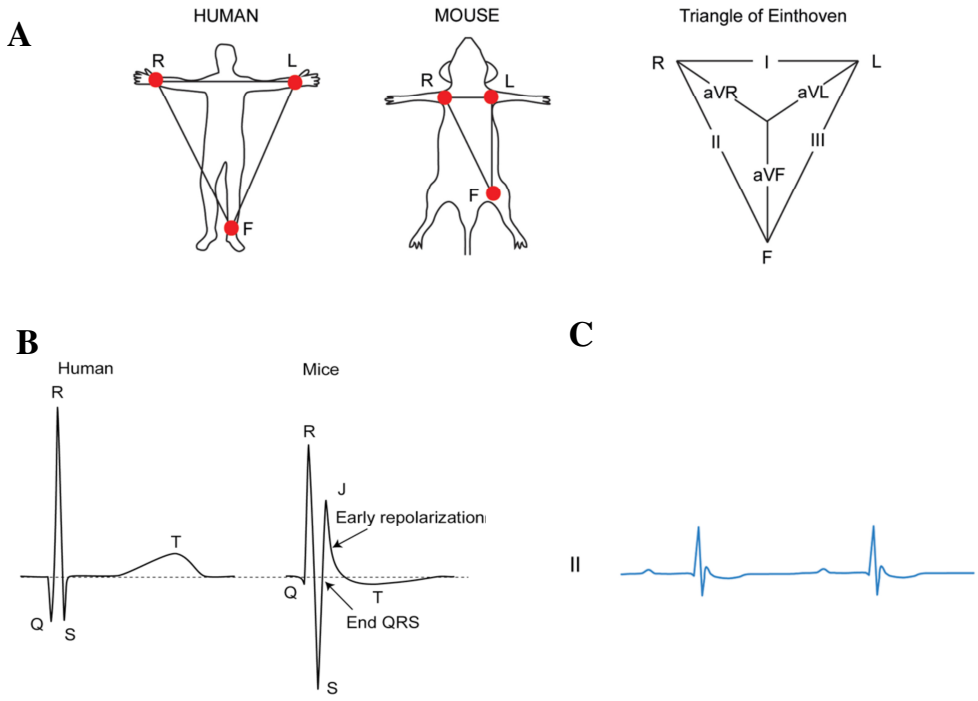

Figure 3.21 The ECG of a human and a mouse.
(A) Schematic drawings of the positions of the leads R, L and F in humans and mice and the triangle of Einthoven respectively **(B)** Schematic representation of the human and murine ECG **(C)** Schematic standard ECG lead II. (Slightly modified from Boukens et al., 2014)

Abnormal ECGs were not found in recordings from XIRP WT mice neither in the sham nor in the TAC group. In contrast, ECG recordings from XIRP1XIRP2 dko TAC mice exhibited an irregular HR and missing P waves in 9.0%, biphasic (bifid) p-waves in 18.2%, and ST elevations in 4.6% of the recordings, while the XIRP1XIRP2 sham mice ECG recordings developed biphasic P waves in 38.5% of the recordings.

3.5.1 Surface ECG parameters

ECG records were non-invasively obtained from 1% isoflurane anesthetized mice on the measurement day. HR, P wave, PQ interval, QRS duration and QT interval are summarized in Table 3.3. In both genotypes there was a tendency to an increased HR in the TAC groups but the level of significance was not reached. P wave duration, PQ interval as well as QT interval were significantly prolonged in XIRP1XIRP2 dko TAC mice compared to their respective controls.
In the XIRP WT TAC mice there was a tendency to prolongation in P wave duration and PQ

Table 3.3 Surface ECG parameters

	XIRP WT ***sham*** (n=6)	**XIRP WT** ***TAC*** (n=5)	**XIRP1XIRP2 dko** ***sham*** (n=15)	**XIRP1XIRP2 dko** ***TAC*** (n=20)
Heart rate (bpm)	517.0 ± 8.5	563.3 ± 25.1	508.1 ± 14.4	520.1± 13.4
P duration (ms)	15.2 ± 1.2	18.0 ± 0.8	14.1 ± 1.2	19.5 ± 0.8[a,b]
PQ (ms)	29.2 ± 0.7	34.4 ± 1.4	32.5 ± 0.4	38.6 ± 1.2[a,b]
QRS (ms)	11.3 ± 1.1	12.3 ± 1.1	9.6 ± 0.2[b]	11.0 ± 0.4
QT (ms)	45.5 ± 3.1	49.6 ± 3.1	41.5. ± 1.5	52.5 ± 2.9[a]

All values are shown as means ± SEM for n mice, statistically significant difference (P< 0.05) by all groups comparison.
[a]; P< 0.05 vs XIRP1XIRP2 dko sham
[b]; P< 0.05 vs XIRP WT sham

interval compared to their controls. Also the QRS complex and the QT interval showed trend to prolongation in the TAC groups. QT interval was longer both TAC genotypes compared to their controls, reaching significance level in the XIRP1XIRP2 dko mice. The tendency prolongation of

QRS and QT interval can be explained by an increase in conduction time in the ventricle probably because of cardiac hypertrophy and fibrosis.

3.5.2 The ECG variations

In this chapter examples for the different ECG variations are given. Fig. 3.22 demonstrates two normal mouse ECG recorded from XIRP WT sham (A) and TAC (B).

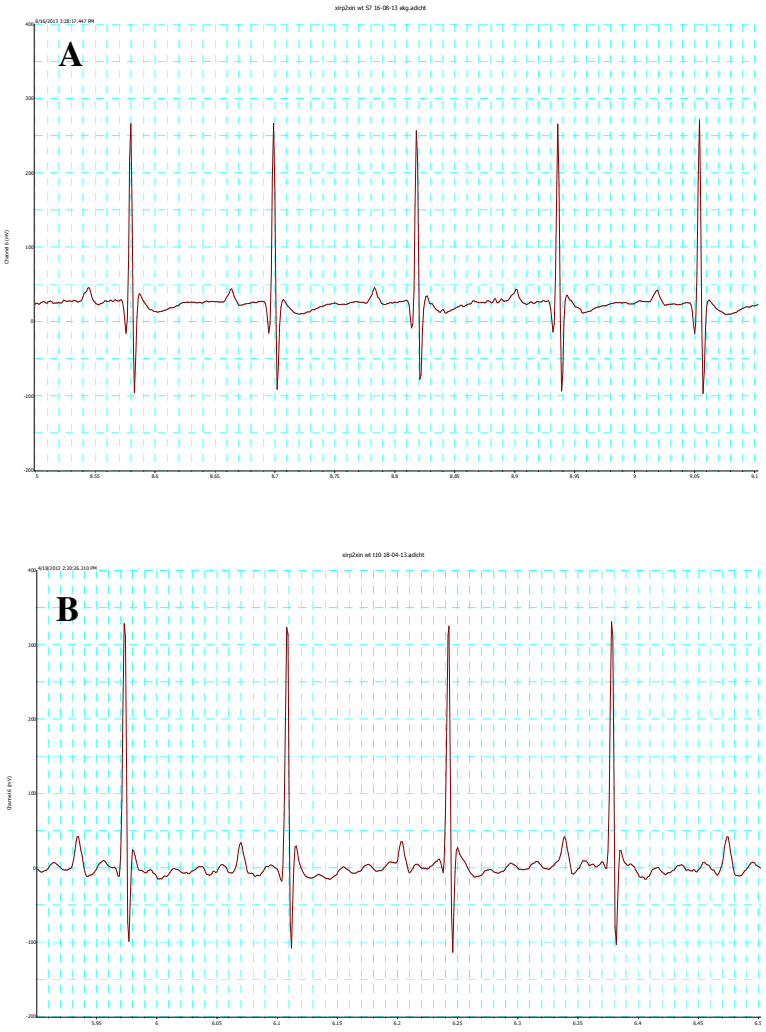

Figure 3.22 ECGs from XIRP WT sham and TAC. ECGs of a XIRP WT sham **(A)** and XIRP WT TAC mouse with normal sinus rhythm are plotted. In **(B)** a 50 Hz disturbance is visible. Digitizing frequency was 1 kHz in all ECGs.

In Figure 3.23 a physiological ECG from a XIRP1XIRP2 dko sham heart is compared to a XIRP1XIRP2 dko TAC heart. The TAC heart exhibits a ventricular extra systole (arrow) followed by a P wave triggered by the sinus rhythm. This P wave is unable to excite the ventricle, possibly due to a refractory AV-node.

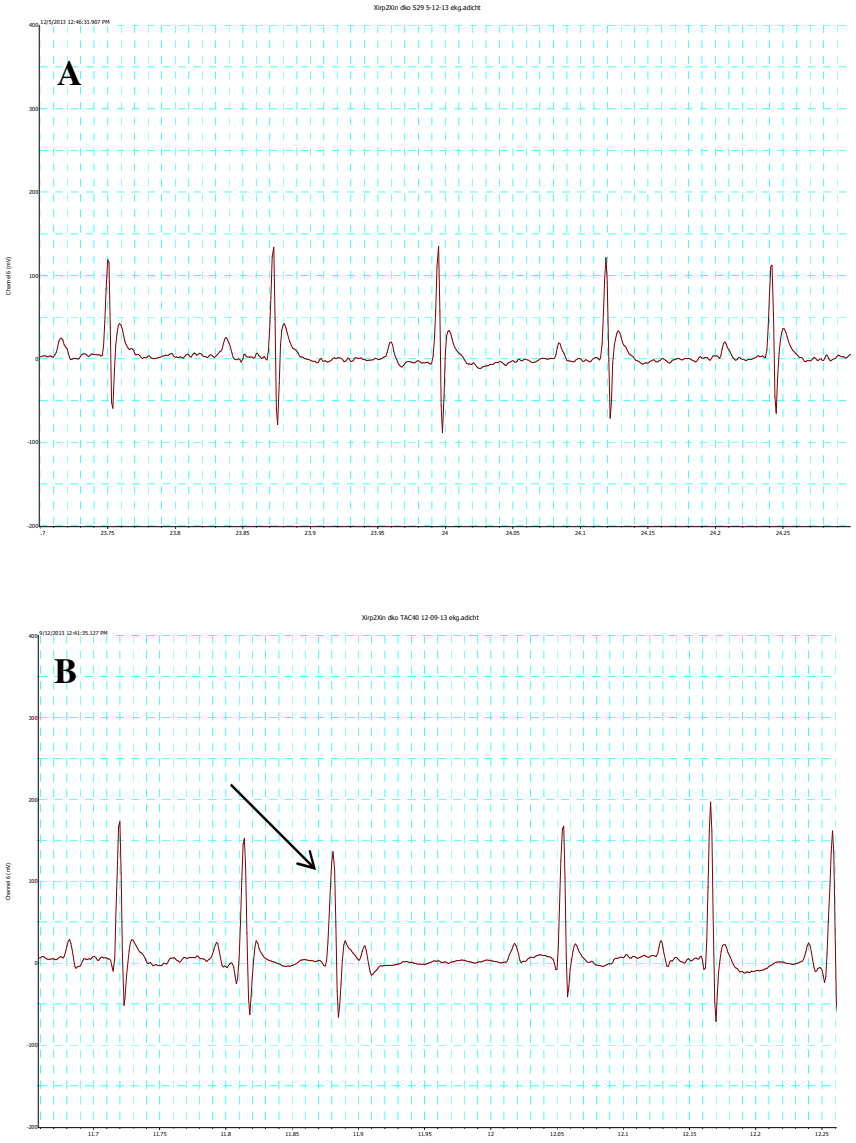

Figure 3.23 ECGs from XIRP1XIrp2 dko sham **(A)** and TAC **(B)** mice.
(A) An ECG with normal sinus rhythm is demonstrated. **(B)** This ECG from a XIRP1XIRP2 dko TAC mouse shows an extra systole (arrow) followed by a P wave and then a pause before the normal sinus rhythm is restored.

Biphasic P waves appeared only in XIRP1XIRP2 dko mice, surprisingly to a higher amount in sham (38%) than in TAC animals. Two examples, one in a sham (A) and one in a TAC (B) animal, are demonstrated in Fig. 3.24.

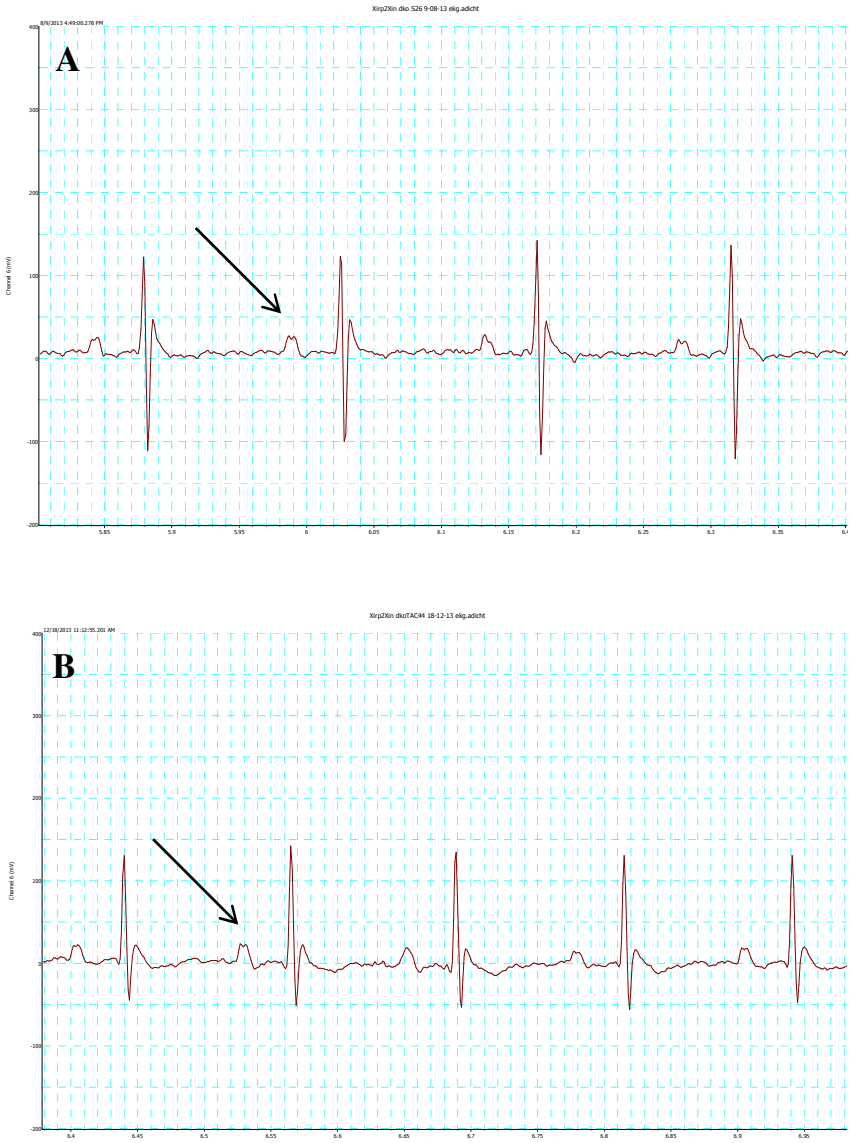

Figure 3.24 ECGs from XIRP1XIRP2 dko sham **(A)** and TAC **(B)** mice.
Both ECGs exhibit biphasic P waves marked by arrows in **(A)** and **(B)**.

One XIRP1XIRP2 dko TAC mouse developed a ST elevation (arrow), which can be taken as an indication for a ischemia. Also biphasic P waves can be identified in figure 3.25.

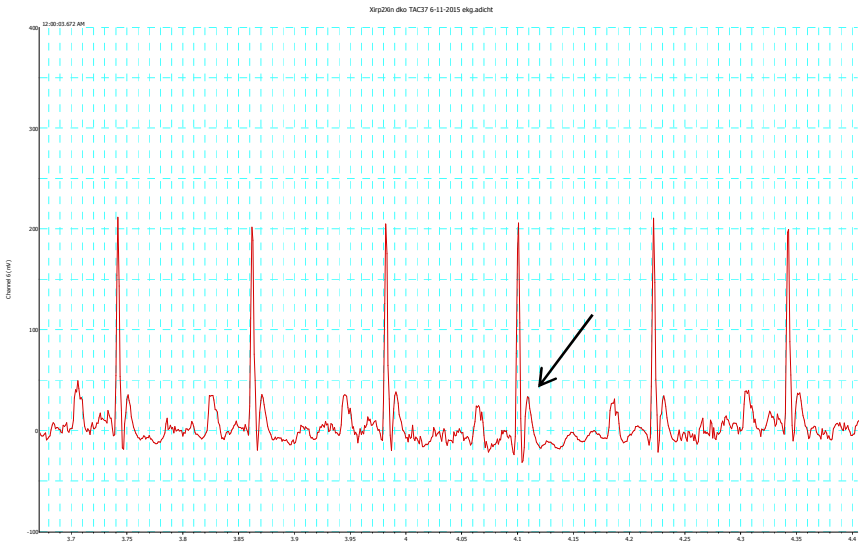

Figure 3.25 ECG from a XIRP1XIRP2 dko TAC mouse.
The ECG of the XIRP1XIRP2 dko TAC mouse exhibits an ST elevation (arrow).

3.6 Comparison of three month old with one year old mice

3.6.1 HW, HW/BW ratio, and HW/TL ratio

To investigate whether the XIRP1XIRP2 dko mice develop a spontaneous cardiac hypertrophy when they become older, one year old mice of the XIRP WT and knockout genotypes were inspected for their heart weight parameters. The data were compared to those of three month old

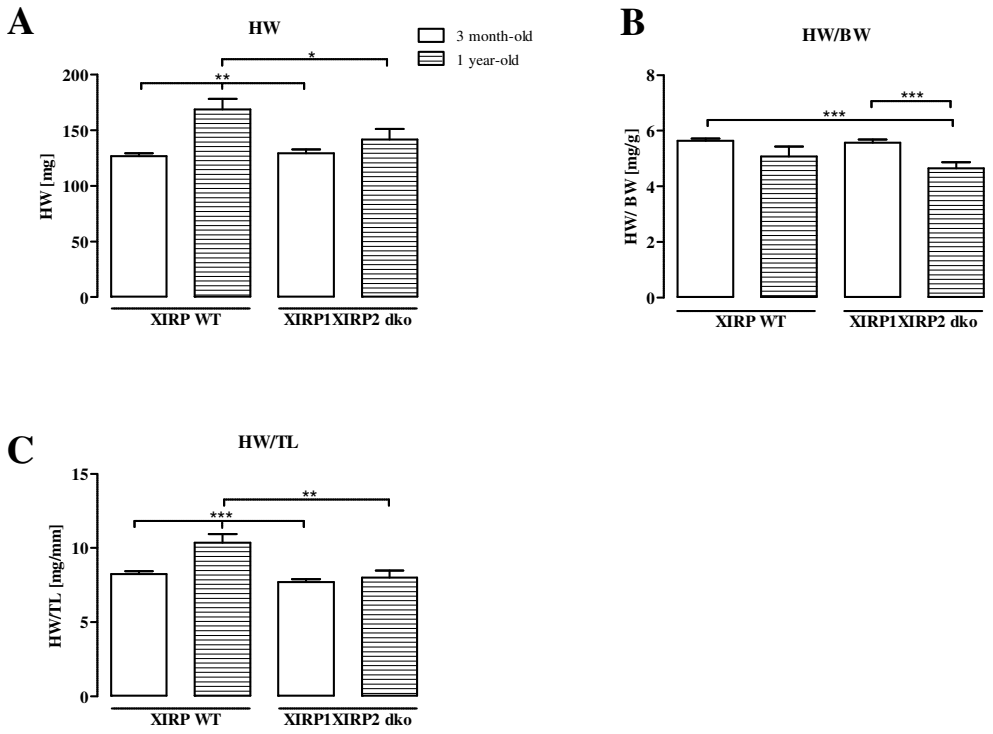

Figure 3.26 HW, HW/BW ratio and HW/TL ratio of XIRP WT and XIRP1XIRP2 dko 3 month-old and 1 year-old mice. HW and HW/TL ratio of XIRP WT 1 year-old mice were significantly higher than all other corresponding groups **(A, C)**. HW/BW ratio of XIRP1XIRP2 dko 1 year-old mice was significantly smaller than the two 3 month old groups. The data are represented as mean ± SEM; n= 3-23 /group, **P*< 0.05 was considered statistically significant.

mice, which have already been presented in chapter 3.1.7. The absolute HW was significantly higher in the case of the older WT animals. However, the XIRP1XIRP2 dko hearts gained only moderately weight during aging, which was not sufficient to reach the level of significance.

Consequently, the HW was significantly higher in one year old WT mice than in the XIRP1XIRP2 dko mice (3 month old XIRP WT HW 127 ± 2.1 mg n= 8 and 1 year-old 168.7 ± 9.5 mg n = 3 vs. 3 month old XIRP1XIRP2 dko HW 129.2 ± 3.8 mg n = 20 and 1 year old 141.7 ± 9.6 mg n = 6). As the animals gained relatively more BW than HW, the HW/BW ratio fell in both genotypes, reaching the level of significance in XIRP1XIRP2 dko mice (3 month old XIRP WT HW/BW ratio 5.6 ± 0.08 n= 11 and 1 year-old 5.03 ± 0.36 mg/g n = 3 vs. 3 month old XIRP1XIRP2 dko HW/BW ratio 5.6 ± 0.1 n = 23 and 1 year old 4.7 ± 0.2 mg/g n = 6). The standardization of HW to TL resulted in a comparable situation as in case of the absolute HW (3 month old XIRP WT HW/TL ratio 8.23 ± 0.19 mg/mm n = 11 and 1 year-old 10.4 ± 0.6 mg/mm n=3 vs 3 month old XIRP1XIRP2 dko HW/TL ratio 7.7 ± 0.2 n = 23 and 1 year old 8.0 ± 0.5 mg/mm n = 5) (Figure 3.26 A, B, and C).

3.6.2 LVW, LVW/BW ratio, and LVW/TL ratio

An equal comparison of LVW, LVW/BW and LVW/TL among the four groups, described in chapter 3.6.1 for the HW parameters, revealed comparable results. The absolute LVW was significantly highest in one year old XIRP WT compared to all other groups (3 month old XIRP WT LVW 96.5 ± 3.2 mg n = 6 and 1 year-old 126.0 ± 4.0 0.3 mg n = 3 vs. 3 month old XIRP1XIRP2 dko LVW 90.3 ± 4.2 n = 9 and 1 year old 98.8 ± 7.1 mg n = 5) (Figure 3.27 A). LVW/BW ratio was smallest in the one year old XIRP1XIRP2 dko compared to the three other groups, reaching significance only in comparison to the three month old groups (3 month old XIRP WT LVW/BW ratio 4.3 ± 0.1 n = 6 and 1 year-old 3.8 ± 0.33 mg/g n = 3 vs. 3 month old XIRP1XIRP2 dko LVW/BW ratio 3.9 ± 0.1 mg/g n = 9 and 1 year old 3.4 ± 0.2 mg/g n = 6). Like LVW, also the LVW/TL ratio was significantly highest compared to all other groups (3 month old XIRP WT LVW/TL ratio 6.2 ± 0.2 mg/mm n = 6 and 1 year-old 7.7 ± 0.2 mg/mm n=3 vs 3 month old XIRP1XIRP2 dko LVW/TL ratio 5.5 ± 0.2 n = 9 and 1 year old 6.0 ± 0.3 mg/mm n = 6) (Figure 3.27 A, B, and C)

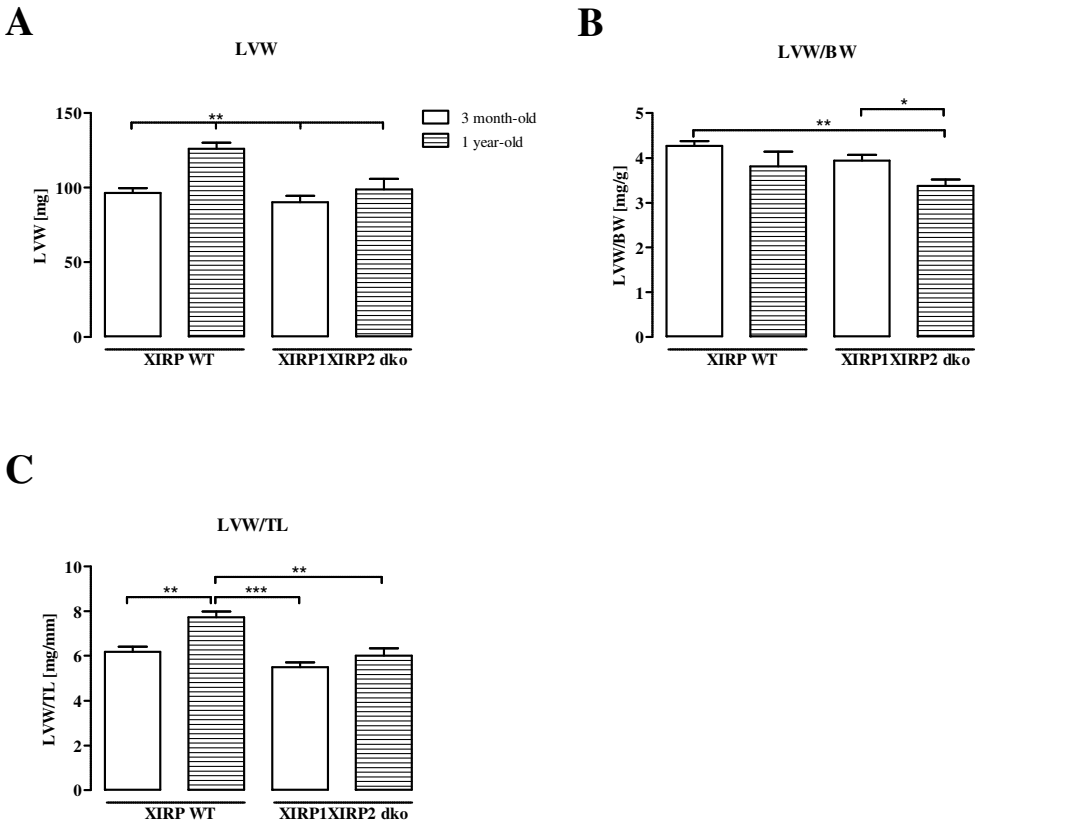

Figure 3.27 LVW, LVW/BW ratio and LVW/TL ratio of 3 month-old and 1 year-old XIRP WT and XIRP1XIRP2 dko mice. LVW and LVW/TL ratio of XIRP WT 1 year-old mice were significantly higher than all other corresponding groups **(A, C)**. LVW/BW ratio of XIRP1XIRP2 dko 1 year-old mice was significantly smaller than that of the two 3 month old groups. The data are represented as mean ± SEM; n= 3-23 /group, **P*< 0.05 was considered statistically significant.

3.6.3 LW, LW/BW ratio, and LW/TL ratio

Like described in the chapters 3.61 and 3.6.2 for HW and LVW parameters also absolute LW was investigated comparably. Absolute LW was highest in the one year old XIRP WT mice, reaching significance only vs the two three month old groups (3 month old XIRP WT LW 150.8 ± 3.0 mg

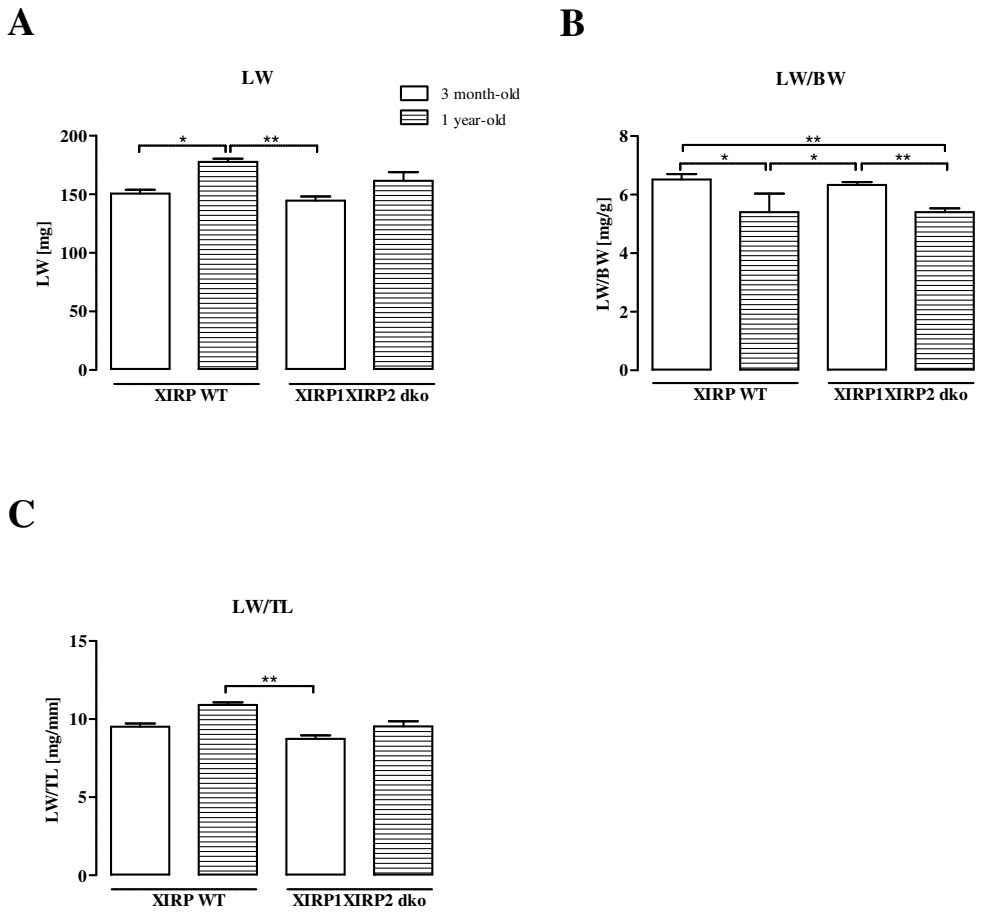

Figure 3.28 LW, LW/BW ratio, and LW/TL ratio of 3 month-old and 1 year-old XIRP WT and XIRP1XIRP2 dko mice. LW was significantly higher in XIRP WT 1 year-old than both 3 month old groups. LW/BW ratio was significantly lower in one year old compared to three month old mice in both genotypes. LW/TL ratio of 1 year-old mice was slightly higher than 3 month-old mice but did not reach level of significance in both genotypes. The data are represented as mean ± SEM; n= 3-20 /group, $*P< 0.05$ was considered statistically significant.

n = 11 and 1 year-old 177.7 ± 2.7 mg n = 3 vs. 3 month old XIRP1XIRP2 dko LW 144.4 ± 4.2 n = 23 and 1 year old 161.3 ± 7.1 mg n = 5) (Figure 3.28 A). In case of LW/BW both one year old groups were significantly smaller than the two 3 month old groups, but they did not differ among each other (3 month old XIRP WT LW/BW 6.5 ± 0.71 n = 11 and 1 year-old 5.4 ± 0.6 mg/g n = 3 vs. 3 month old XIRP1XIRP2 dko LW/BW 6.3 ± 0.1 mg/g n = 23 and 1 year old 5.4 ± 0.1 mg/g n = 6). LW/TL ratio of 1 year-old mice was slightly higher than in 3 month-old mice but not reach level of significance within both genotypes (3 month old XIRP WT LW/TL ratio 9.5 ± 0.2 mg/mm n = 11 and 1 year-old 10.9 ± 0.2 mg/mm n=3 vs 3 month old XIRP1XIRP2 dko LW/TL ratio 8.7 ± 0.2 n = 23 and 1 year old 9.5 ± 0.4 mg/mm n = 6) (Figure 3.28 A, B, and C).

3.6.4 HW, HW/BW ratio and HW/TL ratio after TAC

As a sign for a spontaneous development of cardiac hypertrophy could not be detected in the one year old XIRP1XIRP2 dko mice TAC was applied to these old mice. The development of cardiac hypertrophy was compared between the three month old and the one year old animals. The data of the three month old mice are the same as those presented in chapter 3.2. In the three month old TAC induced a significant increase of HW, HW/BW ratio and HW/TL ratio in both genotypes. However, even in a limited post-test (Sidak´s multiple comparison test) comparing only the four sham groups of interest with the respective TAC groups the one year old animals did not reach the level of significance. This may in part be attributed to the smaller amounts of old animals which were available (XIRP WT 3 month old sham n = 8 vs TAC n = 16; 1 year old sham n = 3 vs. TAC n = 4; XIRP1XIRP2 dko 3 month old sham n = 20 vs. TAC n = 27; 1 year old sham n = 6 vs. TAC n = 13). But the percentage of cardiac growth, which was achieved within 14 days was clearly smaller in the older animals (HW of XIRP WT 3 month old 28.9% vs 1 year old 14.4% growth, of XIRP1XIRP2 dko 3 month old 33.3% vs. 1 year old 25.6% growth) (Fig. 3.29 A).

In case of HW/BW, again the two genotypes of three month old mice reached a significant hypertrophy within 14 days. In the groups of the one year mice the XIRP1XIRP2 dko mice reached the level of significance in the limited post-test also applied in HW. The level of HW/BW gained the older animals during TAC was smaller than in the younger like in case of HW (HW/BW of XIRP WT 3 month old 21.1% vs 1 year old 13.4% growth, of XIRP1XIRP2 dko 3 month old 27.8% vs. 1 year old 22.2% growth) (Fig. 3.29 B).

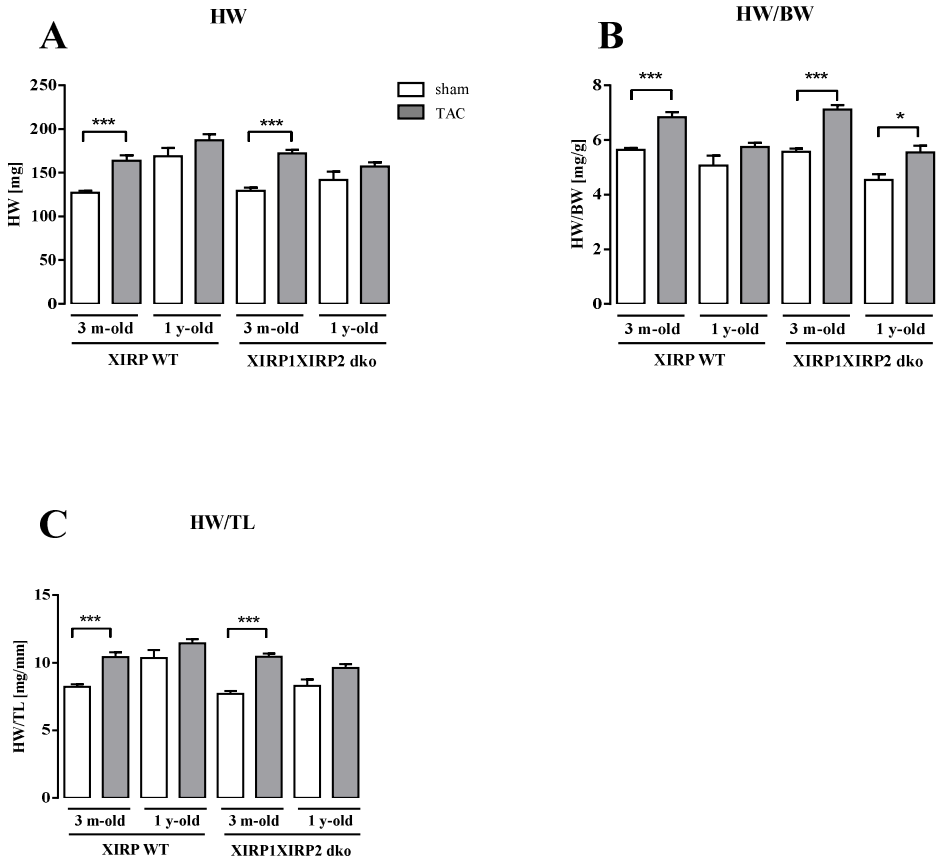

Figure 3.29 HW, HW/BW and HW/TL ratio of 3 month-old and 1 year-old XIRP WT and XIRP1XIRP2 dko mice after 14 days TAC. HW, HW/BW ratio, and HW/TL ratio of 3 month-old mice were significantly increased in both genotypes. For 1 year-old mice the same parameters were increased but only HW/BW of XIRP1XIRP2 dko mice reached the level of significance. The data are represented as mean ± SEM; n= 3-27 /group, **P*< 0.05 was considered statistically significant.

Also in the HW/TL ratio both genotypes of the three month old mice gained a significant hypertrophy within 14 days, whereas the one year old mice did not reach the level of significance within this time even in the limited post-test. The increases in HW/TL were: HW/TL of XIRP WT 3 month old 26.6% vs 1 year old 10.4% growth, of XIRP1XIRP2 dko 3 month old 37.7% vs. 1 year old 15.9% growth (Fig. 3.29 C).

3.6.5 LVW, LVW/BW ratio and LVW/TL ratio after TAC

Like HW also LVW was evaluated after TAC of the one year old mice. The data of the three month old mice are the same as those presented in chapter 3.2. In the three month old mice TAC induced a significant increase of LVW, LVW/BW ratio and LVW/TL ratio in both genotypes. However, even in a limited post-test comparing only the four sham groups of interest with the respective TAC groups the one year old animals XIRP WT did not reach the level of significance in any of the three tested parameters. In contrast, the XIRP1XIRP2 dko TAC mice developed significant hypertrophy in all three parameters. This may in part be attributed to the smaller amounts of old animals which were available (XIRP WT 3 month old sham n = 6 vs TAC n = 8; 1 year old sham n = 3 vs. TAC n = 4; XIRP1XIRP2 dko 3 month old sham n = 9 vs. TAC n = 8; 1 year old sham n = 5 vs. TAC n = 12). But the percentage of cardiac growth, which was achieved within 14 days was clearly smaller in the older animals (LVW of XIRP WT 3 month old 22.0% vs 1 year old 12.5% growth, of XIRP1XIRP2 dko 3 month old 40.0% vs. 1 year old 26.8% growth). Interestingly the differences were only small in case of LVW/BW (LVW/BW of XIRP WT 3 month old 17.3% vs 1 year old 14.2% growth, of XIRP1XIRP2 dko 3 month old 29.4% vs. 1 year old 27.0% growth). (LVW/TL of XIRP WT 3 month old 22.6% vs 1 year old 11.9% growth, of XIRP1XIRP2 dko 3 month old 41.5% vs. 1 year old 25.4% growth)

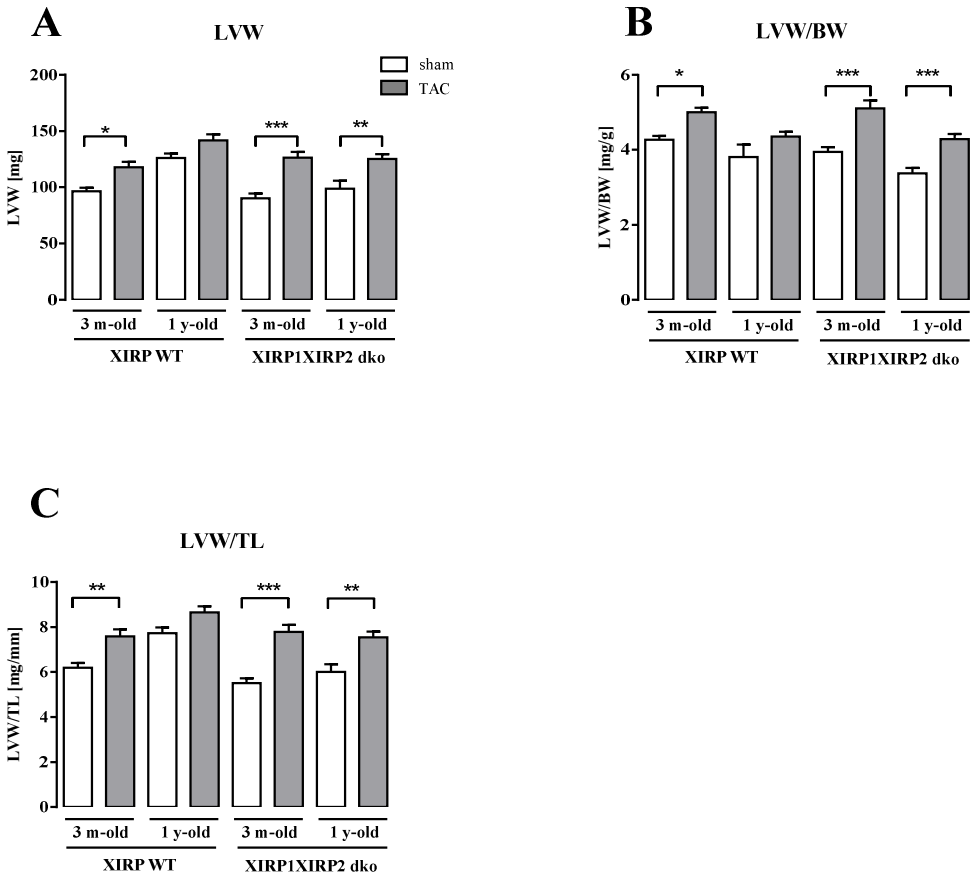

Figure 3.30 LVW, LVW/BW and LVW/TL ratio of 3 month-old and 1 year-old XIRP WT and XIRP1XIRP2 dko mice after 14 days TAC. All three tested parameters (A-C) were significantly increased in 3 month-old mice in both genotypes. In 1 year-old mice the same parameters were significantly increased in XIRP1XIRP2 dko mice. The data are represented as mean ± SEM; n= 3-12 /group, **P*< 0.05 was considered statistically significant.

3.6.6 LW, LW/BW ratio, and LW/TL ratio after TAC

As described in chapter 3.6.4 and 3.6.5 for HW and LVW also the LW of the one year old mice was evaluated after TAC and compared to the data of three month old mice. The data of the three month old mice are the same as those presented in chapter 3.2. In the three month old mice TAC induced a significant increase of LW and LW/TL ratio in both genotypes. In case of LW/BW ratio

only the three month old XIRP1XIRP2 dko 3 exceeded the level of significance.

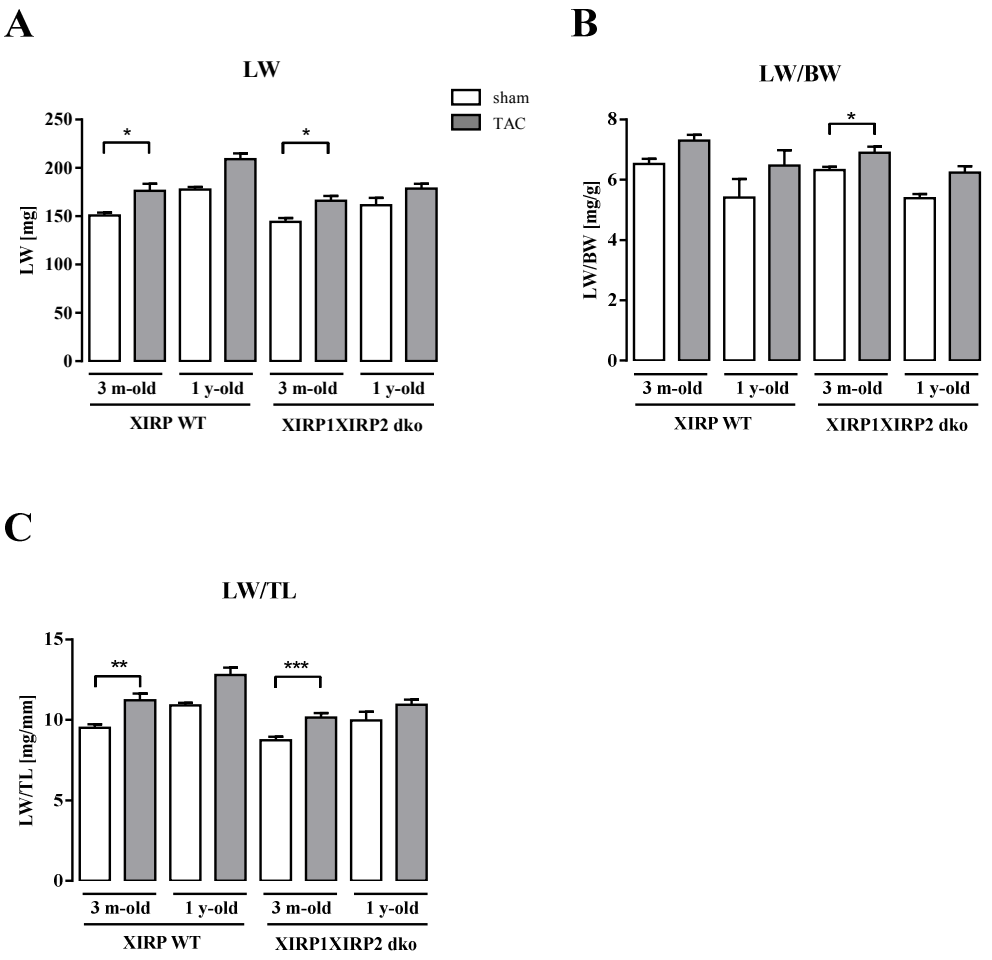

Figure 3.31 LW, LW/BW ratio, LW/TL ratio of 3 month-old and 1 year-old XIRP WT and XIRP1XIRP2 dko mice after 14 days TAC. After 14 days TAC LW (A) LW/TL ratio (C) ratio were significantly increased in both genotypes at 3 month of age, whereas the LW/BW ratio had grown only in the XIRP1XIRP dko mice at this age. In the 1 year old mice a significant influence of TAC was not detected in any of the parameters. The data are represented as mean ± SEM; n= 3-20 /group, **P*< 0.05 was considered statistically significant.

In the one year old mice none of the three LW parameters reached the level of significance even in a limited post-test. Again the groups of old animals were relatively small (XIRP WT 3 month old sham n = 11 vs TAC n = 16; 1 year old sham n = 3 vs. TAC n = 4; XIRP1XIRP2 dko 3 month

old sham n = 23 vs. TAC n = 30; 1 year old sham n = 6 vs. TAC n = 13). But the percentage of lung growth, which was achieved within 14 days was not clearly smaller in the old than in the young mice neither in LW nor in LW/BW ratio nor in LW/TL ratio (LW of XIRP WT 3 month old 16% vs 1 year old 17.7% growth, of XIRP1XIRP2 dko 3 month old 15% vs. 1 year old 5% growth; LW/BW ratio of XIRP WT 3 month old 12% vs 1 year old 19.7% growth, of XIRP1XIRP2 dko 3 month old 9.3% vs. 1 year old 11.5% growth; LW/TL ratio of XIRP WT 3 month old 18.2% vs 1 year old 17.2% growth, of XIRP1XIRP2 dko 3 month old 15.8% vs. 1 year old 9.8% growth).

3.6.7 Hemodynamic parameters in 3 month and 1 year-old mice after 14 days of TAC

TAC surgery significantly increased SAP and LVSP in both genotypes at both ages reaching comparable levels in all groups with one exception in the 1 year XIRP1XIRP2 dko group. In these mice SAP reached only 144 1 ± 2.3 mmHg which was significantly below the 158 ± 5.1 mmHg recorded in their 3 month old littermates (Fig. 3.32 A, B). EDP became elevated in all TAC mice but did not reach to the level of significance the one year old XIRP WT mice (Fig. 3.32 C). HR was significantly elevated in both three month old TAC groups but remained unchanged in the older mice (Fig. 3.32 D). dP/dt_{max} became significantly faster in three month-old TAC XIRP WT mice and showed a trend to increase in the equally old XIRP1XIRP2 dko mice. In the older mice TAC induced a decrease of dP/dt_{max} being significant only in the XIRP1XIRP2 dko mice (Fig. 3.32 E). dP/dt_{min} became faster in all TAC groups of both genotypes and ages but reached significance only in the three month old groups (Fig. 3.32 F).

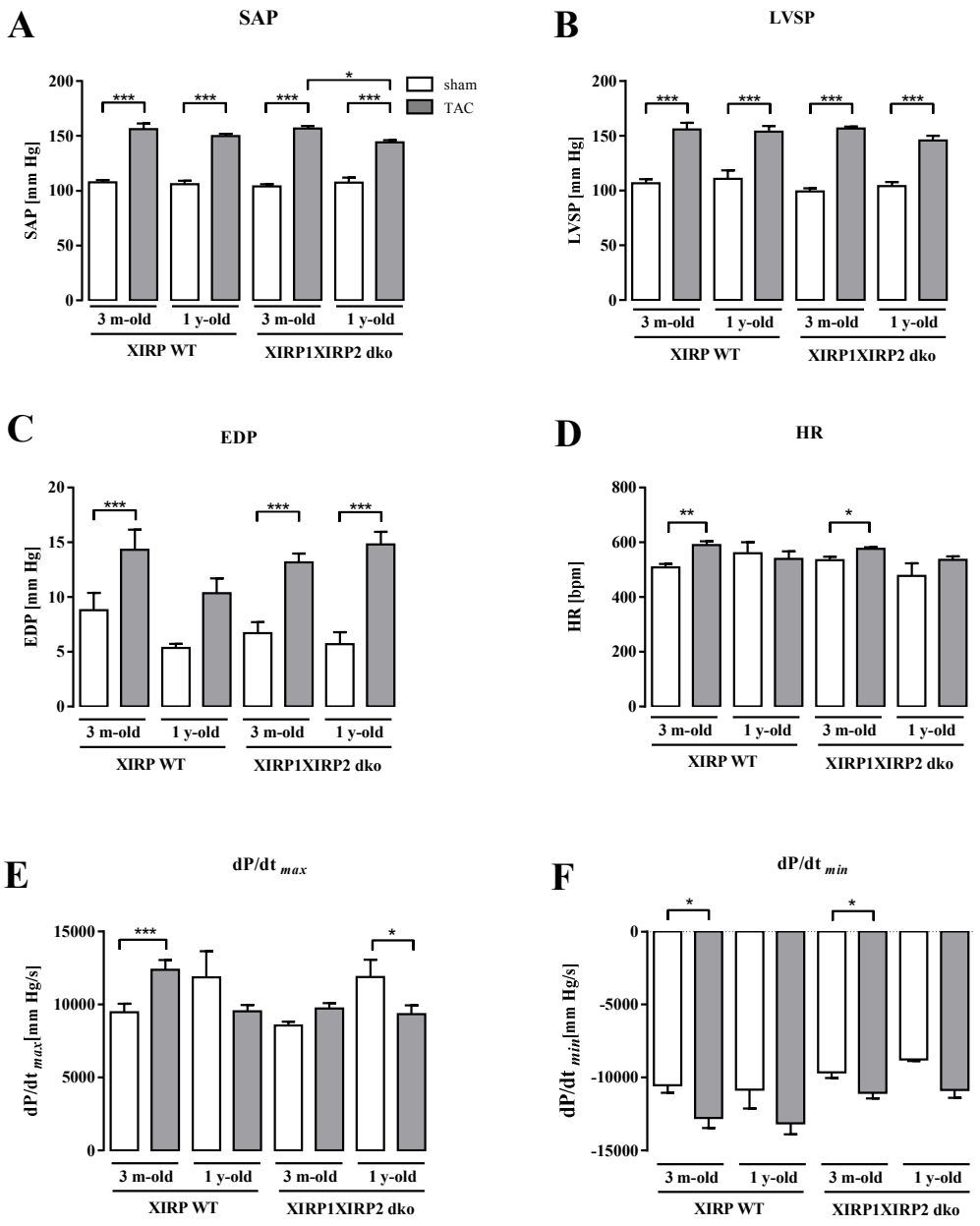

Figure 3.32 Hemodynamic data of XIRP WT and XIRP1XIRP2 dko 3 month-old and 1 year-old mice after 14 days TAC. **(A, B)** TAC surgery increased SAP and LVSP in both genotypes and at both ages. **(C)** EDP was also increased in TAC mice groups, without reaching significance in the 1 year old WT mice. **(D)** HR was significantly elevated in both 3 month old TAC groups **(E, F)** dP/dt_{max} became faster in the 3 month old XIRP1XIRP2 dko TAC mice. dP/dt_{max} became significantly faster in both genotypes in the young groups. The data are represented as mean ± SEM; n= 3-23 /group, **P*< 0.05 was considered statistically significant.

SAP and LVSP 3 month-old: XIRP WT: sham SAP 107.5 ± 2.0 mmHg vs. TAC 160.3 ± 4.5 mmHg; sham LVSP 106.8 ± 3.6 mmHg vs. TAC 158.8 ± 5.1 mmHg; XIRP1XIRP2 dko: sham SAP 104.1 ± 2.0 mmHg vs. TAC 156.8 ± 2.2 mHg; sham LVSP 99.3 ± 2.6 mmHg vs. TAC 156.6 ± 1.8 mmHg; **1 year-old**: XIRP WT sham 106.0 ± 3.2 mmHg vs. TAC 150.0 ± 2.0 mmHg; sham 110.6 ± 7.8 mmHg vs. TAC 153.8 ± 5.3 mmHg; XIRP1XIRP2 dko sham SAP 107.3 ± 4.8 mmHg vs. TAC 144.1 ± 2.3 mmHg; sham LVSP 104.1 ± 3.8 mmHg vs. TAC 145.7 ± 4.7 mmHg.

EDP 3 month-old: XIRP WT: sham 8.8 ± 1.6 mmHg vs. TAC 12.1 ± 2.1 mmHg; XIRP1XIRP2 dko: sham 6.7± 1.0 mmHg vs. TAC 13.2 ± 0.1 mmHg; **1 year-old**: XIRP WT sham 5.4± 0.4 mmHg vs. TAC 10.4 ± 1.4 mmHg; XIRP1XIRP2 dko: sham 5.7± 1.1 mmHg vs. TAC 14.8 ± 1.3 mmHg.

HR 3 month-old: XIRP WT: sham 509.3 ± 11.6 beat/min vs. TAC 590.3 ± 12.6 beat/min; XIRP1XIRP2 dko: sham 535.7± 11.8 beat/min vs. TAC 576.1 ± 6.5 beat/min; **1 year-old**: XIRP WT sham 509.3 ± 11.6 beat/min vs. TAC 590.3 ± 12.6 beat/min; XIRP1XIRP2 dko: sham 535.7 ± 11.8 beat/min vs. TAC 576.1 ± 6.5 beat/min.

dP/dt$_{max}$ 3 month-old: XIRP WT: sham 9470.7 ± 583.8 mm Hg/s vs. TAC 11739.5 ± 610.1 mm Hg/s; XIRP1XIRP2 dko: sham 8570.8 ± 248.8 mm Hg/s vs. TAC 9729.2 ± 349.3 mm Hg/s; **1 year-old**: XIRP WT: sham 11850.2 ± 1799.1 mm Hg/s vs. TAC 9526.4 ± 433.63 mm Hg/s; XIRP1XIRP2 dko sham 11878.6 ± 1192.6 mm Hg/s vs. TAC 9340.27 ± 668.1 mm Hg/s.

dP/dt$_{min}$ 3 month-old: XIRP WT: sham -10525.1 ± 535.2 mm Hg/s vs. TAC -12255.7 ± 767.6 mm Hg/s; XIRP1XIRP2 dko: sham -9651.5 ± 382.5 mm Hg/s vs. TAC -11044.2 ± 381.0 mm Hg/s; **1 year-old**: XIRP WT: sham -10828.1 ± 1309.0 mm Hg/s vs. TAC -13138.0 ± 755.5 0 mm Hg/s; XIRP1XIRP2 dko: sham -8762.7 ± 107.9 mm Hg/s vs. TAC -10837.6 ± 616.7 mm Hg/s.

4 Discussion

The current investigation is focused on the role of Xin repeat-containing proteins (XIRPs) in the heart. In mice and humans the XIRP protein family has two members, XIRP1 and XIRP2. XIRP1 has been reported to be a part of the fascia adherens of the ICD (Sinn et al., 2002) and to co-localize with filamin C and aciulin (Molt et al., 2014). A previous study on XIRP1 deficient mice has revealed a mild cardiac phenotype under resting conditions (Otten et al., 2010). XIRP1 deficient mice exhibited an elevated amount of non-terminal ICDs together with signs of a faster conduction velocity of the ventricular-specific conduction system and subtle changes in the shortening behavior of isolated cardiomyocytes. In a follow-up study (Kebir et al. in prep) the XIRP1 deficient mice were exposed to TAC and these mice developed an extent of cardiac hypertrophy comparable to that of their WT littermates. Also hemodynamic parameters measured 14 days after TAC did not differ between both genotypes. The only parameter which differed clearly between the genotypes after TAC was a higher incidence for ventricular tachycardia after TAC in the XIRP1 deficient mice. In the current study mice deficient of *XIRP1* and hypomorphic of *XIRP2* were investigated, because a possible compensation of the XIRP1 protein deficiency by an up-regulation of the XIRP2 expression should be excluded.

Without stimulation the two genotypes investigated here did not show any macroscopic cardiac differences at three month of age. However, the one year old XIRP1XIRP2 dko mice had significantly smaller HW and LVW than their WT littermates of the same age. Under the stress of TAC the three month old XIRP WT and XIRP1XIRP2 dko mice both developed cardiac hypertrophy. However, the degree of hypertrophy did not vary among the genotypes with respect to the macroscopic cardiac parameters at the age of three month mice. In contrast, the one year old XIRP1XIRP2 dko developed significant cardiac hypertrophy within two weeks whereas the XIRP WT mice exhibited only a tendency to cardiac hypertrophy. One difference between both

genotypes after TAC became obvious at microscopic level. There was a significantly lower degree of cardiac fibrosis in the XIRP1XIRP2 dko mice compared to XIRP WT.

As XIRP1 and XIRP2 are part of the cytoskeleton and are mainly found in the ICDs of the heart, the ICDs were specifically investigated in by antibody staining of isolated cardiomyocytes. The following proteins were visualized by antibodies in cardiomyocytes isolated from hearts of sham and TAC mice of both genotypes: filamin, titin, cadherin, connexin43, myomesin and ryanodine receptors. Interestingly, the cardiomyocytes of the XIRP1XIRP2 dko mice exhibited less non-terminal ICDs than those of the XIRP WT mice. Except the described differences in the distribution of ICDs no further differences in the cytoskeletal proteins were detected.

Finally, the function of the hearts was investigated by arterial and intraventricular pressure catheter recordings and by ECG recordings. Under control conditions the XIRP1XIRP2 dko mice exhibited the same hemodynamic parameters as the XIRP WT mice. Furthermore, both genotypes reacted comparably to TAC stimulation concerning the hemodynamic performance of the hearts. In ECG recordings some genotype differences could be detected: Biphasic P waves appeared more often in XIRP1 XIRP2 dko mice than in XIRP WT. However, this did not depend on the TAC as they appeared most often in the sham and not in the TAC group. Furthermore, TAC induced changes in the ECG parameters i.e. prolongation of P wave duration, of PQ interval, of QRS time and of QT interval were most pronounced and significant in XIRP1XIRP2 dko group and this may be taken as a sign for a slowed down conduction velocity.

4.1 Mouse model

In the current study mice were used as model for research on the cardiovascular system. This seems to be justified as the mouse model it is noteworthy similar to human in case of anatomy, physiology and genetics (Oliver et al., 2007). Human and mouse are both mammals and it has judged that the gene function and physiology are well preserved among them. This is substantiated by the finding that mice and humans exhibit more than 95% genome similarity (Kim et al., 2010). Additionally, mice are small and have a short and accelerated lifespan (one mouse year equals about 30 humans years) that allows the researcher to save costs, space and time required to perform experiments at a manageable speed. Furthermore, the mouse is the only species, which allows to track the function of proteins by the techniques of gene knockout, knockin, and knockdown (Cutler et al., 2007; Oliver et al., 2007).

In contrast to these advantages, some disadvantages of the mouse model have to be taken into account. Concerning cardiovascular research, mice have some differences compared to humans the HR are extremely high and thus there are differences in the recorded ECGs as well as in the underlying action potentials. In order to generate their extremely high HR short action potentials are necessary therefore mice express different K^+ channels in the heart than humans (Nerbonne et al., 2001). Nevertheless, in case of targeted deletion of genes as performed here the mouse is still the only experimental mammalian animal to be used.

4.2 Hypertrophy model (TAC)

Cardiac hypertrophy is an independent risk factor for the development of heart failure. Thus different ways to induce cardiac hypertrophy in animal models have been developed. Among these the TAC model is one of the most widely used microsurgical models which was first established by Rockman et al 1991. Application of the TAC to mice has been shown to cause a proceeding growth of cardiac tissue, which can be demonstrated already three days after the initial surgery (Baumgarten et al., 2006; Ehrentraut et al., 2011; Nakamura et al 2001; Velten et al.,

2012; Weisheit et al., 2014). This growth of cardiac mass reaches its maximum ten to 14 days after the surgery (Meyer et al., 2007; Nakamura et al., 2001). Four weeks after TAC the compensated hypertrophy starts to proceed into dilated cardiac hypertrophy, which may be reached after 6-8 weeks, depending on the severity of obstruction (de Almeida et al., 2010).

To standardize the degree of aortic constriction a 27-gauge needle was used as a placeholder in this study. This treatment allows reducing the inner aortic diameter by 65-70% (Baumgarten et al., 2002).

4.3 TAC-induced changes in macroscopic parameters

4.3.1 Mortality

A good measure for the quality of the surgery by which the TAC is executed is the mortality of the animals. Interestingly, the published mortality values varied over a wide range from < 25% up to >75%. Although the investigators all used the described 27-gauge needles and all applied TAC to male C57BL/6 mice. Mortality rates < 25% were reported by Barrick et al. (2007), Divakaran et al. (2009), Lucas et al. (2010), Rothermel et al. (2005), and Shimura et al. (2008) whereas others obtained 25%–50% (Nakamura et al., 2001; Liao et al., 2002; Skavdahl et al., 2005; Yamamoto et al., 2006; Xu et al., 2008). Higher mortality rates 50%–75% were found by Johnston et al. (2009) and Suryakumar et al. (2010). Mortality rates of greater than 75% have been reported by Jacobshagen et al. (2008) Raher et al. (2008) and Mohammed et al. (2011). The reasons for death can dependend on the expertise of the surgeon i.e. minor experience may lead to bleeding from damaged vessels, respiratory distress, pneumothorax, respiratory failure or HF. In this study, the mortality rate in the sham groups was 0% and in the XIRP WT TAC group it was 10%. These mortality rates are very low compared to those reported above. In the XIRP1 XIRP2 dko the mortality rate was 16.2% which is also low, however genetically modified mice may exhibit different survival rates than WT (Bourajjaj et al., 2008; van Oort et al., 2010).

4.3.2 Body weight

In the group of the three month old mice our XIRP WT and XIRP1XIRP2 dko mice were significantly heavier than the age matched C57BL/6 mice bred in Bonn. But the body weight of these mice was compatible to the body weight information chart of Jackson laboratory, that listed a body weight of 20.2 ± 1.4 g to 21.7 ± 1.5 g for female C57BL/6 mice at the age of 11-13 weeks. In case of stress or sickness mice easily lose body weight TAC surgery is an invasive method that puts strain on the mice. Nevertheless, almost all of the mice had gained a small non-significant amount of body weight after two weeks. Interestingly there was no difference between the TAC and the sham groups. This can be taken as a sign that the animals had recovered nearly completely during the 14 days after surgery.

4.3.3 Age of the mice

According to Flurkey and Harrison (2007) mature life of mice can be divided into three age ranges 3-6 month-old (mature adult), 10-14 month-old (middle aged), and 18-24 month-old (old age). As we know, in human as well as in animals, the aging heart undergoes structural and functional changes that diminish its capability to respond to overload, and to reserve its ability in cardioprotection and repair processes (Lakatta, 2015). Furthermore, the XinAB$^{-/-}$ mice, which can express XinC still, develop fibrosis, conduction defects and signs of cardiomyopathy only at higher age (Gustafson-Wagner et al., 2007). Therefore, in this study two age groups were included the mature adult age 3 month-old (11-13 week-old) and middle aged 12-13 month-old (44-52 week-old). Especially, the 3 month-old mice have been investigated in various publications of our and other groups (Babiker et al., 2006; Baumgarten et al., 2006; Ehrentraut et al., 2011; Kebir et al., in prep; Meyer et al., 2007; Velten et al., 2012; Weisheit et al., 2014). Thus the results gained on this age group can be easily compared earlier ones.

4.3.4 HW, LVW, and LW

The XIRP1XIRP2 dko mice investigated in this study did not develop cardiac hypertrophy spontaneously. According to the literature spontaneous cardiac hypertrophy seemed possible. In the case of the XIRP1 deficient mice two different approaches have been applied, one leading to the XinAB$^{-/-}$ mice which were still able to express the XinC isoform (Gustafson-Wagner et al., 2007). These mice developed cardiac hypertrophy in the higher age spontaneously. On the other hand there are the XinABC$^{-/-}$ which were designed by our group (Otten et al., 2010), these mice did not show cardiac hypertrophy spontaneously nor did they develop a higher degree of cardiac hypertrophy in the case of pressure overload (Kebir et al., in. prep). These mice were crossed with XIRP2 hypomorphic mice described in McCalmon et al. (2010). The XIRP2 hypomorphic mice exhibited a 19% increased HW/BW ratio in the age range of 9-15 weeks (McCalmon et al., 2010). This was attributed to additional growth of cardiac myocytes by the authors. However, the XIRP1XIRP2 dko mice investigated here did not show any sign of spontaneous cardiac hypertrophy even at the age of one year. Even more the one year old XIRP1XIRP2 dko exhibited a significantly lower HW/BW and LVW/BW than their three month old littermates. These lower ratios can be attributed to an increased BW as neither the HW nor the LVW had gained significant amounts of weight after 3 months. In contrast in the XIRP WT mice HW as well as LVW grew significantly after three months. A clear reason for this difference cannot be given here. However, the XinC isoform which is suspected to cause spontaneous cardiac hypertrophy is expressed in the XIRP WT and in the XIRP2 hypomorphic mice but not in the XIRP1XIRP2 dko mice. Therefore one may speculate that the missing XinC could explain the lack growth and thus of spontaneous hypertrophy in these mice.

Pressure overload induced cardiac hypertrophy has been documented in numerous studies. In this study, the XIRP WT developed a 25% increase in HW whereas XIRP1XIRP2 dko reached 39% higher HW after 14 days of aortic banding. HW/BW ratio grew by 22% in XIRP WT TAC mice vs. 27% in XIRP1XIRP2 dko TAC mice. In female C57BL/6 mice Weisheit et al. (2014) gained a

HW/BW of around 30% after 6 days and after around 40% after 21 days. Skavdahl, et al. (2005) detected 31% increase of HW/BW in C57BL5 TAC female mice after 14 days this comparable to the results presented here. However, male C57BL6 exhibited a 64% increase in HW/BW in the same publication. This high cardiac hypertrophy in male mice was also detected by Souders et al. in 2012 who documented the development of cardiac hypertrophy starting day 2 after TAC (25%), at day 7 (71%), at day 14 (63%) and ending at day 28 (64%). This shows that the stable cardiac hypertrophy is reached after 7-14 days. Taken together the cardiac hypertrophy measured in females as HW/BW in this study is significant but somewhat below the values of others.

As TAC induces hypertrophy mainly in the left ventricle the measurement of the weight of this segment of the heart alone gives better resolution. In the present study TAC induced gain in LVW/HW of XIRP1 WT was significant but relatively small 16%, in XIRP1 XIRP2 dko it was 28%. In the investigation of Kebir et al. (in prep.) the TAC induced gain in the female mice amounted to nearly 50% in XIRP1 WT and XIRP1 deficient. Bader et al. (2012) detected 31% increase in LVW/BW female mice after 2 weeks of TAC. Again the values reached here were smaller than those of others. Possibly the banding performed in this study was less firm than that applied by others.

Aortic banding causes an increase in LV afterload which in turn leads to elevation of LV endsystolic volume and also of LV enddiastolic volume. This induces blood congestion in the lung causing lung edema and compensatory fibrosis which is accompanied by leukocyte infiltration and vascular remodeling (Chen et al., 2012). The easiest way to document these remodeling processes in the lung is to determine lung weight. TAC increased LW, LW/BW ratio, and LW/TL ratio this study by 17%, 12% and 18% in XIRP WT vs.; 15%, 10% and 15% in XIRP1XIRP2 dko. However, both TAC groups did not differ significantly. The elevations of LW found here were in concert with the results of Xu et al. (2006) published about 20% in LW/TL after 14 days of TAC.

Advancing age is correlated with an attenuated capacity to develop cardiac hypertrophy due to a decrease of protein synthesis in response to acute pressure overload (Isoyama et al., 1987). In

addition, the older mice (>12 month-old) need more time to develop vascular adaptation after TAC, but they proceed faster to dilated cardiomyopathy than younger mice (3-4 month-old) (Li et al., 2003). Furthermore, de Boer et al. (2013) have reported that aging diminishes the hypertrophic response to TAC. These observations can explain why also in this study, 1 year-old mice of both genotypes exhibited less hypertrophy in response to TAC than their 3 month-old littermates. However, it is worth to mention that the one year old XIRP WT mice did not develop significant cardiac hypertrophy within the 14 days observation period neither in the case of the case HW, HW/BW, and HW/TL nor in the case of LVW, LVW/BW, and LVW/TL. The XIRP1XIRP2 dko mice developed more cardiac hypertrophy than the XIRP WT visible TAC dependent significant increases HW/BW, LVW, LVW/BW and LVW/TL. This may be taken as a sign for a higher sensitivity to TAC in the XIRP1XIRP2 dko mice. Possible reasons for that will be discussed in chapter 4.3.5

4.3.5 Left ventricular, septum thickness, and cardiac fibrosis

LaPlace's law adopted to the heart says that left ventricular wall stress caused by an increased transmural pressure can be reduced by increasing wall diameter.

K = P * r / (2 * d)
K: wall stress
P: intraventricular pressure
r: radius of the ventricular chamber
d: wall diameter.

In case of an increased intraventricular pressure due to the TAC a compensatory rise in wall diameter is expected to maintain the normal ejection fraction of the heart (Lorell and Carabello, 2000). Consequently, the detection of the left ventricular wall diameter is a meaningful parameter, which was measured in the septum as well as in the wall between the papillary muscles. 2 weeks after TAC there was a significant increase in left ventricular wall and septum thickness in both genotypes (XIRP WT by about 175% and XIRP1XIRP2 dko by about 150%). Although the relative increase seems to be smaller in XIRP1XIRP2 dko significant differences between the

genotypes could not be detected. Nevertheless, the increases in wall thickness detected here are consistent with those from other studies like 155% in Chen et al. (2013) and like 125% in Speerschneider et al. (2013). These observations are also consistent with echocardiographic imaging after TAC for 2 weeks, which also demonstrated significant increases of LV wall thickness (Gao et al., 2000; Lai et al., 2012; Liao et al., 2002; Tanaka et al., 1996; Xu et al., 2008; Youn et al., 1999). Interestingly, did the increases in wall thickness in this investigation fit nicely to those from others although the weight gains were somewhat below the values in the literature.

Also in human patients that suffer from aortic stenosis (AS) it has been shown previously that pressure overload usually led to increased LV wall thickness and concentric hypertrophy (Faggiano et al., 1994; Kehat et al., 2010). Concentric hypertrophy has been documented as the most common LV geometric remodeling pattern in patients with severe symptomatic AS (Antonini-Canterin et al., 2003).

The concentric hypertrophy is qualified by the increase in the width of individual cardiomyocytes in parallel (Kehat et al., 2010). In addition, chronic pressure overload exhibited increased collagen accumulation between cardiomyocytes and myocyte fascicles (Weber et al., 1988) as well as accumulation of ECM and fibrosis followed by cardiac stiffness and then inadequate filling leads to insufficiency diastole function (Kehat and Molketin, 2010).

In this study TAC induced more cardiac fibrosis in three month old XIRP WT mice (4%) than in XIRP1XIRP2 dko mice (2%). This interesting difference may be in conjunction with AngII. In the introduction it has been mentioned that the *XIRP2* gene has an AngII sensitive region in its promotor. In their study McCalmon et al. (2010) demonstrated that AngII and the "myocyte enhancer factor 2A", MEF2A, are both able to stimulate the promotor activity of *XIRP2*.

AngII and MEF2A acted synergistically i.e. applied together they stimulated more than 10x, applied alone they stimulate 2.5x and 3.6x. In a model of AngII induced cardiac hypertrophy the XIRP2 hypomorphic mice displayed attenuated cardiac hypertrophy, fibrosis, and apoptosis. As AngII is indirectly attributing to pressure overload induced cardiac hypertrophy (Müller et al., 2013), the reduced cardiac fibrosis in our XIRP1XIRP2 dko mice may be explained by the

reduced AngII signaling in these mice, especially since AngII has been shown to be pro-fibrotic by interaction with TGFβ_1 signaling (reviewed in Leask 2015).

4.3.6 Cardiomyocyte parameters

In a comparison of the cardiomyocyte dimensions the length of the XIRP1XIRP2 dko sham cells proved to be significantly longer and less wide than the XIRP WT sham cardiomyocytes. This seems to be in contrast to the observation that the whole hearts did not differ between the genotypes. But as the length and width are contrary this may level out in the tissue. Interestingly, the isolated cardiomyocytes of XinABC$^{-/-}$ were also slightly but significantly longer than their WT counterparts (Otten et al., 2010).

In case of the development of concentric cardiac hypertrophy one would expect an increase in cellular width due to the assembly of new myofibrils in parallel (Byus et al., 2007; Kehat and Molkentin, 2010). After TAC cardiomyocytes became shorter and wider in both genotypes, however, level of significance was only reached in the XIRP1XIRP2 dko cells. These observations seem to be in line with development of concentric cardiac ventricular hypertrophy.

As XIRP1 and XIRP2 are part of the cytoskeleton and are mainly found in the ICDs of the heart, the ICDs were investigated by antibodies directed against cadherin, connexin43 and filaminA/C d1-2. Non-terminal ICDs were detected in a significantly lower amount in XIRP1XIRP2 dko sham cells (3.44 ± 0.2) than in XIRP WT sham cells (4.7 ± 0.3). TAC seemed to increase non terminal ICDs further in the XIRP WT sham cells (5.1 ± 0.3) but not in the XIRP1XIRP2 dko sham cells (3.36 ± 0.2). At the first glimpse this result seems to be surprising, because Otten et al. (2010) found an elevated number of non-terminal ICDs in XinABC$^{-/-}$ cardiomyocytes. However, the number was around 8 per cell there compared to about 4 - 5 in their WT cardiomyocytes. Thus the amount non-terminal ICDs in the XIRP WT here seems to be comparable to that of Otten et al. (2010). But the non-terminal ICDs of the XIRP1XIRP2 dko sham and TAC cells are extremely low.

In an effort to detect further differences in the cytoskeleton various antibodies were applied, against myomesin located in the M band, against a Z-band epitope of titin, and against ryanodine receptor as part of the triads. The localization of these proteins was neither influenced by the genotype nor by the TAC treatment. This is somewhat surprising as one may expect that synthesis of new myofibrils should require a complete remodeling of the cytoskeleton, a process on which the absence of both XIRP proteins should exert influence. However, the failure of the detection changes may also be explained by the relatively late time point after the aortic constriction. As mentioned in chapter 4.3.4 the cardiac hypertrophy in mice develops mainly between day two and seven after TAC and between one week and four weeks after TAC the amount of cardiac hypertrophy is relatively stable. For the detection of dynamic changes which could help to unmask the role the XIRP proteins further, earlier time points after TAC should be observed.

4.4 TAC-induced changes in the hemodynamic parameters

The genetic differences between the XIRP WT and XIRP1XIRP2 dko mice did not influence of hemodynamic parameters recorded here in the sham mice neither in the in the month old group (c.f. table 3.2) nor in one year old group (chapter 3.6.7). Thus spontaneous differences in the cardiac function could be detected.

Inducing hypertrophic cardiac remodeling by increasing the afterload will induce mechanical stress to the ICDs, which in turn may cause difference due to the absence of both XIRP proteins. The primary pro-hypertrophic stimulus in the TAC model is a pre-stenotic elevation of blood pressure. Therefore it is important classify the rise in blood pressure obtained by the aortic constriction.

After 14 days of TAC SAP was significantly elevated by about 150% to around 160 mmHg in both young groups (XIRP WT: 160.3 mmHg (149.0%), XIRP1XIRP2 dko: 156.8 mmHg (150.6%)). An increase in SAP by about 150% can be taken as an indication for a successful TAC surgery. Comparable elevations of systolic BP have published in previous studies on female mice, Patten et al. (2008) (157.5%, 149.0 mmHg), Witt et al. (2008) (160.0%, TAC 160 mmHg) and Xu

et al. (2008) (144.0% 153.0 mmHg). Furthermore, the one year old mice which were exposed to TAC here also reached SAP values in the same range as the young mice (XIRP WT TAC 150.0 mmHg increase 141%; XIRP1XIRP2 dko SAP 144 mmHg increase 135%). The blood pressure reactions gained in the older mice were lower than in the younger ones, which points to a reduced ability to compensate the increased afterload. In the old XIRP1XIRP2 dko the gained pressures were lower than in the old XIRP WT although only the XIRP1XIRP2 dko developed a significant cardiac hypertrophy.

The TAC-induced changes in the hemodynamic parameters can also be taken as a measure for cardiac performance. The higher the LVEDP increases the worse is the condition of the ventricle and the elevated LVEDP induces a progressive congestion of blood in the lungs. The LVEDP rose in both genotypes and age groups (3 month-old: XIRP WT from 8.8 to 12.1 mmHg; XIRP1XIRP2 dko from 6.7 to 13.2 mmHg; 1 year-old: XIRP WT from 5.4 to 10.4 mmHg; XIRP1XIRP2 dko from 5.7 to 14.8 mmHg). All these increases can be regarded as moderate with the exception of the one year old XIRP1XIRP2 dko in which TAC increased the EDP by 9.1 mmHg. Patten et al. (2008) also reported an increase in LVEDP in three month old female mice from 3.1 mm Hg to 11.8 mm Hg, which is in the same range as our values.

In case of a compensated hypertrophy cardiac output (CO) is also maintained by increasing the heart rate. Significant up-regulations of HR after two weeks TAC could be proven in both genotypes of the three month old mice but not in the one year old groups.

Another sign of compensated cardiac hypertrophy is an up-regulation of dP/dt_{max}. After 14 days of TAC both genotypes groups of young exhibited significantly higher dP/dt_{max} values than the respective sham groups. Differences among the genotypes were found. The hearts of the young mice were able to compensate the elevated afterload significant by up-regulation of dP/dt_{max} detectable only in a limited comparison (Fig. 3.20). However, XIRP1XIRP2 dko TAC developed significantly dP/dt_{max} values than the respective WT mice. In contrast, the one year old mice were not able to up-regulate dP/dt_{max} but exhibited down-regulation of the contractility, reaching the

level of significance in the XIRP1XIRP2 dko mice. dP/dt_{min} was increased in all groups, being significant only in the two groups of young animals.

Taken together, according to the cardiac performance of the two young groups seem to be in the stage of compensated cardiac hypertrophy. Whereas the older mice seemed to have proceeded further on the way to HF. However, significant genotype differences were small.

4.5 TAC-induced changes in the ECG

TAC is a standard procedure to generate pressure overload in mice, causing LV hypertrophy. The ECG was applied here to evaluate electrical activity within the heart. The ECG analysis revealed that biphasic P waves appeared more often in XIRP1 XIRP2 dko mice then in XIRP WT. Interestingly, XIRP1XIRP2 dko exhibited more biphasic P waves in sham than in TAC conditions. Left atrium enlargement causes broad biphasic P waves in ECG lead II, because a large atrium results in a delay of the complete depolarization from right atrium to left atrium (Levine, Coyne & Colvin, 2015). Furthermore, pressure overload can induce atrium enlargement by increased left atrium afterload (Patel et al., 2009). But as biphasic P waves were more frequent in sham than in TAC XIRP1XIRP2 dko mice TAC does not seem to influence this phenomenon here. But two other atrial parameters P wave duration and PQ time were prolonged by the TAC in both genotypes. However, the level of significance was only reached in the XIRP1XIRP2 dko. The general prolongation may be attributed increased conductance distances because of an increased atrium or to a slowed conduction velocity.

ST elevation is a classical hallmark of acute myocardial infarction. In the mouse ST segment represents mainly the ventricular repolarization. But also left ventricular hypertrophy especially of the septum is a common condition that is associated with ST segment elevation. However, ST elevation caused by septum enlargement is not as obvious as in myocardial infarction (Coppola et al., 2013). In this study ST elevation found in one of the XIRP1XIRP2 dko TAC mice.

The study by Boulaksil et al. (2010) documented after 2 weeks TAC mice showed rapid structural and electrical remodeling leading to QRS and QT interval prolongation. This consistent with our

results on QRS and QT interval, as both TAC groups displayed a trend to prolongation of these values. In case of QT time XIRP1XIRP2 dko TAC mice reached the level of significance. QRS complex prolongation indicates a delayed activation of the ventricles, due to either a slowed down impulse conduction or an increased conduction distance due to cardiac enlargement (Wiegerinck et al., 2006). In aortic constriction the mice developed fibrosis which associated with slowing conduction, but fibrosis was significantly higher in the XIRP WT than in the XIRP1XIRP2 dko. Therefore fibrosis may here not be the most important factor for the prolonged QRS complex and QT interval.

Another reason may be a changed structure of the ICDs. In the XinAB$^{-/-}$ hearts, which spontaneously develop a disrupted ICD structure and cardiac hypertrophy, a prolonged QT interval was recorded (Gustafson-Wagner et al., 2007). Interestingly, signs of a faster conduction velocity of the ventricular-specific conduction system were detected in the XinABC$^{-/-}$ mice. This faster conduction velocity was attributed to the increased number of ICDs in these mice (Otten et al., 2010). In the XIRP1XIRP2 dko mice decreased number of lateral ICDs could be shown here, which can contribute to the prolonged QT interval detected here.

XinABC$^{-/-}$ mice exposed to TAC had a higher incidence for the development of ventricular tachycardia after electrical induction (Kebir et al. in prep). This parameter was not investigated in the present study. However, both XIRP proteins are localized in the ICD and their absence in XIRP1XIRP2 dko mice may cause reorganization of the ICDs especially during the hypertrophic remodeling. The reorganized ICDs of XIRP1XIRP2 dko mice may lead to lowered cell-to-cell coupling a thus a prolonged QT interval. But this observation needs further substantiation. In summary, TAC induced changes in ECG parameters were most pronounced and significant in XIRP1XIRP2 dko group and may be taken as a sign for a slowed down conduction velocity.

4.6 Conclusion

In the present study we sought to determine the role of XIRP1 and XIRP2 proteins in cardiac structure and function. Furthermore, cardiac hypertrophic remodeling was induced in order to enlighten the functions of the XIRP proteins during structural adaptation of the cardiomyocytes to increased load. We hypothesized that an additional knock-down of XIRP2 may help to unravel the functions of both XIRPs in the murine heart as an up-regulation of XIRP2 may not be able substitute a XIRP1 deficiency. Therefore, XinABC$^{-/-}$ mice (Otten et al., 2010) were crossed with XIRP2 hypomorphic mice (McCalmon et al., 2010) and referred as XIRP1XIRP2 dko mice.

The XIRP1XIRP2 dko mice exhibited a mild cardiac phenotype, without developing a spontaneous cardiac hypertrophy. The hypothesis that XinABC$^{-/-}$ mice do not develop severe phenotype because XIRP2 is able to replace the functions of XIRP1 could not be confirmed. Surprisingly, the phenotype of the XIRP1XIRP2 dko mice was even less pronounced than that of the XIRP2 hypomorphic mice, because the XIRP1XIRP2 dko sham mice did not develop a spontaneous cardiac hypertrophy in contrast to the XIRP2 hypomorphic mice. A possible reason for that could be the missing XinC isoform in the XIRP1XIRP2 dko mice which seems to play a role in the development of cardiac hypertrophy and failure. However, this is not proven by the experiments performed here.

Only a few genotype-dependent differences could be detected. Regarding spontaneously appearing differences, a reduced amount of non-terminal ICDs was seen in fluorescence microscopy and a high rate of biphasic P waves was recorded in the XIRP1XIRP2 dko sham mice. As the reduced non-terminal ICDs were detected in ventricular cells and the biphasic P waves originate in the atrium these two observations could not be directly correlated. During hypertrophic remodeling a few additional XIRP dependent changes were observed. The fibrosis induced by cardiac overload was less distinct in XIRP1XIRP2 dko mice than in XIRP WT. XIRP2 has been shown to be involved in AngII signaling as its promoter is sensitive to AngII. AngII is known to enhance cardiac fibrosis, thus the missing XIRP2 may help to reduce the development of fibrosis during hypertrophic growth.

Finally, some functional effects of the XIRP1XIRP2 deficiency were detected in ECG recordings: prolongation of P wave duration, of PQ interval and of QT interval. These may be taken signs for reduced conduction velocity in the XIRP1XIRP2 dko TAC mice. As the XIRP1XIRP2 dko TAC mice exhibit less non-terminal ICDs a reduction of cellular coupling may follow, which could contribute to reduce conduction velocity. However, this hypothesis needs further substantiation by more refined ECG recordings.

5 Abstract

The proteins of intercalated discs (ICDs) are components of the cardiac cytoskeleton which forms the scaffold of cardiomyocytes and thus helps to maintain cell shape, provide tissue integrity, and to stabilize the sarcomeric proteins. Part of the cytoskeleton are the Xin repeat containing proteins 1 and 2 (XIRP1 and XIRP2), which are located in ICDs of the mammalian heart. XIRP1 and XIRP2 have been detected in the adherens junctions of the ICDs and play critical roles in the cardiac development and the structural integrity of ICDs. XIRP1-null mice created by our group exhibited a mild cardiac phenotype with increasing non-terminal ICDs and an increased intraventricular conduction velocity. Also the application of elevated afterload to XIRP1 deficient mice to induce hypertrophic cardiac remodeling did not lead to a more severe phenotype. Possibly lack of XIRP1 protein was compensated by XIRP2 up-regulation. Therefore XIRP1 deficient mice were crossed with XIRP2 knockdown mice (XIRP1 XIRP2 dko). We hypothesized that an additional knock-down of XIRP2 may help to unravel the functions of both XIRPs in the murine heart in case of normal and elevated afterload.

XIRP wild-type (XIRP WT) and XIRP1XIRP2 dko female mice of about 12 weeks or one year age were assigned to transverse aortic constriction , TAC, or sham surgery. Surgeries were performed on anesthetized (2 vol % isoflurane) mice provided i.p. with analgesia (buprenorphine 0.065 mg/kg body weight, BW). A 27 gauge needle was used to standardize the degree of aortic constriction. After 14 days of TAC or sham, hemodynamic parameters were recorded by a pressure catheter in mild anesthesia (heart rate, HR, ~500 min^{-1}). Furthermore, surface electrocardiography was performed under the same conditions.

Different morphometric parameters were measured: body weight, BW; heart weight, HW; left ventricular weight, LVW; lung weight, LW; tibia length, TL. From explanted hearts single cardiomyocytes were prepared by retrograde Langendorff-perfusion, proteins of interest were localized in the isolated cardiomyocytes by antibodies and visualized by immunofluorescence microscopy. Representative hearts from the different groups were embedded in paraffin and

sections from 4 different areas were cut. In light microscopy the diameters of the septum and the ventricular wall were determined as well as the amount of cardiac fibrosis, visualized by Masson's trichrome stain.

14 days after TAC surgery the XIRP WT and XIRP1XIRP2 dko mice of three month age had developed significant cardiac hypertrophy compared to the sham animals. However, both genotypes did not differ with respect to the measured morphological parameters (HW, HW/BW, HW/TL; LVW, LVW/BW, LVW/TL; LW, LW/BW; LW/TL). Also the diameters of septum and ventricular wall were significantly increased by the TAC but did not exhibit genotype differences. But TAC induced cardiac fibrosis was significantly higher in XIRP WT than in XIRP1XIRP2 dko mice. Protein localization performed by fluorescence microscopy revealed that XIRP1XIRP2 dko mice exhibited independently of TAC significantly less non-terminal ICDs than XIRP WT mice, whereas the number of terminally situated ICDs was not altered. Localization of proteins in the M-band, the Z-discs and the triads was neither influenced by genotype nor by TAC.

The TAC elevated the systolic arterial pressure, SAP, and the left ventricular systolic pressure, LVSP, significantly by ~ 150% in both genotypes. Also the left ventricular end-diastolic pressure, LVEDP, HR, and the measures for contractility, maximal velocity of pressure increase, dP/dt_{max}, as well as maximal velocity of pressure decrease, dP/dt_{min}, were all up-regulated in response to TAC, however to the same degree in both genotypes.

Abnormal ECG parameters were never recorded from XIRP WT mice neither in the sham nor in the TAC group. In contrast, ECG recordings from XIRP1XIRP2 dko sham mice exhibited biphasic P waves in 38.5% of the recordings. XIRP1XIRP2 dko TAC mice showed biphasic P waves in 18% of the evaluations, irregular HR, missing P waves and even ST elevations were detected. TAC induced a prolongation of P wave duration, PQ interval and QT interval in both genotypes. As the amount of prolongation was higher in the XIRP1XIRP2 dko TAC mice only these reached the level of significance.

To find out whether there are genotype dependent phenomena which appear only in older age also 1 year-old mice of both genotypes underwent sham and TAC surgery. They were evaluated for

the macroscopic morphological parameters and for the hemodynamics. The mice did not spontaneously develop any genotype dependent differences during aging. The cardiac growth gained within 14 days after TAC surgery was clearly smaller in the older mice than in the younger ones. Within this time span hypertrophic cardiac growth reached the level of significance only in the XIRP1XIRP2 dko mice, although both groups of mice responded to the excessive afterload by comparably increased levels of SAP, LVSP, and LVEDP.

Taken together, only a few genotype-dependent differences could be detected. Regarding spontaneously appearing differences, a reduced amount of non-terminal ICDs were seen in fluorescence microscopy and a high rate of biphasic P waves were recorded in the XIRP1XIRP2 dko sham mice. As the reduced non-terminal ICDs were detected in ventricular cells and the biphasic P waves originate in the atrium these two observations could not be directly correlated. TAC dependent fibrosis was less distinct in XIRP1XIRP2 dko mice. This may possibly originate in a changed angiotensin II, AngII, signaling. As XIRP2 expression has been shown to be influenced by AngII, its absence in turn may disturb AngII signaling, which is known to enhance fibrosis. Prolongation of P wave duration, PQ interval, QRS complex, and QT interval may be taken signs for reduced conduction velocity in the XIRP1XIRP2 dko TAC mice. These mice also exhibit less non-terminal ICDs which could contribute to reduced conduction velocity. However, this hypothesis needs further substantiation by more refined ECG recordings.

6 References

Annes JP (2003) Making sense of latent TGFβ activation. J. Cell Sci. 116: 217-224.

Antonini-Canterin F, Huang G, Cervesato E, Faggiano P, Pavan D, Piazza R, Nicolosi GL (2003) Symptomatic aortic stenosis: does systemic hypertension play an additional role? Hypertension 41: 1268-1272.

Babiker FA, Lips D, Meyer R, Delvaux E, Zandberg P, Janssen B, van Eys G, Grohe C, Doevendans PA (2006) Estrogen receptor β protects the murine heart against left ventricular hypertrophy. Arterioscler Thromb Vasc Biol 26: 1524-1530.

Bader M, Westphal C, Schubert C, Prelle K, Penkalla A, Fliegner D, Petrov G, Regitz-Zagrosek V (2012) Effects of estrogen, an ERα agonist and raloxifene on pressure overload induced cardiac hypertrophy. PLoS ONE 7: e50802.

Baicu CF, Stroud JD, Livesay VA, Hapke E, Holder J, Spinale FG, Zile MR (2003) Changes in extracellular collagen matrix alter myocardial systolic performance. Am J Physiol Heart Circ Physiol. 284: H122-H132.

Barrick CJ, Rojas M, Schoonhoven R, Smyth SS, Threadgill DW (2007) Cardiac response to pressure overload in 129S1/SvImJ and C57BL/6J mice: temporal- and background-dependent development of concentric left ventricular hypertrophy. Am J Physiol Heart Circ Physiol 292: H2119-H2130.

Baumgarten G, Kim S-C, Stapel H, Vervölgyi V, Bittig A, Hoeft A, Meyer R, Grohé C, Knuefermann P (2006) Myocardial injury modulates the innate immune system and changes myocardial sensitivity. Basic Res Cardiol 101: 427-435.

Baumgarten G, Knuefermann P, Kalra D, Gao F, Taffet GE, Michael L, Blackshear PJ, Carballo E , Sivasubramanian N, Mann DL. (2002) Load-dependent and -independent regulation of proinflammatory cytokine and cytokine receptor gene expression in the adult mammalian heart. Circulation 105: 2192-2197.

Bernardo BC, Weeks KL, Pretorius L, McMullen JR (2010) Molecular distinction between physiological and pathological cardiac hypertrophy: experimental findings and therapeutic strategies. Pharmacol Ther 128: 191-227.

Berne RM, Levy MN, Koeppen BM, Stanton BA (2008) Berne & Levy Physiology. Pennsylvania: Mosby/Elsevier

Boron (2009) Medical Physiology. Philadelphia: Saunders,

Boulaksil M, Winckels SKG, Engelen MA, Stein M, van Veen TAB, Jansen JA, Linnenbank AC, Bierhuizen MFA, Groenewegen WA, van Oosterhout MFM, Kirkels JH, de Jonge N, Varro A, Vos MA, de Bakker JMT, van Rijen HVM (2010) Heterogeneous connexin43 distribution in heart failure is associated with dispersed conduction and enhanced susceptibility to ventricular arrhythmias. Eur J Heart Fail 12: 913-921.

Bourajjaj M, Armand AS, Martins PADC, Weijts B, van der Nagel R, Heeneman S, Wehrens XH, De Windt LJ (2008) NFATc2 is a necessary mediator of calcineurin-dependent cardiac hypertrophy and heart failure. J Bio Chem 283: 22295-22303.

Buys ES, Raher MJ, Blake SL, Neilan TG, Graveline AR, Passeri JJ, Llano M, Perez-Sanz TM, Ichinose F, Janssens S, Zapol WM, Picard MH, Bloch KD, Scherrer-Crosbie M (2007) Cardiomyocyte-restricted restoration of nitric oxide synthase 3 attenuates left ventricular remodeling after chronic pressure overload. Am J Physiol Heart Circ Physiol 293: H620-H627.

Calaghan SC, Le Guennec JY, White E (2004) Cytoskeletal modulation of electrical and mechanical activity in cardiac myocytes. Prog Biophys Mol Biol 84: 29-59.

Candido R (2003) A breaker of advanced glycation end products attenuates diabetes-induced myocardial structural changes. Circ Res 92: 785-792.

Chen H, Hwang H, McKee LAK, Perez JN, Regan JA, Constantopoulos E, LaFleur B, Konhilas JP (2013) Temporal and morphological impact of pressure overload in transgenic FHC mice. Front Physiol 4: 205

Chen Y, Guo H, Xu D, Xu X, Wang H, Hu X, Lu Z, Kwak D, Xu Y, Gunther R, Huo Y, Weir EK (2012) Left ventricular failure produces profound lung remodeling and pulmonary hypertension in mice: heart failure causes severe lung disease. Hypertension 59: 1170-1178.

Cherepanova O, Orlova A, Galkin VE, van der Ven PF, Fürst DO, Jin JP, Egelman EH (2006) Xin-repeats and nebulin-like repeats bind to F-actin in a similar manner. J Mol Biol 356: 714–723.

Choi S, Gustafson-Wagner EA, Wang Q, Harlan SM, Sinn HW, Lin JL, Lin JJ (2007) The intercalated disc protein, mXinα, is capable of interacting with β-catenin and bundling actin filaments. J Biol Chem. 282: 36024-36036.

Chopra A, Tabdanov E, Patel H, Janmey PA, Kresh JY (2011) Cardiac myocyte remodeling mediated by N-cadherin-dependent mechanosensing. Am J Physiol Heart Circ Physiol 300: H1252-H1266.

Chu PH, Chen J (2011) The novel roles of four and a half LIM proteins 1 and 2 in the cardiovascular system. Chang Gung Med J 34: 127-134.

Clark KA, McElhinny AS, Beckerle MC, Gregorio CC (2002) Striated muscle cytoarchitecture: an intricate web of form and function. Annu Rev Cell Dev Biol 18: 637-706.

Clemen CS, Herrmann H, Strelkov SV, Schröder R (2013) Desminopathies: pathology and mechanisms. Acta Neuropathol 125: 47-75.

Clemen CS, Stöckigt F, Strucksberg K-H, Chevessier F, Winter L, Schütz J, Bauer R, Thorweihe J-M, Wenzel D, Schlötzer-Schrehardt U, Rasche V, Krsmanovic P, Katus HA, Rottbauer W, Just S, Müller OJ, Friedrich O, Meyer R, Herrmann H, Schrickel JW, Schröder R (2015) The toxic effect of R350P mutant desmin in striated muscle of man and mouse. Acta Neuropathol 129: 297-315.

Cohn JN, Ferrari R, Sharpe N (2000) Cardiac remodeling-concepts and clinical implications: a consensus paper from an international forum on cardiac remodeling. J Am Coll Cardiol 35: 569-582.

Coppola G, Carità P, Corrado E, Borrelli A, Rotolo A, Guglielmo M, Nugara C, Ajello L, Santomauro M, Novo S (2013) ST segment elevations: always a marker of acute myocardial infarction? Indian Heart J 65: 412-423.

Costanzo LS (2010) Costanzo Physiology (5th Ed). Pennsylvania, USA: Saunders.

Cutler G, Marshall LA, Chin N, Baribault H, Kassner PD (2007) Significant gene content variation characterizes the genomes of inbred mouse strains. Genome Res 17: 1743-1754.

de Almeida AC, van Oort RJ, Wehrens XH (2010) Transverse aortic constriction in mice. J Vis Exp 38: 1729.

de Boer M, van Deel ED, de Kleijnen M , Hoeijmakers JHJ. and Duncker D J. (2013) Diverse effects of aging on the cardiac response in pathological left ventricular remodeling and dysfunction. FASEB J 27: 1194.2.

Deschamps A, Spinale FG (2006) Pathways of matrix metalloproteinase induction in heart failure: bioactive molecules and transcriptional regulation. Cardiovasc Res 69: 666-676.

Desmouliere A, Geinoz A, Gabbiani F, Gabbiani G (1993) Transforming growth factor-β 1 induces α-smooth muscle actin expression in granulation tissue myofibroblasts and in quiescent and growing cultured fibroblasts. J Cell Biol 122: 103-11.

Divakaran V, Adrogue J, Ishiyama M, Entman ML, Haudek S, Sivasubramanian N, Mann DL (2009) Adaptive and maladptive effects of SMAD3 signaling in the adult heart after hemodynamic pressure overloading. Circ Heart Fail 2: 633-642.

Dorn GW, Robbins J, Sugden PH (2003) Phenotyping hypertrophy: eschew obfuscation. Circ Res 92: 1171-1175.

Drees F, Pokutta S, Yamada S, Nelson WJ, Weis WI (2005) α-catenin is a molecular switch that binds E-cadherin-β-catenin and regulates actin-filament assembly. Cell 123: 903-915.

Ehrentraut H, Weber C, Ehrentraut S, Schwederski M, Boehm O, Knuefermann P, Meyer R, Baumgarten G (2011) The toll-like receptor 4-antagonist eritoran reduces murine cardiac hypertrophy. Eur J Heart Fail 13: 602-610.

Fabiato A (1985) Time and calcium dependence of activation and inactivation of calcium-induced release of calcium from the sarcoplasmic reticulum of a skinned canine cardiac purkinje cell. J Gen Physiol 85: 247-289.

Factor SM (1994) Role of extracellular matrix in dilated cardiomyopathy. Heart Fail 9: 260–268.

Faggiano P ST, Rusconi C, Ghizzoni G, Marchetti A, Sorgato A (1994) Left ventricular geometric adaption to chronic pressure overload: differences between systemic hypertension and valvular aortic stenosis: an echocardiographic study. Am J Noninvas Cardiol 8: 346–351.

Fatkin D, Otway R, Richmond Z (2010) Genetics of dilated cardiomyopathy. Heart Fail Clin 6: 129-140.

Flurkey K CJ, Harrison DE (2007) The mouse in aging research. In: Fox JG ea, editors (ed) The mouse in biomedical research. American College Laboratory Animal Medicine (Elsevier), Burlington, MA, pp 637–672.

Frank O (1895) Zur Dynamik des Herzmuskels. Z. Biol 32: 370-437.

Fürst DO, Osborn M, Nave R, Weber K (1988) The organization of titin filaments in the half-sarcomere revealed by monoclonal antibodies in immunoelectron microscopy: a map of ten nonrepetitive epitopes starting at the Z Line extends close to the M Line. J Cell Biol 106: 1563-1572.

Gao XM, Dart AM, Dewar E, Jennings G, Du XJ (2000) Serial echocardiographic assessment of left ventricular dimensions and function after myocardial infarction in mice. Cardiovasc Res 45: 330-338.

Geiger B, Bershadsky A, Pankov R, Yamada KM (2001) Transmembrane crosstalk between the extracellular matrix-cytoskeleton crosstalk. Nat Rev Mol Cell Biol 2: 793-805.

Gerdts E (2008) Left ventricular structure in different types of chronic pressure overload. Eur Heart J Suppl 10: E23-E30.

Goltz D RE, Besmens M, Huss S, Kirfel J, Meyer R, Büttner R The loss of the LIM-only protein FHL2 protects the heart against pressure induced cardiac hypertrophy and remodeling process. PloS One (in revision).

Gontier Y, Taivainen A, Fontao L, Sonnenberg A, van der Flier A, Carpen O, Faulkner G, Borradori L (2005) The Z-disc proteins myotilin and FATZ-1 interact with each other and are connected to the sarcolemma via muscle-specific filamins. J Cell Sci 118: 3739-3749.

Granzier HL, Campbell KB (2006) New insights in the role of cardiac myosin binding protein C as a regulator of cardiac contractility. Circ Res 99: 795-797.

Green KJ, Böhringer M, Gocken T, Jones JC (2005) Intermediate filament associated proteins. Adv Protein Chem 70: 143-202.

Grosskurth SE, Bhattacharya D, Wang Q, Lin JJ-C (2008) Emergence of Xin demarcates a key innovation in heart evolution. PLoS ONE 3: e2857.

Gullestad L, Ueland T, Vinge LE, Finsen A, Yndestad A, Aukrust P (2012) Inflammatory cytokines in heart failure: mediators and markers. Cardiology 122: 23-35.

Gustafson-Wagner EA, Sinn HW, Chen YL, Wang DZ, Reiter RS, Lin JLC, Yang B, Williamson RA, Chen J, Lin CI, Lin JJ (2007) Loss of mXinα, an intercalated disk protein, results in cardiac hypertrophy and cardiomyopathy with conduction defects. Am J Physiol Heart Circ Physiol 293: H2680-H2692.

Guyton AC & Hall JE (2006) Textbook of medical physiology (11th Ed). Philadelphia, Pennsylvania, USA: Elsevier.

Harvey PA, Leinwand LA (2011) The cell biology of disease: cellular mechanisms of cardiomyopathy. J Cell Biol 194: 355-365.

Hein S, Kostin S, Heling A, Maeno Y, Schaper J (2000) The role of the cytoskeleton in heart failure. Cardiovasc Res 45: 273-278.

Ho CY (2010) Hypertrophic cardiomyopathy: for heart failure clinics: genetics of cardiomyopathy and heart failure. Heart Fail Clin 6: 141-159.

Huang HT, Brand OM, Mathew M, Ignatiou C, Ewen EP, McCalmon SA, Naya FJ (2006) Myomaxin is a novel transcriptional target of MEF2A that encodes a Xin-related α-actinin-interacting protein. J Biol Chem 281: 39370-39379.

Hutchinson KR, Saripalli C, Chung CS, Granzier H (2015) Increased myocardial stiffness due to cardiac titin isoform switching in a mouse model of volume overload limits eccentric remodeling. J Mol Cell Cardiol 79: 104-114.

Isoyama S, Wei JY, Izumo S, Fort P, Schoen FJ, Grossman W (1987) Effect of age on the development of cardiac hypertrophy produced by aortic constriction in the rat. Circ Res 61: 337-345.

Jacobshagen C, Gruber M, Teucher N, Schmidt AG, Unsold BW, Toischer K, Van PN, Maier LS, Kogler H, Hasenfuss G (2008) Celecoxib modulates hypertrophic signalling and prevents load-induced cardiac dysfunction. Eur J Heart Fail 10: 334-342.

Jane-Lise S, Corda S, Chassagne C, Rappaport L (2000) The extracellular matrix and the cytoskeleton in heart hypertrophy and failure. Heart Fail Rev 5: 239-250.

Johnston RK, Balasubramanian S, Kasiganesan H, Baicu CF, Zile MR, Kuppuswamy D (2009) 3 Integrin-mediated ubiquitination activates survival signaling during myocardial hypertrophy. FASEB J 23: 2759-2771.

Jung-Ching Lin J, Gustafson-Wagner EA, Sinn HW, Choi S, Jaacks SM, Wang DZ, Evans S, Li-Chun Lin J (2005) Structure, Expression, and Function of a Novel Intercalated Disc Protein, Xin. J Med Sci 25: 215-222.

Kassiri Z, Khokha R (2005) Myocardial extra-cellular matrix and its regulation by metalloproteinases and their inhibitors. Thromb Haemost 93: 212-219.

Kebir S, Schuld J, Orfanos Z, Linhart M, Lamberz C, van der Ven PFM, Schrickel J, Kirfel G, Fürst DO, Meyer R Xin contributes protection against ventricular arrhythmia in cardiac hypertrophy (in preparation).

Kehat I, Davis J, Tiburcy M, Accornero F, Saba-El-Leil MK, Maillet M, York AJ, Lorenz JN, Zimmermann WH, Meloche S, Molkentin JD (2010) Extracellular signal-regulated kinases 1 and 2 regulate the balance between cccentric and concentric cardiac growth. Circ Res 108: 176-183

Kehat I, Molkentin JD (2010) Molecular pathways underlying cardiac remodeling during pathophysiological stimulation. Circulation 122: 2727-2735.

Kemp CD, Conte JV (2012) The pathophysiology of heart failure. Cardiovasc Pathol 21: 365-371.

Kim IY, Shin JH, Seong JK (2010) Mouse phenogenomics, toolbox for functional annotation of human genome. BMB Rep 43: 79-90.

Klabunde RE (2011) Cardiovascular physiology concepts Lippincott Williams & Wilkins

Koteliansky VE, Glukhova MA, Gneushev GN, Samuel JL, Rappaport L (1986) Isolation and localization of filamin in heart muscle. Eur J Biochem 156: 619-623.

Krüger M, Linke WA (2009) Titin-based mechanical signalling in normal and failing myocardium. J Mol Cell Cardiol 46: 490-498.

Lai NC, Gao MH, Tang E, Tang RY, Guo T, Dalton ND, Deng AH, Tang T (2012) Pressure overload-induced cardiac remodeling and dysfunction in the absence of interleukin 6 in mice. Lab Invest 92: 1518-1526.

Lakatta EG (2015) So! What's aging? Is cardiovascular aging a disease? J Mol Cell Cardiol 83: 1-13.

Leask A (2015) Getting to the heart of the matter. Circ Res 116: 1269-1276.

Levine S, Coyne BJ, Colvin LC (2015) Clinical exercise electrocardiography. Burlington, Massachusetts, USA: Boston Medical Publishing.

Li J, Radice GL (2010) A new perspective on intercalated disc organization: implications for heart disease. Dermatol Res Pract 2010: 1-5.

Li YH, Reddy AK, Ochoa LN, Pham TT, Hartley CJ, Michael LH, Entman ML, Taffet GE (2003) Effect of age on peripheral vascular response to transverse aortic banding in mice. J Gerontol A: Biolo Sci Med Sci 58: B895-B899.

Li YY, McTiernan CF, Feldman AM (1999) Proinflammatory cytokines regulate tissue inhibitors of metalloproteinases and disintegrin metalloproteinase in cardiac cells. Cardiovasc Res 42: 162-172.

Liao RL, Jain M, Cui L, D'Agostino J, Aiello F, Luptak I, Ngoy S, Mortensen RM, Tian R (2002) Cardiac-specific overexpression of GLUT1 prevents the development of heart failure attributable to pressure overload in mice. Circulation 106: 2125-2131.

Lin X, Ruan X, Anderson MG, McDowell JA, Kroeger PE, Fesik SW, Shen Y. (2005) siRNA-mediated off-target gene silencing triggered by a 7 nt complementation. Nucleic Acids Res 33: 4527-4535.

Lorell BH, Carabello BA (2000) Left ventricular hypertrophy : pathogenesis, detection, and prognosis. Circulation 102: 470-479.

Lucas JA, Zhang Y, Li P, Gong K, Miller AP, Hassan E, Hage F, Xing D, Wells B, Oparil S, Chen YF (2010) Inhibition of transforming growth factor-β signaling induces left ventricular dilation and dysfunction in the pressure-overloaded heart. Am J Physiol Heart Circ Physiol 298: H424-H432.

Lyon RC, Zanella F, Omens JH, Sheikh F (2015) Mechanotransduction in cardiac hypertrophy and failure. Circ Res 116: 1462-1476.

Marian AJ (2010) Hypertrophic cardiomyopathy: from genetics to treatment. Eur J Clin Invest 40: 360-369.

McCalmon SA, Desjardins DM, Ahmad S, Davidoff KS, Snyder CM, Sato K, Ohashi K, Kielbasa OM, Mathew M, Ewen EP, Walsh K, Gavras H, Naya FJ (2010) Modulation of angiotensin II-mediated cardiac remodeling by the MEF2A target gene Xirp2. Circ Res 106: 952-960.

Meyer R, Schreckenberg R, Kretschmer F, Bittig A, Conzelmann C, Grohé C, Schlüter K-D (2007) Parathyroid hormone-related protein (PTHrP) signal cascade modulates myocardial dysfunction in the pressure overloaded heart. Eur J Heart Fail 9: 1156-1162.

Milner DJ, Taffet GE, Wang X, Pham T, Tamura T, Hartley C, Gerdes MA, Capetanaki Y (1999) The absence of desmin leads to cardiomyocyte hypertrophy and cardiac dilation with compromised systolic function. J Mol Cell Cardiol 31: 2063-2076.

Modica-Napolitano JS, Singh KK (2004) Mitochondria as targets for detection and treatment of cancer. Expert Rev Mol Med 4: 1-19.

Mohammed SF, Storlie JR, Oehler EA, Bowen LA, Korinek J, Lam CSP, Simari RD, Burnett JC, Redfield MM (2012) Variable phenotype in murine transverse aortic constriction. Cardiovasc Pathol 21: 188-198.

Molt S, Buhrdel JB, Yakovlev S, Schein P, Orfanos Z, Kirfel G, Winter L, Wiche G, van der Ven PF, Rottbauer W, Just S, Belkin AM, Fürst DO (2014) Aciculin interacts with filamin C and Xin and is essential for myofibril assembly, remodeling and maintenance. J Cell Sci 127: 3578-3592.

Monreal G, Nicholson LM, Han B, Joshi MS, Phillips AB, Wold LE, Bauer JA, Gerhardt MA (2008) Cytoskeletal remodeling of desmin is a more accurate measure of cardiac dysfunction than fibrosis or myocyte hypertrophy. Life Sci 83: 786-794.

Muller P, Kazakov A, Semenov A, Jagoda P, Friedrich EB, Bohm M, Laufs U (2013) Ramipril and telmisartan exhibit differential effects in cardiac pressure overload-induced hypertrophy without an additional benefit of the combination of both drugs. J Cardiovasc Pharmacol Ther 18: 87-93.

Nakamura A, Rokosh DG, Paccanaro M, Yee RR, Simpson PC, Grossman W, Foster E (2001) LV systolic performance improves with development of hypertrophy after transverse aortic constriction in mice. Am J Physiol Heart Circ Physiol 281: H1104-H1112.

Nerbonne JM, Kass RS (2005) Molecular physiology of cardiac repolarization. Physiol Rev 85: 1205-1253.

Nerbonne JM, Nichols CG, Schwarz TL, Escande D (2001) Genetic manipulation of cardiac K^+ channel function in mice: what have we learned, and where do we go from here? Circ Res 89: 944-956.

Nivala M, de Lange E, Rovetti R, Qu Z (2012) Computational modeling and numerical methods for spatiotemporal calcium cycling in ventricular myocytes. Front Physiol 3: 114.

Noorman M, van der Heyden MA, van Veen TA, Cox MG, Hauer RN, de Bakker JM, van Rijen HV (2009) Cardiac cell-cell junctions in health and disease: electrical versus mechanical coupling. J Mol Cell Cardiol 47: 23-31.

Oliver PL, Bitoun E, Davies KE (2007) Comparative genetic analysis: the utility of mouse genetic systems for studying human monogenic disease. Mamm Genome 18: 412-424.

Olson EN (2004) A decade of discoveries in cardiac biology. Nat Med 10: 467-474.

Opie LH, Commerford PJ, Gersh BJ, Pfeffer MA (2006) Controversies in ventricular remodelling. Lancet 367: 356-367.

Otten C, van der Ven PF, Lewrenz I, Paul S, Steinhagen A, Busch-Nentwich E, Eichhorst J, Wiesner B, Stemple D, Strähle U, Fürst DO, Abdelilah-Seyfried S (2012) Xirp proteins mark injured skeletal muscle in zebrafish. PLoS ONE 7: e31041.

Pacholsky D, Vakeel P, Himmel M, Löwe T, Stradal T, Rottner K, Fürst DO, van der Ven PF (2004) Xin repeats define a novel actin-binding motif. J Cell Sci 117: 5257–5268.

Patel DA, Lavie CJ, Milani RV, Shah S, Gilliland Y (2009) Clinical implications of left atrial enlargement: a review. Ochsner J 9: 191-196.

Patten RD, Pourati I, Aronovitz MJ, Alsheikh-Ali A, Eder S, Force T, Mendelsohn ME, Karas RH (2008) 17 β-estradiol differentially affects left ventricular and cardiomyocyte hypertrophy following myocardial infarction and pressure overload. J Card Fail 14: 245-53.

Patterson SW, Starling EH (1914) On the mechanical factors which determine the output of the ventricles. J Physiol 48: 357-379.

Perriard JC, Hirschy A, Ehler E (2003) Dilated cardiomyopathy: a disease of the intercalated disc? Trends Cardiovasc Med 13: 30-38.

Raher MJ, Thibault HB, Buys ES, Kuruppu D, Shimizu N, Brownell AL, Blake SL, Rieusset J, Kaneki M, Derumeaux G, Picard MH, Bloch KD, Scherrer-Crosbie M (2008) A short duration of high-fat diet induces insulin resistance and predisposes to adverse left ventricular remodeling after pressure overload. Am J Physiol Heart Circ Physiol 295: H2495-H2502.

Rockman HA, Ross RS, Harris AN, Knowlton KU, Steinhelper ME, Field LJ, Jr Ross J, Chien KR (1991) Segregation of atrial-specific and inducible expression of an atrial natriuretic factor transgene in an in vivo murine model of cardiac hypertrophy. Proc Natl Acad Sci U S A 88: 8277-8281.

Rothermel BA, Berenji K, Tannous P, Kutschke W, Dey A, Nolan B, Yoo KD, Demetroulis E, Gimbel M, Cabuay B, Karimi M, Hill JA (2005) Differential activation of stress-response signaling in load-induced cardiac hypertrophy and failure. Physiol Genomics 23: 18-27.

Rueckschloss U, Isenberg G (2001) Cytochalasin D reduces Ca^{2+}currents via cofilin-activated depolymerization of F-actin in guinea-pig cardiomyocytes. J Physiol 537: 363-370.

Rueckschloss U, Isenberg G (2004) Contraction augments L-type Ca^{2+} currents in adherent guinea-pig cardiomyocytes. J Physiol 560: 403-411.

Sarantitis I, Papanastasopoulos P, Manousi M, Baikoussis NG, Apostolakis E (2012) The cytoskeleton of the cardiac muscle cell. Hellenic J Cardiol 53: 367-379.

Schrickel JW, Fink K, Meyer R, Grohé C, Stoeckigt F, Tiemann K, Ghanem A, Lickfett L, Nickenig G, Lewalter T (2009) Lack of gelsolin promotes perpetuation of atrial fibrillation in the mouse heart. J Interv Card Electrophysiol 26: 3-10.

Sequeira V, Nijenkamp LL, Regan JA, van der Velden J (2013) The physiological role of cardiac cytoskeleton and its alterations in heart failure. Biochim Biophys Acta 1838: 700-722.

Severs NJ, Bruce AF, Dupont E, Rothery S (2008) Remodelling of gap junctions and connexin expression in diseased myocardium. Cardiovasc Res 80: 9-19.

Shimura M, Minamisawa S, Takeshima H, Jiao Q, Bai Y, Umemura S, Ishikawa Y (2008) Sarcalumenin alleviates stress-induced cardiac dysfunction by improving Ca^{2+} handling of the sarcoplasmic reticulum. Cardiovasc Res 77: 362-370.

Sheikh F, Ross RS, Chen J (2009) Cell-cell connection to cardiac disease. Trends Cardiovasc Med 19: 182-190.

Silverthorn DU (2008) Human physiology: an integrated approach (5th Ed), San Francisco , USA: Benjamin Cummings.

Sinn HW, Balsamo J, Lilien J, Lin JJ (2002) Localization of the novel Xin protein to the adherens junction complex in cardiac and skeletal muscle during development. Dev Dyn 225: 1-13.

Siwik DA, Chang DL, Colucci WS (2000) Interleukin-1β and tumor necrosis factor α decrease collagen synthesis and increase matrix metalloproteinase activity in cardiac fibroblasts in vitro. Circ Res 86: 1259-1265.

Siwik DA, Colucci WS (2004) Regulation of matrix metalloproteinases by cytokines and reactive oxygen/nitrogen species in the myocardium. Heart Fail Rev 9: 43-51.

Skavdahl M, Steenbergen C, Clark J, Myers P, Demianenko T, Mao L, Rockman HA, Korach KS, Murphy E (2005) Estrogen receptor-β mediates male-female differences in the development of pressure overload hypertrophy. Am J Physiol Heart Circ Physiol 288: H469-H476.

Souders CA, Borg TK, Banerjee I, Baudino TA (2012) Pressure overload induces early morphological changes in the heart. Am J Pathol 181: 1226-1235.

Speerschneider T GS, Metoska A, Olesen S P, Calloe K, Thomsen M B (2013) Development of heart failure is independent of K^+ channel-interacting protein 2 expression. J Physiol 591: 5923–5937.

Spinale F, Zellner JL, Johnson WS, Eble DM, Munyer PD (1996) Cellular and extracellular remodeling with the development and recovery from tachycardia-induced cardiomyopathy: changes in fibrillar collagen, myocyte adhesion capacity and proteoglycans. J Mol Cell Cardiol 28: 1591-1608.

Spinale FG, Tomita M, Zellner JL, Cook JC, Crawford FA, Zile MR (1991) Collagen remodeling and changes in LV function during development and recovery from supraventricular tachycardia. Am J Physiol 261: H308-H318.

Suryakumar G, Kasiganesan H, Balasubramanian S, Kuppuswamy D (2010) Lack of β3 integrin signaling contributes to calpain-mediated myocardial cell loss in pressure-overloaded myocardium. J Cardiovasc Pharmacol 55: 567-573.

Tagawa H, Rozich JD, Tsutsui H, Narishige T, Kuppuswamy D, Sato H, McDermott PJ, Koide M, Cooper G (1996) Basis for increased microtubules in pressure-hypertrophiedcardiocytes. Circulation 93: 1230-1243.

Tanaka N, Dalton N, Mao L, Rockman HA, Peterson KL, Gottshall KR, Hunter JJ, Chien KR, Ross J (1996) Transthoracic cchocardiography in models of cardiac disease in the mouse. Circulation 94: 1109-1117.

van der Ven PF, Obermann WM, Lemke B, Gautel M, Weber K, Fürst DO (2000) Characterization of muscle filamin isoforms suggests a possible role of gamma-filamin/ABP-L in sarcomeric Z-disc formation. Cell Motil Cytoskeleton 45: 149-162.

van der Ven PF, Ehler E, Vakeel P, Eulitz S, Schenk JA, Milting H, Micheel B, Fürst DO (2006) Unusual splicing events result in distinct Xin isoforms that associate differentially with filamin c and Mena/VASP. Exp Cell Res 312: 2154-2167.

van Oort RJ, Respress JL, Li N, Reynolds C, De Almeida AC, Skapura DG, De Windt LJ, Wehrens XHT (2010) Accelerated development of pressure overload-induced cardiac hypertrophy and dysfunction in an RyR2-R176Q knockin mouse model. Hypertension 55: 932-938.

Velten M, Duerr GD, Pessies T, Schild J, Lohner R, Mersmann J, Dewald O, Zacharowski K, Klaschik S, Hilbert T, Hoeft A, Baumgarten G, Meyer R, Boehm O, Knuefermann P (2012) Priming with synthetic oligonucleotides attenuates pressure overload-induced inflammation and cardiac hypertrophy in mice. Cardiovasc Res 96: 422-432.

Vinkemeier U, Obermann W, Weber K, Fürst D.O. (1993) The globular head domain of titin extends into the center of the sarcomeric M band. cDNA cloning, epitope mapping and immunoelectron microscopy of two titin-associated proteins. J Cell Sci 106: 319-330.

Walker MG (2001) Pharmaceutical target identification by gene expression analysis. Mini Rev Med Chem 1: 197-205.

Wang DZ, Reiter RS, Lin JL, Wang Q, Williams HS, Krob SL, Schultheiss TM, Evans S, Lin JJ (1999) Requirement of a novel gene, Xin, in cardiac morphogenesis. Development 126: 1281-1294.

Wang Q, Lin JL, Reinking BE, Feng HZ, Chan FC, Lin CI, Jin JP, Gustafson-Wagner EA, Scholz TD, Yang B, Lin JJ (2010) Essential roles of an intercalated disc protein, mXinβ, in postnatal heart growth and survival. Circ Res 106: 1468-1478.

Wang Q, Lin JL, Wu KH, Wang DZ, Reiter RS, Sinn HW, Lin CI, Lin CJ (2012) Xin proteins and intercalated disc maturation, signaling and diseases. Front Biosci (Landmark Ed) 17: 2566-2593.

Wang Q, Lu TL, Adams E, Lin JL, Lin JJ(2013) Intercalated disc protein, mXinα, suppresses p120-catenin-induced branching phenotype via its interactions with p120-catenin and cortactin. Arch Biochem Biophys 535: 91-100.

Watabe-Uchida M (1998) α -catenin-vinculin interaction functions to organize the apical junctional complex in epithelial cells. J Cell Biol 142: 847-857.

Weber KT, Brilla CG (1992) Myocardial fibrosis and the renin-angiotensin-aldosterone system. J Cardiovasc Pharmacol 20: S48-S54.

Weber KT, Janicki JS, Shroff SG, Pick R, Chen RM, Bashey RI (1988) Collagen remodeling of the pressure-overloaded, hypertrophied nonhuman primate myocardium. Circ Res 62: 757-765.

Weber KT, Sun Y, Tyagi SC, Cleutjens JP. (1994) Collagen network of the myocardium: function, structural remodeling and regulatory mechanisms. J Mol Cell Cardiol 26: 279-292.

Weisheit C, Zhang Y, Faron A, Köpke O, Weisheit G, Steinsträsser A, Frede S, Meyer R, Boehm O, Hoeft A, Kurts C, Baumgarten G (2014) Ly6Clow and not Ly6Chigh macrophages

accumulate first in the heart in a model of murine pressure-overload. PLoS ONE 9: e112710.

Weisser-Thomas J, Kempelmann H, Nickenig G , Grohé C ,Djoufack P , Fink K , Meyer R (2015) Influence of gelsolin deficiency on excitation contraction coupling in adult murine cardiomyocytes. J Physiol Pharmacol 66: 373-383.

Wiegerinck RF, Verkerk AO, Belterman CN, van Veen TA, Baartscheer A, Opthof T, Wilders R, de Bakker JM, Coronel R (2006) Larger cell size in rabbits with heart failure increases myocardial conduction velocity and QRS duration. Circulation 113: 806-813.

Witt H, Schubert C, Jaekel J, Fliegner D, Penkalla A, Tiemann K, Stypmann J, Roepcke S, Brokat S, Mahmoodzadeh S, Brozova E, Davidson MM, Ruiz Noppinger P, Grohe C, Regitz-Zagrosek V (2008) Sex-specific pathways in early cardiac response to pressure overload in mice. J Mol Med (Berl) 86: 1013-1024.

Xu J, Gong NL, Bodi I, Aronow BJ, Backx PH, Molkentin JD (2006) Myocyte enhancer factors 2A and 2C induce dilated cardiomyopathy in transgenic mice. J Biol Chem 281: 9152-9162.

Xu X, Fassett J, Hu X, Zhu G, Lu Z, Li Y, Schnermann J, Bache RJ, Chen Y (2008) Ecto-5'-nucleotidase deficiency exacerbates pressure-overload-induced left ventricular hypertrophy and dysfunction. Hypertension 51: 1557-1564.

Yamamoto K, Ohishi M, Katsuya T, Ito N, Ikushima M, Kaibe M, Tatara Y, Shiota A, Sugano S, Takeda S, Rakugi H, Ogihara T (2006) Deletion of angiotensin-converting enzyme 2 accelerates pressure overload-induced cardiac dysfunction by increasing local angiotensin II. Hypertension 47: 718-726.

Youn HJ, Rokosh G, Lester SJ, Simpson P, Schiller NB, Foster E (1999) Two-dimensional echocardiography with a 15-MHz transducer is a promising alternative for in vivo measurement of left ventricular mass in mice. J Am Soc Echocardiogr 12: 70-75.

7 Appendix

7.1 List of figures

1.1	Structure of the heart, and course of blood flow through the heart chambers and heart valves	1
1.2	Mechanical and humoral factors affecting cardiac output	3
1.3	The structure of cardiac myocytes	5
1.4	A diagrammatic representation of three structural zones of the Intercalated disc	6
1.5	Anatomy of the sarcomere	7
1.6	Selected cytoskeletal filament linkages in the sarcolemma of Cardiomyoctes	10
1.7	Proposed model for XIRP1 (XinB) localization at the adherens junction of the intercalated disc	13
1.8	Action potential of a ventricular cardiomyocyte	16
1.9	Excitation contraction coupling in cardiac muscle	17
1.10	The ventricular pressure curves	18
1.11	Classification of ventricular remodeling patterns	21
2.1	An overview of experimental protocols	29
2.2	Transverse aortic constriction	30
2.3	The setup for small animal surgeries	34
2.4	The surgical instruments	34
2.5	Hair removing	36
2.6	Endotracheal intubation	36
2.7	Mini-ventilator and the endotracheal tube connection	37
2.8	The transverse aortic constriction	38
2.9	The calibration equipment	40
2.10	The PowerLab/8SP	40
2.11	Screen shot of units conversion	41
2.12	Pressure catheter insertion	43
2.13	The blood pressure setting dialog	44
2.14	LabChart window sheet	45
2.15	The heart perfusion	46

2.16	Tissue embedding station	48
2.17	Microtome	49
2.18	Mounting the paraffin block on a piece of hardwood using a heated knife	49
2.19	The image J setting scale	51
2.20	The left ventricular thickness measurement by Image J	51
2.21	The scale and the tibia length measurement	52
3.1	Western-blot analysis of whole hearts from WT and XIRP1XIRP2 dko mice	64
3.2	Fluorescence microscopic visualization of immunofluorescence stainings in cryosections of hearts from XIRP WT and XIRP1XIRP2 dko mice	65
3.3	Body weight (BW) of the mice of all genotypes	66
3.4	The tibia length (TL) of the mice of all genotypes	67
3.5	HW, HW/BW ratio, HW/TL ratio of XIRP WT and XIRP1XIRP2 dko mice	68
3.6	LVW, LVW/BW ratio, LVW/TL ratio of XIRP WT and XIRP1XIRP2 dko mice	69
3.7	LW, LW/BW ratio, LW/TL ratio of XIRP WT and XIRP1XIRP2 dko mice	70
3.8	HW, HW/BW ratio, HW/TL ratio of XIRP WT and XIRP1XIRP2 dko mice	72
3.9	LVW, LVW/BW ratio, LVW/TL ratio of XIRP WT and XIRP1XIRP2 dko mice	73
3.10	LW, LW/BW ratio, LW/TL ratio of XIRP WT and XIRP1XIRP2 dko	74
3.11	Comparison of septum thickness between XIRP1XIRP2 dko and XIRP WT	75
3.12	Light microscopic photographs of transverse sections of hearts trichrome stained according to Masson from the four groups	76
3.13	Light microscopic photographs of transverse sections of hearts trichrome stained according to Masson from the four groups	77
3.14	Quantified area of fibrosis in sham and TAC hearts of both genotypes	78
3.15	Microscopic evaluation and immunolocalization of myomesin, RyRs , and filaminC d16-20 in isolated cardiomyocytes	79
3.16	Microscopic evaluation and immunolocalization of filaminA/C d1-2, titin, andconnexin43 in isolated cardiomyocytes	80

3.17 Microscopic evaluation and immunolocalization of filaminA/C d1-2, titin, andcadherin in isolated cardiomyocytes 81
3.18 Cardiomyocyte length and width 82
3.19 The single cardiomyocyte and number of terminal and non-terminal ICDs 84
3.20 Hemodynamic data of XIRP WT and XIRP1XIRP2 dko female after TAC 86
3.21 The ECG of a human and a mouse 87
3.22 ECGs from XIRP WT sham and TAC. ECGs of a XIRP WT sham 89
3.23 ECGs from XIRP1XIrp2 dko sham 90
3.24 ECGs from XIRP1XIRP2 dko sham 91
3.25 The ECG from XIRP1XIRP2 dko TAC mice 92
3.26 HW, HW/BW ratio and HW/TL ratio of XIRP WT and XIRP1XIRP2 dko 3 month-old and 1 year-old mice 93
3.27 LVW, LVW/BW ratio and LVW/TL ratio of 3 month-old and 1 year-old XIRP WT and XIRP1XIRP2 dko mice 95
3.28 LW, LW/BW ratio, and LW/TL ratio of 3 month-old and 1 year-old XIRP WT and XIRP1XIRP2 dko mice 96
3.29 HW, HW/BW ratio and HW/TL ratio of 3 month-old and 1 year-old XIRP WT and XIRP1XIRP2 dko mice after 14 days TAC 98
3.30 LVW, LVW/BW ratio and LVW/TL ratio of 3 month-old and 1 year-old XIRP WT and XIRP1XIRP2 dko mice after 14 days TAC 100
3.31 LW, LW/BW ratio, LW/TL ratio of 3 month-old and 1 year-old XIRP WT and XIRP1XIRP2 dko mice after 14 days TAC 101
3.32 Hemodynamic data of XIRP WT and XIRP1XIRP2 dko 3 month-old and 1 year-old mice after 14 days TAC 103

7.2 List of tables

1. 1 The Nomenclature of XIRPs 12
3.1 Development of BW from the operation to the measurement day 71
3.2 The hemodynamic data of XIRP WT and XIRP1XIRP2 dko mice 85
3.3 Surface ECG parameters 88

8 Declaration

I hereby declare that this dissertation has been written only by the undersigned and without any assistance from third parties. Furthermore, I confirm that no sources have been used in the preparation of this dissertation other than those indicated in the dissertation itself. This dissertation was not submitted in any form for another degree at any university or other institution of tertiary education.

Bonn, 30th July 2015

Tippaporn Bualeong

9 Acknowledgements

First and foremost, I would like to express my special gratitude to my supervisor Prof. Dr. Rainer Meyer for giving me the great opportunity to learn several valuable lessons and the opportunity to carry out the great research projects in his laboratory and also the cooperative projects in his group. I would like to greatly appreciate him for his exceptional, scientific supervision, motivation, and for believing in me throughout my doctoral studies.

I am thankful especially to Prof. Dr. Dieter O. Fürst for his scientific supervision, support, and giving me to work in this project.

I would like to thank the members of my doctoral committee, Prof. Dr. Gerhard von der Emde and PD. Dr. Gerhild van Echten-Deckert for their time, as part of my dissertation committee.

I would like to give my special thanks to Dr. med. Diane Goltz, Dr. med. dent. Lina Gölz, Dr.med. Sied Kebir, and Dr. med. Paul Markowski**,** whom instructed me on the surgery techniques.

I am grateful to people who contributed to my project, particularly Julia Schuld for her experimental support and inputs into my work; and Hanne Bock for her friendship, understanding, and motivation during difficult moments throughout my work, and of course for her experimental support and invaluable advices.

Furthermore, I would like to thank all the other wonderful coworkers I was allowed to meet during my study time at the “Institut für Physiologie II”, “Institut für Zellbiologie”, and “Anatomisches Institut” whose have been patient, friendly, and always ready for help. It was a real pleasure to work and share this time with you all.

I gratefully acknowledge the scholarship received towards my study from the staff development program of Naresuan University, Thailand.

Finally, I would like to thank my parents, my sister, and my friends for their continuous support and understand during different steps of my study.

10 Poster and presentations

Tippaporn Bualeong, Sied Kebir, Michael Wolf, Dorothea Hof, Pascal Knüfermann, Georg Baumgarten, Heidi Ehrentraut, Rainer Meyer (2013). The Influence of Toll-like receptor 2 and 9 on the development of cardiac hypertrophy.
Poster and presentation, 92nd Annual Meeting of the German Physiological Society, Heidelberg, Germany

Tippaporn Bualeong, Seid Kebir, Michael Wolf, Pascal Knüfermann, Georg Baumgarten, Heidi Ehrentraut, Rainer Meyer (2014). Toll-like receptor 2 deficiency exacerbates cardiac hypertrophy in pressure overload.
Poster and presentation, Growth and Wasting in Heart and Skeletal Muscle, Keystone symposia, Santa Fe, New Mexico USA

Heidi Budde, Tippaporn Bualeong, Ilona Schirmer, Diana Cimiotti, Philip Steinwascher, Avinash Appukutan, Andreas Mügge, Yury ladilov, Kornelia Jaquet (2015). Soluble adenylyl cyclase plays a critical role in cardiac disease.
Poster, Heart Failure, 81st Annual Meeting of the Deutsche Kardiologe Gesellschaft Congress, Mannheim, Germany